MOLECULAR MODIFICATION OF DYE CONSTITUENTS THROUGH GRAFTING ANCHORING GROUPS AND PI-SPACERS: TOWARDS DSSCs APPLICATION

Geradius Deogratias

A Dissertation Submitted in Partial Fulfillment of the Requirements for the Degree of Doctor of Philosophy in Materials Science and Engineering of the Nelson Mandela African Institution of Science and Technology

Arusha, Tanzania

June, 2021

ABSTRACT

Triphenylamine based dyes molecular modification by grafting anchoring groups and π-spacers was performed within computational framework aimed at potential materials for dye-sensitized solar cells (DSSCs) application. For the modification, benzothiadiazole-like spacers, heterocyclic anchoring groups and heteroatom doping have been taken into account. The reported structural and optoelectronic properties of the dyes were realized through density functional theory and time-dependent density functional theory using B3LYP and CAM-B3LYP functionals coupled with 6-31G(d,p) and 6-31G+(d,p) basis sets. The findings show that presence of atoms of nitrogen and sulphur in the π-spacers has a beneficial impact on the material's properties, whereas the branched π-spacer impairs the electronic light absorption characteristics of the sensitizers. The heterocyclic anchoring units result in a bathochromic shift with maximum absorption within 450 − 600 nm. The computed light-harvesting efficiencies, excited-state lifetimes, electron injection and regeneration abilities prove that dyes with heterocyclic anchoring groups to be potential candidates for DSSC applications. The heteroatom doping demonstrates that the chalcogens enhance the absorption and fluorescent emission spectra of the isolated dyes in the visible and near infra-red regions with maximum wavelength 504 – 556 nm and 637 – 732 nm, respectively. Simulation of the dyes attachment to the TiO_2 surface was undertaken; two models of the crystal surface considered, TiO_2 slab and hydrogenated $(TiO_2)_6$ cluster. Among possible adsorption modes of the dye@TiO_2 complexes, monodentate, bidentate and tridentate, the bidentate mode was found thermodynamically more favourable. In both, individual dyes and dye@TiO_2 complexes, less electronegative dopants contributed to the improvement of the UV-Vis spectra and redistribution of electron density. The calculated energies of the dye@TiO_2 attachment relate to dopant heteroatoms; stronger binding is observed in the complexes with heavier heteroatoms – selenium and tellurium. The adsorption energy magnitudes range between 0.11 − 1.75 eV for the TiO_2 slab and 7.61 − 9.48 eV for $(TiO_2)_6$ cluster. Energy difference between the two binding models was found to correspond to the enthalpy of sublimation of TiO_2 from the TiO_2 anatase. One can anticipate that systematic modification of dyes' building blocks may lead to novel materials with suitable characteristics for application in DSSCs.

DECLARATION

I, Geradius Deogratias, do hereby declare to the Senate of the Nelson Mandela African Institution of Science and Technology that this dissertation is my own original work and that it has neither been submitted nor concurrently submitted for a degree or similar award in any other institution.

Geradius Deogratias

_____ _____

Name and Signature of the Candidate **Date**

The above declaration is confirmed

Prof. Alexander Pogrebnoi

_____ _____

Name and Signature of Supervisor (1) **Date**

Prof. Tatiana Pogrebnaya

_____ _____

Name and Signature of Supervisor (2) **Date**

Prof. Nicola Seriani

_____ _____

Name and Signature of Supervisor (3) **Date**

COPYRIGHT

CERTIFICATION

The undersigned certify that they have read and hereby recommend for acceptance by the Nelson Mandela African Institution of Science and Technology a the dissertation entitled: "Molecular Modification of Dye Constituents through Grafting Anchoring Groups and pi-Spacers: Towards DSSCs Application" and recommend for examination in partial fulfilment of the requirements for the degree of Doctor of Philosophy in Materials Science and Engineering of the Nelson Mandela African Institution of Science and Technology.

Prof. Alexander Pogrebnoi

_____ _____

Name and Signature of Supervisor (1) **Date**

Prof. Tatiana Pogrebnaya

_____ _____

Name and Signature of Supervisor (2) **Date**

Prof. Nicola Seriani

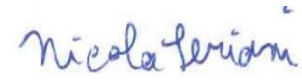

_____ _____

Name and Signature of Supervisor (3) **Date**

ACKNOWLEDGMENT

First and foremost, I would like to thank the Almighty God, the giver of life; without the Almighty God there is no variation or shadow due to change; without him, I am puny and powerless.

I want to extend my deepest gratitude to my supervisors, Prof. Nicola Seriani, Prof. Tatiana Pogrebnaya and Prof. Alexander Pogrebnoi. The freedom to explore, share opinions and ideas during the research period was excellent under their supervision. Their enthusiasm for research made a strong impression on me and I hope I will deliver the same in the future. Heartfelt thanks should as well go to Prof. Nuha Wazzan and Ms. Ohoud S. Al-Qurashi from the Chemistry Department, Faculty of Science, King Abdulaziz University, Jeddah, Saudi Arabia for their kind support and providing access to the King Abdulaziz University's High-Performance Computing Centre (Aziz Supercomputer) (http://hpc.kau.edu.sa).

Similarly, I would like to thank Prof. Revocatus Machunda (Dean, School of MEWES) and Dr. Thomas Kivevele (HoD, MESE Department) for providing a supportive environment to carry out my studies and their leadership attributes. I extend my heartfelt thanks to the AfDB Project Manager at NM-AIST, Mr. Julius Lenguyana for providing the excellent atmosphere to carry out my research activities. Furthermore, I wish to thank Ms. Analyce Ichwekeleza (Dean of Students), Ms. Victoria Ndossi, Ms. Silvia Ndakidemi (Students Welfare Office), Mr. Adam Mawenya, Ms. Leah Gonda and Ms. Joyce Martin for their dedicated assistance from IT department. I gain place my record and my sincere gratitude to Mr. Haji Chomba, Ms. Christina Dominick, Ms. Florence George and Ms. Eunice Mwakang'ata for their exceptional work in MEWES Dean's Office; I also owe the entire NM-AIST community.

I pass my heartfelt gratitude to my friend Dr. Fortunatus Rwegasira Jacob; it is whole-heartedly appreciated that your great advice proved monumental towards the success of this work. Also, I extend my sincere appreciation to colleagues Aristide G. Lambura, Catherine Paschal, Clemence Ansbert, Edwin R. Ndibalema, Dr. Daniel S. Madulu, Edwiga Renald, Faith Mpondo, Fina Lesafi, Geni Juma, Godiana H. Philipo, Hegespo H. Mwanyika, Paul Lucas, Plassidius J. Chengula, Rene Costa, Siri Abihudi, Stephano Hanolo, Tusekile Alfred, Wilson Mahene and many others. I wish to thank all the people whose assistance was a milestone in the three years' culmination.

I wish to acknowledge the support and great love of my family, especially my beloved wife Lidath, thank you for taking care of our beautiful daughters throughout this long commitment of your time, you are such a special person and I am so fortunate to call you my wife. My sincere appreciation goes to the family of Mr. Daisle Kileo and Mrs. Restituta Kamala, my father Mzee Deogratias Kikumi; my father-in-law, Mr. Dominick Kikumi, Rev. Fr. Respicius R. Kamala, Mr. Fortunatus Kikumi and all members of Kikumi family have been kind and supportive to me over the last several years.

Lastly, I would like to express my sincere appreciation to my employer, the University of Dar es Salaam, for granting me a study leave. I gratefully acknowledge the African Development Bank (AfDB) 's financial support, the United Republic of Tanzania through project number P-Z1-IA0-016 and grant number 2100155032816; I very much appreciate the support received from the International Centre for Theoretical Physics (ICTP) through the short-term visit scheme.

May God bless you far more abundantly than all you can ever ask or think (Ephesians 3:20).

DEDICATION

To my wonderful daughters

Lisa Kemilembe, Laureen Kaumbya and Linda Asiimwe

and

To my loving grandparents, the late Mzee Leonard Kamara Kikumi and Bi Paschazia Kokwihyukibwa Kikumi, to my mother, the late Bi Faustina and mother-in-law Bi Leonida

and

To my friends and mentors, the late

Prof. Egid B. Mubofu and Prof. Paul O'Brien.

TABLE OF CONTENTS

LIST OF TABLES

LIST OF FIGURES

LIST OF ABBREVIATIONS AND SYMBOLS

a-Si	Amorphous Silicon
B3LYP	Becke's Three Parameters Gradient-Corrected Exchange Potential and The Lee-Yang-Parr Gradient-Corrected Correlation Potential
BB	Bridging Bidentate
BE	Binding Energy
BT	Bridging Tridentate
BTZ	Benzothiadiazole
C.E	Counter Electrode
CA	Cyanoacrylic Acid
CAM-B3LYP	Coulomb-Attenuating Method Combined with B3LYP
CB	Conduction Band
CPCM	Conductor-Like Polarizable Continuum Model
c-Si	Crystalline Silicon
DFT	Density Functional Theory
DFT-D3	Dispersion-Corrected Density Functional Theory Calculations
DMF	Dimethylformamide
DSSCs	Dye-Sensitized Solar Cells
EA	Electron Affinity
EA_a	Adiabatic Electron Affinity
EA_v	Vertical Electron Affinity
ECP	Effective Core Potentials
EEP	Electron Extraction Potential
ESOP	Excited-state Oxidation Potential
FEDAM	Full-Electron Donor-Acceptor Map
FMOs	Frontier Molecular Orbitals
FTO	Fluorine-Doped Tin Oxide
GGA	Gradient-Correlated Approximation
GSOP	Ground State Oxidation Potential
HEP	Hole Extraction Potential
HOMO	Highest Occupied Molecular Orbital
ICT	Intramolecular Charge Transfer
IP	Ionization Potential

IP_a	Adiabatic Ionization Potential
IP_v	Vertical Ionization Potential
IR	Infra-Red
ITO	Indium-Doped Tin Oxide
LANL2DZ	Los Alamos National Laboratory 2 Double Zeta
LHE	Light-harvesting Efficiency
LUMO	Lowest Unoccupied Molecular Orbital
M	Monodentate
MMFF94	Merk Molecular Force Field
MOs	Molecular Orbitals
MPW1PW91	Modified Perdew–Wang Exchange and Perdew–Wang 91
PCE	Power Conversion Efficiencies
PV	Photovoltaic
TCO	Transparent Conductive Oxides
TD-DFT	Time-Dependent Density Functional Theory
THF	Tetrahydrofuran
TPA	Triphenylamine
U	Coulombic Repulsion
UV-Vis	Ultraviolet-Visible
XC	Exchange-Correlation

CHAPTER ONE

INTRODUCTION

1.1 Background of the Problem

It is undisputed that the high quality of life and modern civilization is dependent on the availability, acceptability, efficiency and affordability of energy (Pachauri, 2011; Ren & Sovacool, 2014; Tongsopit *et al*., 2016). Here, availability refers to geographical and geological existence of energy resources, adequacy of supply and lower risk of supply disruption (Narula, 2014). The acceptability is high if it provides reduced waste generation such as CO_2, SO_x, NO_x emissions (Narula, 2014). Affordability relates to the economic dimension that influences households and industries' energy prices (Ren & Sovacool, 2014; Tongsopit *et al*., 2016). Energy is considered to have a multiplier effect on education, water supply, health, transport, industry, agriculture and other tertiary sectors (Narula, 2014; Pachauri, 2011).

Ever-growing energy demand is among the most critical and most significant challenges facing the world today. With the continually growing population associated with improved living standards, more energy is required to cater to the need. For example, for many years, the world has noted a rapid depletion of fossil fuel reserves (Li *et al*., 2006; Pimental, 1976; Pimentel *et al*., 1994). However, in recent years, the Malthusian fear of running out of fossil fuels has largely been overtaken by environmental concerns imposed by fossil fuels include ambient air pollution, deforestation, soil, contamination of potable water, inhalation of polluted air, higher accident risks, reduced ecological health and fossil fuel induced climate change (Li *et al*., 2019; Narula, 2014; Wang *et al*., 2020; Wang *et al*., 2019; Ahmed *et al*., 2013; Solangi *et al*., 2011; Tsoutsos *et al*., 2005). Table 1 shows the current status of the discovered global fossil fuels reserves. It can be observed from Reserves to Production (R/P) ratios that the time available to depletion of fossil fuels is well below two centuries.

Table 1: Total global reserves for the fossil fuels worldwide by the end of 2018, data collected by British Petroleum (BP)

Fossil fuel	Reserves	R/P ratio (Years)
Crude Oil	1729.7 thousand million barrels	50.0
Natural gas	6951.8 trillion cubic feet	50.9
Coal	1.05 trillion tons	132

Fossil fuels cannot continue to dominate energy in a couple of decades to come for two reasons. Firstly, it is highly likely that most reserves will all have peaked by 2030. Secondly, due to greater emphasis to shift from the use of fossil fuels following environmental concerns as fossil fuels are responsible for an estimated 74% of all CO_2 emissions (Bashmakov *et al*., 2007; Moriarty & Honnery, 2012). More importantly, Ray's (2019) study shows that the levelized cost of energy for utility-scale PV plants is less than conventional fossil fuel generators in most countries. The recent levelized cost of energy analysis show that, the levelized cost of energy range for utility-scale PV is 32 to 44 USD per MWh while natural gas combined cycle plants range between 44 to 68 USD per MWh (Ray, 2019); that means a drastic decrease in prices for PV system components was observed from 394 to 44 USD for the ten year period (2009-2019).

Therefore, to meet the future global energy demand, renewable energy sources are considered the best alternative to fossil fuels. Renewable energy sources are those resources that can be used to produce energy, again and again, e.g., solar energy, biomass energy, wind energy, geothermal energy etc. and are also often called alternative sources of energy. Renewable energy sources present many advantages over conventional fossil fuels as most of them are not expected to deplete over time like natural resources and also do not evolve CO_2 or any solid and liquid waste products (Ahmed *et al*., 2013; Solangi *et al*., 2011; Tsoutsos *et al*., 2005).

1.1.1 Renewable Energy Sources

Over the past few decades, renewable energy sources have resulted in the flattening of the CO and CO_2 emission curves from 2014 to 2016 (Sinha & Shahbaz, 2018; Zheng *et al*., 2018). Thus, from the observed ecological and economic impact in section 1.1, the energy transition is inevitable to avoid the catastrophic effects posed by climate change and significantly reduce the cost to end-users by instituting cost-effective technologies. This is in line with the Intergovernmental Panel goals on the Climate Change report projecting net-zero greenhouse gas emissions by 2040 and 2055 (Davidson, 2019). Renewable sources of energy represent a viable alternative for satisfying the ever-increasing energy demand.

Compared to other renewables, solar possess irreplaceable merits of cleanness, demonstrating the great potential to fulfill global energy demands towards the realization of the future sustainable environment (Dhere, 2007; Hosseini & Wahid, 2020). While hydropower, wind

power and geothermal can be limited on geographical grounds, solar energy is the most available source on earth (Kumar *et al*., 2020). Approximately 30% of the solar energy that strikes the Earth's surface gets reflected and about 3.9×10^{24} MJ incident solar energy is received by Earth's surface annually, which is about ten thousand times more than current global energy consumption (Joshi *et al*., 2011). More interestingly, solar energy is clean, environmentally friendly and freely available. This provides the confidence that solar energy is capable of meeting the current and future global energy demands. Solar energy can be converted into electricity using photovoltaic (PV) technologies. In the past few years, PV technologies such as silicon solar cells, perovskite solar cells and dye-sensitized solar cells (DSSCs) present a high potential for down-scaled electricity cost rendering the technology competitive with other energy sources (Zhang *et al*., 2020).

1.1.2 Generations of Photovoltaic Solar Cells

Crystalline silicon (c-Si) solar cells found in the first generation of solar cells (Table 2) dominate the market and account for ~90% share of the photovoltaic energy due to their high power conversion efficiency (PCE) and long-term reliability exhibiting high efficiency among photovoltaic device landscape (Green *et al*., 2020). The best PCE of c-Si solar cells is about 25% and 22% on the lab and commercial scale, respectively (Green, 2015). The c-Si solar cells require 99.9999% purity for precursors in the fabrication; the purification process is often expensive and laborious (Marques *et al*., 2019). Also, p-n homojunction formed by a thermal doping process and softicated technology adds directly to the manufacturing plant capital cost and photovoltaic modules (Kavlak *et al*., 2018; Kim *et al*., 2020). Furthermore, there are underlying health issues associated with the manufacturing of c-Si, such as inhalation of hazardous fumes from dopant gases and vapours such as B_2H_6, $POCl_3$ and PH_3. For example, during the deposition in a chamber, toxic gasses P_2O_5 and Cl_2 can be generated from the liquid form of $POCl_3$. Other poisonous fumes can be encountered during reactor and wafer cleaning and the removal of dopant oxides when HNO_3, HF and NaOH are used (Fthenakis, 2018). The second generation, also known as thin-film solar cells, is constituted by copper zinc tin sulphide (CZTS), copper indium gallium diselenide (CIGS), cadmium telluride (CdTe), amorphous silicon (a-Si) and thin-film crystalline silicon (Table 2) they contain the photoactive material prepared using thin-film techniques. The second-generation utilizes only a few micrometers thick layers (thin-film) of semiconductor deposited on low-cost substrates such as flexible plastic, glass, stainless steel. Most solar cells in this

generation exhibit the highest PCE between 10% and 29% (Green *et al*., 2020; Jackson *et al*., 2015).

Table 2: The generations of solar cell technologies

1st Generation Silicon PV	2nd Generation Thin Film	3rd Generation Emerging PV
Monocrystalline (Mono c-Si) Polycrystalline (Poly c-Si),	Amorphous silicon (a-Si) Metal Chalcogenides (CdTe, CZTS, CIGS) Group III-V (GaInP, GaAs)	DSSCs, Quantum dots, Perovskite and Organic

Contrary to the first-generation solar cells, second-generation solar cells offer lower manufacturing cost, less material required and larger area deposition. However, poor charge transport is a major limiting factor for these solar cells, which inhibits the commercialization and results in the investigation of third-generation PV technologies.

1.1.3 Dye-Sensitized Solar Cells

The third-generation includes dye-sensitized solar cells (DSSCs), concentrating photovoltaic technology, organic solar cells and novel and emerging solar cell concepts. The sensitized solar cells have achieved tremendous consideration over the traditional silicon-based PV technology owing to their non-toxic nature, low manufacturing cost and the higher theoretical limit of PCE (Graetzel *et al*., 2012; Khan & Kim, 2019; Marziano *et al*., 2017; Tamang *et al*., 2016; Wang *et al*., 2016).

Inspired by nature, DSSCs mimic charge separation processes that take place in the plant during photosynthesis. Owing to their economic feasibility and unique features such as straightforward synthesis routes of material (Zhang *et al*., 2018), light-weight, high flexibility (Yugis *et al*., 2015), relatively high efficiency, environmental friendliness as well as excellent performance even under diverse lighting conditions, DSSCs are considered as potential alternatives to the traditional inorganic and silicon solar cells (Hug *et al*., 2014; James & Contractor, 2018). The competitive characteristics make them the ideal choice for both indoor and outdoor applications.

Since the seminal work by O'Regan and Grätzel (1991), the world has noted a progressive increase in the efficiency of DSSCs. The highest registered light-to-electric energy conversion efficiency of DSSCs is ~15% under standard AM 1.5 irradiation (Kakiage *et al*., 2015; Upadhyaya *et al*., 2013). However, DSSCs suffer from several limitations including,

electrolyte leakage under extreme weather conditions, low PCE, degradation of materials, expensive materials such as rhodium, ruthenium; all these together limits the large-scale industrial application of DSSCs.

Suitability, versatile materials and performance under mild conditions are among the advantages of DSSCs; these factors make DSSCs cost-effective compared to earlier PV devices. The main components of DSSCs include a substrate (conductive substrate or film-coated substrate), semiconductor nanostructure/photoanode (usually TiO_2, ZnO, et cetera), electrolytes and dye as photosensitizer and catalyst coated counter electrode. Dye molecules are chemically bound to the TiO_2 surface, for the effective operation of DSSCs requires that sensitizer fulfill a few criteria:

(i) The extended-spectrum in UV and near infra-red (NIR) regions is of interest to provide a good overlap with solar emission spectrum for high photocurrent response.

(ii) The extinction coefficient or the dye's oscillator strength should be high over the whole absorption spectrum to absorb most of the light.

(iii) The dye's excited-state lifetime must be long enough for efficient charge injection into the conduction band (CB) of a semiconductor with a low possibility of charge recombination.

(iv) The sensitizers of interest must demonstrate suitable energy level alignment with the CB of a semiconductor (−4.05 eV for TiO_2) (Fujisawa *et al*., 2017) and the redox potential of I^-/I_3^- electrolyte (−4.8 eV) (Zhang *et al*., 2009). Experiences have shown that for efficient charge injection into the CB and subsequent dye regeneration, the difference between the excited-state potential (ESOP) of the dye and semiconductor CB (that is, the free energy of charge injection ΔG_{inj}) should be at least ~0.2 eV (by magnitude), while the difference between the ground state oxidation potential (GSOP) of the dye and electrolyte redox couple (free energy of dye regeneration ΔG_{reg}) should be at least, ~0.4 eV (Pastore *et al*., 2010; Wei *et al*., 2016; Zanjanchi & Beheshtian, 2019).

(v) Dyes must possess an anchoring group to improve the chemical bonding when bound to a semiconductor surface; the anchoring group is also used as a bridge for electron injection.

(vi) The sensitizer should be soluble in some solvents for adsorption on the electrode.

(vii) The photosensitizer should demonstrate chemical, electrochemical and thermal stability under long illumination times in the electrolyte media.

1.1.4 Working Principle of Dye-Sensitized Solar Cells

Contrary to the 1st and 2nd generations, DSSC configuration combines two phases (solid and liquid), the function of light absorption is separated from charge carrier transport. While for Si-based solar cells, charge separation relies on the built-in electrical field, in DSSCs, current is generated when a photon absorbed by a dye molecule gives rise to electron injection into the conduction band of the semiconductor (Hsu *et al*., 2004; Matsushita *et al*., 2017).

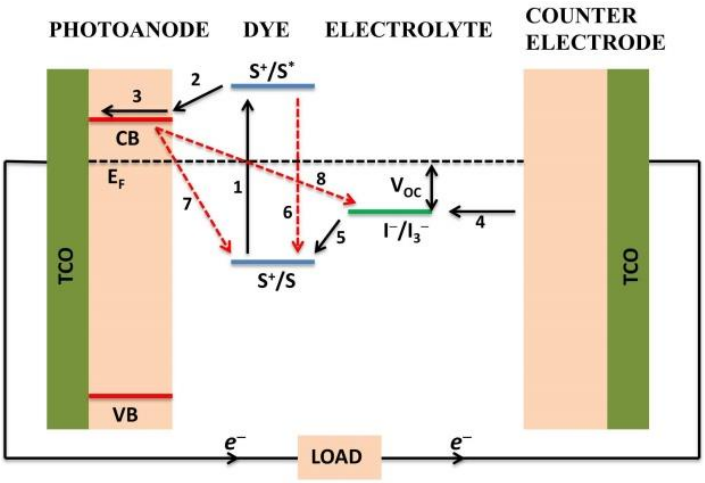

Figure 1: Schematic diagram of the charge transfer mechanism and energy level alignment

Further advances rely entirely on continued investigations on the DSSC's components such as two glass substrates of transparent conductive oxides (TCO) layer of fluorine-doped tin oxide (FTO) or indium-doped tin oxide (ITO), a mesoporous semiconductor metal-oxide layer (for example, TiO_2), a monolayer of dye molecules, an electrolyte containing a redox couple of iodide/tri-iodide electrolyte and a platinum counter electrode (Grätzel, 2003; Shakeel *et al*., 2017). Generally, operation of a DSSC involves four key steps: (a) the sensitizers are adsorbed on the semiconductor photoanode for light absorption; (b) the electrons in the excited-state are injected into the conduction band (CB) of the semiconductors; (c) the injected electron travels through the CB to the external circuit to produce electric current. The electron travels through the external wire and is collected by the transparent conductive substrate of a counter electrode; (d) the redox system is regenerated through the counter electrode.

Therefore, proper energy level alignment is required for efficient charge transfer in DSSCs. For example, it is needed that the energy level of the lowest unoccupied molecular orbital (LUMO) of the dye must be more positive than the CB of TiO_2. In contrast, the highest occupied molecular orbital (HOMO) energy must be more negative than the electrolyte's redox potential (Liu *et al*., 2019b). The highlight of the electron transfer mechanism and the energy level alignment for DSSCs is shown in Fig. 1. The mechanism can be explained in eight steps: (1) Photoexcitation, (2) Electron injection, (3) charge travel through CB to external circuit, (4) Reduction of the redox mediator, (5) Dye regeneration and (6-8) Recombination (Kumar *et al*., 2020; Omar *et al*., 2020; Yan *et al*., 2020).

The continuous transfer of electrons in the system described in Table 3 creates energy harvested through DSSCs. The PCE of DSSCs is dependent on the four energy levels in the components: the HOMO in the ground state and LUMO of the excited-state of the dye, the chemical potential of the mesoporous semiconducting electrode and the redox potential of the electrolyte (Mahadevi & Sumathi, 2020). Efforts have been devoted to exploring new materials to increase solar PCE of DSSCs (Bourass *et al*., 2016; Guo *et al*., 2016). Furthermore, introducing the concepts of nature-inspired fractal-based design techniques is critical in ensuring that the high-efficiency DSSC transforms from small-scale laboratory levels to sizeable industrial production.

A sensitizer is the crucial component of DSSC; if carefully selected, it can play a vital role in achieving durability and high PCE (Han *et al*., 2014). Investigation and synthesis of metal-organic dyes such as ruthenium and zinc complexes have enabled a rapid increase in solar cell efficiencies (Chaitanya *et al*., 2014; Chen *et al*., 2006; Huang *et al*., 2010; Xie *et al*., 2015). It is well established that sensitizer's stability is dependent on the anchoring group (Perini *et al*., 2013; Murakami *et al*., 2014). Generally, carboxylic acid-based anchoring groups such as cyanoacrylic acid have been commonly used in DSSCs due to good injection efficiency and excellent electron coupling between dyes and semiconductors.

However, under long illumination times in the presence of water or at elevated temperature, carboxylic groups may dissociate from the semiconductor's surface resulting in reduced sensitizer loading, consequently leading to low PCE (Jia *et al*., 2019). Other drawbacks associated with organic sensitizers include narrow and blue-shifted absorption bands that reduce light-harvesting capabilities (Lee *et al*., 2011). Furthermore, poor sensitizer adsorption, aggregation and faster electron recombination result in reduced PCE of the cells.

Therefore, studies on various components of DSSCs need to be undertaken, for example modification of internal structures of the dyes cause broad coverage of the UV-Visible spectrum up to near infra-red regions, thereby increasing the quantity of captured photons.

Table 3: The detailed charge transfer mechanism in the dye-sensitized solar cells operating principle

1.	Photoexcitation	The sensitizers absorb sunlight and generate excitons, after absorption of ($h\nu$), the sensitizer (dye) changes from ground state (S) to the excited-state (S^*). During this stage, the transition of an electron from HOMO to LUMO occurs through the process: $S + h\nu \rightarrow S^*$. The number of photons absorbed dictates the PCE. Note that electrons are injected from the LUMO level into the CB of the photoanode and the holes are injected from the HOMO level into the redox electrolyte.
2.	Electron injection	The photo-generated electrons from the dyes are injected rapidly into the CB of the SC leaving the dye in an oxidized state, S^+ through the reaction: $S^* \rightarrow S^+ + e^-$(injected).
3.	Energy generation	Subsequently, the injected electrons diffuse to the FTO layer as the main driving force for charge transport in the mesoporous TiO_2 film then travel through the external circuit and arrive at the cathode counter electrode C.E. e^-(injected) + C.E $\rightarrow$ e^-(C.E) + electrical energy.
4.	Reduction of the redox mediator	The I_3^- in the electrolyte receives an electron and become reduced to I^- at the C.E. The regenerative circle is: $I_3^- + 2\cdot e^-$(C.E) $\rightarrow 3\cdot I^-$(C.E).
5.	Dye regeneration	The oxidized dye, S^+ is brought to the ground state, S by receiving an electron from I^-. The expression here describes the regenerative circle: $S^+ + \frac{3}{2}\cdot I^- \rightarrow S + \frac{1}{2}\cdot I_3^-$.
6.	Recombination	Direct recombination of the excited dye that is reflected by the excited-state-lifetime.
7.	Recombination	The next recombination process is the injection of electrons in the TiO_2 with oxidized dyes: $S^+ + e^-(TiO_2) \rightarrow 3\cdot I^-$(anode)
8.	Recombination	In this stage, the recombination of injected electrons in the TiO_2 with acceptors in the electrolyte: $I_3^- + 2\cdot e^-(TiO_2)$

Moreover, stability of the dye when bound to the semiconductor is also a major challenge in DSSCs, different approaches such as the use anchoring group of different morphology lead to enhanced stability. If well investigated, both modification of the internal units (π-spacers) and anchoring groups may result into appropriate energy level matching and improved stability. In this dissertation, molecular diversification is thought in order to address the observed

shortcomings, design and investigation of novel sensitizers by introducing π-spacers and anchoring groups have been carried out.

1.2 Statement of the Problem

In the last two decades, DSSCs have gained widespread attention due to their advantageous characteristics such as production costs, ease of fabrication process and tunable optical properties. To date, efficiency for DSSC has reached 17% under standard AM 1.5 irradiation (Cui *et al*., 2020; Cui *et al*., 2019). Despite the recorded efficiency (Cui *et al*., 2020; Cui *et al*., 2019), challenges such as narrow absorption range, low absorption intensity, low stability on the semiconductor, poor charge injection and dye regeneration processes, photo-degradation and recombination continue to hinder commercialization of DSSC devices. Nevertheless, there is growing appreciation that materials modification is likely to boost DSSCs efficiencies. Thus, many studies are inspired by existing challenges; considerable efforts are underway to improve stability and increase the power conversion efficiency.

Sensitizers have been reported through several studies by incrementally changing existing sensitizers' structures or testing hundreds of compounds and the expensive synthesis of new ones in the laboratory; these practical means are often costly and time-consuming. Thus, this indicates an urgent need to understand the properties of the materials under investigation at a molecular level before embarking on experiments. This will eventually lead to the invention of materials with desirable properties.

Therefore, in this work, attention is paid to triphenylamine (TPA) dye constituents studying both electronic and optical dyes properties as they are essential in the fabrication of DSSCs. Through quantum chemical methods, molecular modification of TPA-based dyes has been carried out by grafting anchoring groups and π-spacers to enhance the photo-electronic and charge transfer properties of materials under consideration.

1.3 Rationale of the Study

Renewable energy, specifically solar power, presents a considerable potential to replace environmentally problematic sources of energy. Successful and efficient harvesting of solar energy entirely relies on solar cells. The advantages of DSSCs outweigh those of conventional tools such as Si-solar cells, thus successful design and fabrication of DSSCs with higher power conversion.

1.4 Research Objectives

1.4.1 General Objective

To perform molecular modification of dye constituents by grafting highly conjugated units and anchoring groups towards the improvement of sensitizing properties in dye-sensitized solar cells.

1.4.2 Specific Objectives

(i) To determine the geometrical structure and vibrational frequencies of designed materials using quantum computational methods.

(ii) To determine the effects of an extended conjugated system and anchoring groups on optical and electronic properties of designed dyes.

(iii) To assess the influence of heterocyclic anchoring groups against cyanoacrylic anchoring group on the optoelectronic properties.

(iv) To compare the influence of heteroatom-doped π-linkers and anchoring group morphology on the optoelectronic properties.

(v) To assess the binding stability of the designed materials on TiO_2 semiconductor using $(TiO_2)_6$ cluster and TiO_2 anatase 101 slab.

1.5 Research Questions

(i) Are the calculated geometrical parameters and vibrational frequencies corresponding to equilibrium geometries?

(ii) What is the best combination of π-linker and anchoring group that exhibit excellent optoelectronic properties?

(iii) The heterocyclic anchoring groups demonstrate better optoelectronic properties compared to dyes featuring cyanoacrylic acid anchoring group?

(iv) What is the effect of heteroatom-doping in the π-linkers on optoelectronic properties?

(v) Which among the designed sensitizer demonstrate strong binding energy when attached to TiO_2 semiconductor?

1.6 Significance of the Study

Many works have been carried out in DSSCs by investigation of various components of the device. The DSSCs' PCE improvement has been growing at a slow pace; this is associated with the low level of understanding of chemical processes such as electron transfer within the material itself and the semiconductor at the molecular level.

Therefore, this study will help screen out compounds with desirable properties to be considered potential materials for DSSCs application before the practical experiments are undertaken to ensure that devices are obtained at reasonable prices. High prices of solar modules often arise from experiments that are based on trial and error technique during the identification of potential materials. The findings reported here will reduce unfriendly emissions such as CO_2 resulting from other conventional sources of energy such as coal. Also, the study will significantly reduce the risk of exposure to poisonous materials such as ruthenium as it offers environmentally friendly material. Finally, DSSCs will enable electrification at a low cost as the materials and methods involved are cheap and the synthesis routes involved are simple compared to their counterparts.

1.7 Delineation of the Study

To enhance the materials' optical and electronic characteristics, the research was carried out using computational approaches; modifications were made to methoxy substituted triphenylamine dyes. Two key parts of the D-π-A architecture model were considered (π-spacer and anchoring group). In addition to improving power conversion efficiency, the designed and investigated materials aim to scale down the solar cells' costs by considering organic sensitizers. In this research, the benchmark material shows $\sim 5 - 8\%$ power conversion efficiencies. The reported findings are based on computational approaches the designed materials demonstrating characteristics of interest are proposed for further experimental investigations. Therefore, it is anticipated that higher power conversion efficiencies will be demonstrated among the built novel materials compared to benchmark materials.

CHAPTER TWO

LITERATURE REVIEW

2.1 The Dye-Sensitized Solar Cells History

The first panchromatic film able to render the image of a scene realistically into black and white followed the work of Vofel in 1873, demonstrated that silver halide alone could not show any response towards the visible light (Narayan, 2012). The idea was further proved by Moser in 1887. However, the voltage produced was too low to be used as a photovoltaic device about 0.04 V. Hishiki and Gerischer in 1965 and 1968 respectively were able to improve Moser's DSSC by showing that zinc oxide can be supersensitive by applying concentrated single or two cyanine and bengal dyes solution (Gerischer *et al*., 1968; Namba & Hishiki, 1965). A subsequent study was conducted by introducing rhodamine B dyes on the ZnO system (Daltrozzo & Tributsch, 1975). The replacement of ZnO with TiO_2 by Spitler and Calvin in 1977 produced important results which showed the relationship between current density and the two factors of the dye, i.e., the amount adsorbed on the TiO_2 surface and the pH of the solution used in dye adsorption processes (Spitler & Calvin, 1977).

However, the use of DSSCs in photovoltaic remained rather unsuccessful until the first discovery of a simple device capable of converting sunlight into electricity aided by regenerative photochemical processes in 1991 by Michael Grätzel and Brian O'Regan, where nanostructured electrodes which assisted efficient charge injection were developed with the efficiency of 7%. This was a turning point and significant to motivate the search for similar materials with improved properties (Souza *et al*., 2018; Kavan & Grätzel, 1989; O'Regan & Grätzel, 1991; Rho *et al*., 2018; Wan *et al*., 2018).

A number of metal-based complexes, porphyrins, phthalocyanines have been considered in DSSCs applications. Ruthenium-containing dyes have so far demonstrated excellent photovoltaic performance over other metal-based complexes (Hagfeldt *et al*., 2010). However, elevated production cost and high levels of toxicity hamper their production and application at a large scale (Juhász *et al*., 2018).

2.2 Triphenylamine Based Dyes

Triphenylamine (TPA) has been widely used as an excellent donor unit; they are extensively used in DSSCs as functional materials (Agarwala & Kabra, 2017; Mahmood, 2016). Presence

of propeller-shaped triphenyl groups prevents aggregation by inducing non-planarity. Furthermore, TPA is known for its electron-donating solid ability and hole-transport properties (Mahmood, 2016).

Owing to the diversity of molecular design, it has been demonstrated that systematic modification of sensitizers by introducing donor units (D), internal molecular units known as π-linker/π-spacer (π) and anchoring groups (A) can help to improve the optical, electronic and chemical reactivity parameters, eventually resulting in high photovoltaic performance (Ellis *et al*., 2013; Ferdowsi *et al*., 2018; Mahmood, 2016). The anchoring group determines the bonding degree between the sensitizer and the semiconductor surface. It plays a crucial role in electron-transfer processes and absorption, while π-spacers are highly conjugated units that facilitate intramolecular charge transfer (ICT).

Different molecular architectures such as D-π-A, D-D-π-A, D-A-π-A and D-π-π-A, et cetera, are often thought consisting of donor groups and π-spacers: coumarin, phenothiazine (Chen *et al*., 2016), benzene, thiophene (Luo *et al*., 2016), furan (Lin *et al*., 2009), triphenylamine (Liang *et al*., 2007), carbazole (Venkateswararao *et al*., 2014), et cetera, have been widely investigated. Thus, TPA donor derivatives have found applications in DSSCs and other organic electronic applications. They demonstrated sufficient fluorescence within the visible and near infra-red regions; it is also possible to carry out facile functionalization onto these donors groups. Furthermore, it is possible to improve intermolecular charge transfer, fluorescence, charge injection and dye regeneration characteristics of the material through systematic incorporation of π-spacers and anchoring groups into main structures, the design of a longer π-conjugated sensitizer molecule results in a broader coverage of the absorption region (Han *et al*., 2014). However, dyes with extended π-conjugated units suffer from low stability under irradiation of high energy photons and allow easy formation of unfavourable π-stacks (Han *et al*., 2014; Lee *et al*., 2015; Marinado *et al*., 2010; Wu *et al*., 2012).

Benzothiadiazole (BTZ) and thiophene are extensively investigated π-linkers as they lead to a stabilised molecular conformation, enhanced favourable π-π-stacking and formation of intramolecular and intermolecular links. In addition to the BTZ in the D-π-A, other π-linkers can be added in order to improve ICT. For example, auxiliary π-linkers such as furan, pyrrole, thiophene, selenophene and tellurophene can be inserted to obtain D-π-π-A molecular architecture for tuning dye's spectral properties.

Velusamy and co-workers (2005) investigated the effect on the variation of heteroatom by replacing sulfur of BTZ with selenium in a D-π-BTZ-π-A in the thiophene linked compounds (D3 and D4) and to the phenylene linked derivatives (D1 and D2) (see Table 4). The introduced a BTZ unit into the conjugated backbone resulted in the absorption band's shift to the near-IR. The intensity of absorption for Se-containing dye was less compared to S-containing dye. However, both dyes exhibited comparable efficiency (Velusamy *et al*., 2005).

Table 4: The maximum wavelength, open-circuit voltage, short-circuits current density, fill factor and efficiency for triphenylamine-based materials upon the modification

Dye	λ_{max}, nm	V_{OC}, mV	J_{SC}, mA cm^{-2}	FF	η, %
D1	491	546	10.44	0.66	3.77
D2	502	524	8.35	0.67	2.97
D3	541	517	3.21	0.69	1.15
D4	544	474	3.57	0.66	1.11
D5	514	775	11.88	0.75	6.88
D6	523	744	14.32	0.72	7.67
D7	506	794	12.08	0.75	7.17
D8	522	769	13.84	0.683	7.27
D9	525	755	12.84	0.737	7.15
D10	549	720	14.57	0.740	7.77
D11	516	693	14.49	0.702	7.05
D12	530	720	15.20	0.733	8.02

Furthermore, the D3 was studied in both isolated and TiO_2 complex forms in different solvents. For the isolated dye, λ_{max} of 361 nm was measured in THF solution at room temperature while a red-shift was observed for the complex (518 nm) measured in acetonitrile with 0.1 M $TBAPF_6$ (Lee *et al*., 2011). Upon modifying D3 by introducing the alkoxy group to the para direction, red-shift in the electronic spectra was observed with increased efficiency to 7.30% from 3.81%.

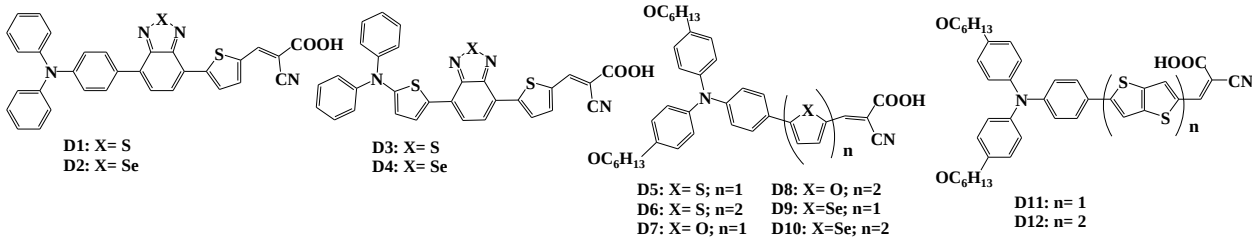

Figure 2: The sensitizers containing sulfur and selenium heteroatoms in the π-linkers and multiple units of π-linkers

The π-conjugated linkers (thiophene, bithiophene, furan, bifuran, selenophene and biselenophene) embedded in the framework of D-π-A with dihexyloxy-substituted TPA donor and the cyanoacrylic acid acceptor (D5 − D10) were reported by Li *et al*. (2009) the influence of heteroatoms on photocurrents and photovoltages investigated through quantum chemical calculations. The electronegativity effect for the selenophene series results in more evident absorptivity and red-shifted electronic spectra. For the first time, Li *et al*. (2009) demonstrated that furan and selenophene could be employed as building blocks of sensitizers in stable DSSCs.

Increasing the dye's conjugated backbone improves the fundamental characteristics of interest such as planarity, which results in the improvement of intramolecular charge transfer of the resulting dyes (Sun *et al*., 2020; Yao *et al*., 2016). For example, to enhance the LHE and other optical and electronic properties of D11 (Xu *et al*., 2008), a second thienothiophene was fussed into D11 to obtain bisthienothiophene containing dye D12 (Zhang *et al*., 2009). Both dyes contain dihexyloxy-substituted on the terminal phenyl rings of TPA with cyanoacrylic acid as an anchoring group. The efficiency for D12 was found to be higher by ~0.97% compared to D11 under AM 1.5 irradiation 100 mW cm^2. Additionally, the authors reported the efficiency after one-week aging; the cell showed excellent stability by keeping 92% of its initial efficiency. Thienothiophene units are known for their influence in stabilizing molecular structures and thus have been used in the engineering of the low energy gap polymers wide applications (Lee & Sotzing, 2001; Neef *et al*., 1999; Sotzing & Lee, 2002).

Significance differences in the PCE and photoelectronic properties for the dyes tuned through variation of the π-conjugated linkers were noted for the dyes composed of a triazatruxene donor and a cyanoacrylic acid acceptor group using D-π-A framework (Qian *et al*., 2013). The π-linkers thiophene, furan and benzene were used, resulting in 6.1, 5.5 and 5.1 PCE (in %), respectively. The studied dyes' electronic properties were carried out using THF solvent; each dye exhibited two major absorption bands at 280 − 350 and 400 − 550 nm.

The ligand containing Zn(II) coordinated networks with pyridyl and carboxylate furan, thiophene and selenophene were synthesized at elevated temperatures in DMF solvent (Hua & D'Alessandro, 2017). Thiophene and selenophene-containing dyes demonstrated similar linear bond angles, unlike furan, which showed bent resulting in unpredictable topologies and structures. Therefore, the dyes containing furan, thiophene and selenophene highlighted the critical role of the linearity within the ligand. Furthermore, it was revealed that the

replacement of sulfur by other heteroatoms in the five-membered ring with furan, selenophene or thienothiophene would greatly influence the photovoltaic performance parameters (Wang *et al*., 2015).

In DSSC, a sensitizer directly interacts with a mesoporous oxide layer made of nanometre-sized particles (usually TiO_2) through anchoring group. Also, it cannot be excluded that both internal architectural design and anchoring group may impact the overall performance of the cell (Chen *et al*., 2006; Sundin & Abrahamsson, 2018). It is required that anchoring groups are electrically conducting, hydrolytically stable and oxidation-resistant over pH variations (Materna *et al*., 2017). Among many anchoring groups, carboxylic (COOH) and phosphonic acids ($P(O)(OH)_2$) emerge as commonly used in DSSCs (Galoppini, 2004; Materna *et al*., 2017). However, the widely used anchoring group still suffers from several drawbacks: limited stability in aqueous environments, photodegradation during device operation and dissociation on semiconductor's surface.

Diverse anchoring groups such as benzoic acid, tropolone, rhodanine, 2 - (3 –oxo-2, 3 – dihydroinden – 1 - ylidene) - malononitrile, 8 - carboxylquinoline and 8 - hydroxyquinoline have been investigated. It was been demonstrated that, variation of achoring groups can result in the improvement of PCE. For example, in the study by Guo and co-workers (2016) reported the increase in efficiency from 4.90% to 7.66% for cyanoacrylic acid and hydantoin anchoring groups, respectively. However, the investigation on heterocyclic units as anchoring groups remains insufficient, including the underlying influences on dye's absorption response, the free energy of charge injection and dye regeneration and interface electron transfer properties on the semiconductor surface. In this regard, investigation for different anchoring groups with excellent binding ability to the semiconductor is essential to replace conventional carboxylic acid-based anchoring groups. A limited number of experimental and theoretical studies exist on the heterocyclic units as anchoring groups in DSSCs (Feng *et al*., 2019; Guo *et al*., 2016; Zhang *et al*., 2018). The currently limited investigations manifest that heterocyclic units are alternatives to carboxylic acid-based anchoring roups.

2.3 Theoretical Framework

A general electronic structure problem and the numerical solution through Density Functional Theory (DFT) and Time-Dependent Density Functional Theory (TD-DFT) are considered in this work. The open challenges in materials science today are the understanding and

prediction of the properties and the route to synthesize materials of target properties. Computation chemistry/physics is used for the prediction of the properties/characteristics of molecules and solids. The high level of accuracy in predicting various phenomena resulted in the popularity of computational methods in different research disciplines ranging from energy, health, waste and environmental pollution (Andreoni & Yip, 2020). In many scenarios, multiscale materials modeling is brought in due to its ability to interrelate the descriptions of a system at various length scales ranging from the atomic/molecular level (such as the description of electronic structure) to the microscopic scale $\rightarrow$ mesoscopic scale $\rightarrow$ macroscopic scales (Andreoni & Yip, 2020). The coupling between theory and experiment is expected to result in cost-effective investigations and thus the community can benefit from the materials innovation. This dissertation involves the formulation of hypothesis and testing through simulation and then obtained materials that exhibit desirable properties can further be subjected to physical experiments.

2.4 Overview on Quantum Chemistry

The revelation of exciting phenomena such as energy quantization and wave-particle duality of light occurred in the early 19th century. Since then, many significant contributions have been witnessed in quantum mechanics' evolution and Erwin Schrödinger made the most famous contribution in 1926. Schrödinger proposed that a physical system is described entirely by a wave function Ψ. Generally, no physical property can be drawn directly from Ψ, the product between Ψ and its complex conjugate Ψ^* ($\Psi^*\Psi = |\Psi|^2$) represents a probability density. The probability of finding a particle described by Ψ in a volume element $d\mathbf{r}$ is given by:

$$p(\mathbf{r}) = |\Psi(\mathbf{r})|^2 d\mathbf{r}$$

By taking into account the normalization criterion, the probability of finding a particle within the region must be equal to a unit:

$$\int |\Psi|^2 d\tau = \langle \Psi | \Psi \rangle = 1$$

where $d\tau$ represents the integration over the entire space and the wave function can be obtained by solving the as the time-independent Schrödinger equation:

$$\hat{H}\Psi(\mathbf{r}, \mathbf{R}) = i\hbar\partial_t \Psi(\mathbf{r}, \mathbf{R})$$

where $\hat{H}$ is the Hamiltonian or energy operator and contains expressions for kinetic and potential energy, the expectation value of a measurable quantity given by $\hat{A}$ (for example, the angular momentum) calculated as:

$$\langle A \rangle = \frac{\int \Psi^* \hat{A} \Psi d\tau}{\int \Psi^* \Psi d\tau} = \frac{\langle \Psi | \hat{A} | \Psi \rangle}{\langle \Psi | \Psi \rangle}$$

For interacting chemical systems, the solution Schrödinger equation cannot be found through analytical methods. The many-body Hamiltonian describing a system of *N* electrons and *M* nuclei is defined as:

$$\hat{H} = -\sum_{i=1}^{N} \frac{1}{2} \nabla_i^2 - \sum_{A=1}^{M} \frac{1}{2m_{\mathrm{A}}} \nabla_{\mathrm{A}}^2 - \sum_{i=1}^{N} \sum_{A=1}^{M} \frac{Z_{\mathrm{A}}}{r_{i\mathrm{A}}} + \sum_{i=1}^{N} \sum_{j>i}^{N} \frac{1}{r_{ij}} + \sum_{\mathrm{A}=1}^{M} \sum_{\mathrm{B}>1}^{M} \frac{Z_{\mathrm{A}} Z_{\mathrm{B}}}{R_{\mathrm{AB}}}$$

where **r** and ***R*,** *m* and *Z* denote the electrons and nuclei intermolecular distances, mass and nuclear charge, respectively, ($r_{ij} = |r_i - r_j|$), all values in atomic units. The first and second terms represent the kinetic energy of the electrons and nuclei, respectively, while the third term represents the Coulomb attraction between electrons and nuclei, the fourth and fifth terms are the electron-electron Coulomb attraction and nuclei-electron Coulomb of repulsion, respectively.

The time evolution of the interacting electrons and nuclei are described through the time-dependent Schrödinger equation:

$$\hat{H} \Psi(\mathbf{r}, \mathbf{R}, t) = i\hbar \partial_t \Psi(\mathbf{r}, \mathbf{R}, t)$$

where the electron-nuclear wavefunction $\Psi(\mathbf{r}, \mathbf{R}, t)$ describes the state of the system over time and $\hbar$ is the reduced Planck's constant.

2.4.1 The Born-Oppenheimer Approximation

The Born-Oppenheimer approximation is the basic concept underlying the description of the quantum states of molecules. The Born-Oppenheimer (BO) approximation states that since electrons move with several orders of magnitude faster than the heavier nuclei. Using the BO approximation, it is possible to separate the motion of the nuclei and electrons. Due to its simplicity and high level of accuracy, BO is routinely applied. By applying the Born-Oppenheimer approximation, the kinetic energy term in the Hamiltonian equation disappears and the Coulombic repulsion between the nuclei become reduced to a constant $V_{N\,N}$ and is added to the electronic energy. The purely electronic Hamiltonian equation can be written as:

$$\widehat{H} = -\sum_{i=1}^{N}\frac{1}{2}\nabla_i^2 - \sum_{i=1}^{N}\sum_{A=1}^{M}\frac{Z_{\mathrm{A}}}{r_{i\mathrm{A}}} + \sum_{i=1}^{N}\sum_{j>i}^{N}\frac{1}{r_{ij}}$$

With this approximation, the nuclei can be considered moving on a potential energy surface (PES). Therefore, only the electronic Schrödinger equation can be solved to give the electronic wavefunction. The electronic Schrödinger equation can be written as:

$$\widehat{H}_{\mathrm{el}}\Psi_{\mathrm{el}}(\mathbf{r};\mathbf{R}) = E_{\mathrm{el}}\Psi_{\mathrm{el}}(\mathbf{r};\mathbf{R})$$

The solutions to the electronic Schrödinger equation can be approximated by constructing wavefunctions. For example, Slater determinants of one-electron wavefunctions, which is the foundation of the so-called wavefunction methods such as Hartree-Fock (HF), configuration interaction and coupled-cluster are commonly used. The latter is a very accurate method; however, it is computationally expensive.

2.4.2 Density Functional Theory

Density Functional Theory (DFT) is a model that is based on the quantum mechanical treatment of material and focuses mainly on electron density instead of the many-body wave function to reduce the computational difficulty. Although formally exact, all known DFT protocols need to be fed with some empirical expressions, meaning they are not strictly *ab initio* methods although sometimes referred to as such. Density Functional Theory is used to solve molecular structures and vibrational frequencies, relative energies and thermochemistry, electric properties, magnetic properties, hydrogen bonds and weakly bound systems and chemical reactivity, to mention a few. Density Functional Theory has a wide gain range of applications and attracted researchers' attention in several fields to solve quantum chemical problems. As the real electronic wavefunction is a function of 3N variables, this requires high memory to solve the problem. Thus, it would be highly advantageous to describe the system instead of using the electronic density $\rho(\mathbf{r})$; the function of only three variables. Theoretically, this is possible by using DFT due to the Hohenberg-Kohn theorem.

(i) Hohenberg-Kohn Theorem

The first Hohenberg-Kohn theorem states that, “There is a unique external potential (determined up a purely time-dependent function) that reproduces the given electron density”.

Thus the Hamiltonian and hence all ground-state properties, are determined solely by the electron density.

In many-body Hamiltonian fixes the ground state of the system under consideration, it determines the groundstate many-body wavefunction Ψ and thus the above theorem ensures that this itself is also a unique functional of the groundstate density. Consequently, the kinetic and electron-electron interaction energies will also be functionals of $\rho(\mathbf{r})$.

$E = E[\rho], \qquad \Psi = \Psi[\rho]$

and thus the energy is a functional of ρ such that $E_0 = E\left[\rho_0(\mathbf{r})\right]$ and therefore $E[\rho(\mathbf{r})] = \left\langle \Psi[\rho(\mathbf{r})] \middle| \widehat{H} \middle| \Psi[\rho(\mathbf{r})] \right\rangle$

The Born-Oppenheimer approximation results into:

$$E_{\text{el}}[\rho] = \int \rho(\mathbf{r}) V_{eN} d\mathbf{r} + F_{HK}[\rho]$$

Where $F_{HK}[\rho] = T[\rho] + V_{ee}[\rho]$ is a universal functional in the sense that it has the same dependence on the electron density for any system, independent of the external potential concerned; it is known as the Hohenberg-Kohn functional. While T and V_{ee} are the kinetic energy and electron-electron interaction operator, respectively.

The second Hohenberg-Kohn theorem is the DFT analogue to the variational principle. This theorem states that: For any trial density ρ' in an external potential V_{ext}, so that any density found to yield lower energy is a better approximation of the groundstate electron density.

$$E[\rho'] = \int \rho'(\mathbf{r})\, V_{\text{ext}} d\mathbf{r} + T[\rho'] + V_{\text{ext}}[\rho'] \geq E_0$$

The second theorem is valid only for the ground state; it assumes the use of exact functionals. Taken together with the first theorem, it ensures that if the exact functionals are used, the true wavefunction can be found in a variational sense. The problem is that the functional form of F_{HK}, albeit system-independent and universally valid, is unknown.

(ii) Kohn-Sham Theory

To simplify the task of finding the universal functional, Kohn and Sham (1965) suggested introducing a fictitious system with non-interacting electrons but with the same electronic density as the real system. Due to the non-interacting electrons, this reference system can be described using one-electron so-called Kohn-Sham (KS) orbitals.

$$\widehat{H}_{\mathrm{R}}\psi_i(\mathbf{r}) = \varepsilon_i\psi_i(\mathbf{r})$$

The non-interacting Hamiltonian can be defined as:

$$\widehat{H}_{\mathrm{R}} = -\frac{1}{2}\nabla^2 + \nu_{\mathrm{R}}(\mathbf{r})$$

The reference potential $\nu_{\mathrm{R}}(\mathbf{r})$, ensures that the system has the same density as the real system, such that:

$$\rho(\mathbf{r}) = \sum_{i=1}^{N}\left|\psi_i(\mathbf{r})\right|^2$$

Following the introduction of orbitals, the kinetic energy of the electrons in the reference system is well-defined, the energy of the reference system can be written as:

$$E_{\mathrm{R}}[\rho] = \underbrace{-\frac{1}{2}\sum_{i=1}^{N}\left\langle\psi_i\middle|\nabla^2\middle|\psi_i\right\rangle}_{\mathrm{T_s}[\rho]} + \int \nu_{\mathrm{R}}(\mathbf{r})\rho(\mathbf{r})d\mathbf{r}$$

By using the kinetic energy and approximate, the electron-electron interaction with the simple Coulombic repulsion (or Hartree term) for as a first approximation of the reference system, the resulting expression for the energy of the real system can be written as:

$$E[\rho] = \mathrm{T_s}[\rho] + \frac{1}{2}\iint\frac{\rho(\mathbf{r})\rho(\mathbf{r}')}{|\mathbf{r}-\mathbf{r}'|}d\mathbf{r}d\mathbf{r}' + \int \nu_{\mathrm{ion}}(\mathbf{r})\rho(\mathbf{r})d\mathbf{r} + E_{\mathrm{xc}}$$

where the exchange-correlation functional, $E_{\mathrm{xc}}[\rho]$, is defined as the error in approximating the energy with the reference kinetic energy and Hartree term, the $E_{\mathrm{xc}}[\rho]$ can be expressed as:

$$E_{\mathrm{xc}}[\rho] = T_{\mathrm{e}}[\rho] - T_{\mathrm{s}}[\rho] + U_{\mathrm{ee}}[\rho] - \frac{1}{2}\iint\frac{\rho(\mathbf{r})\rho(\mathbf{r}')}{|\mathbf{r}-\mathbf{r}'|}d\mathbf{r}d\mathbf{r}'$$

It follows, from the expressions of the energy of the real systems and the reference, the reference potential defining the reference system is given by:

$$\nu_{\mathrm{R}}(\mathbf{r}) = \underbrace{\int\frac{\rho(\mathbf{r})}{|\mathbf{r}-\mathbf{r}'|}d\mathbf{r}'}_{\nu_{\mathrm{H}}(\mathbf{r})} + \nu_{\mathrm{ion}}(\mathbf{r}) + \underbrace{\frac{\partial E_{\mathrm{xc}}[\rho]}{\partial\rho}}_{\nu_{\mathrm{xc}}(\mathbf{r})}$$

As it can be observed, the reference potential is dependent on the density and the Kohn-Sham equations must be solved in a self-consistent manner from an initial guess of $\rho(\mathbf{r})$.

CHAPTER THREE

MATERIALS AND METHODS

3.1 The Investigated Sensitizers

In this study, the proposed sensitizers were designed based on TPA by introducing π-linkers, anchoring groups and heteroatoms. Figure 3 presents the molecular structures obtained through variation of π-linkers while Fig. 4 and Fig. 5 show the geometries obtained through variation of heterocyclic anchoring groups and heteroamtoms, respectively.

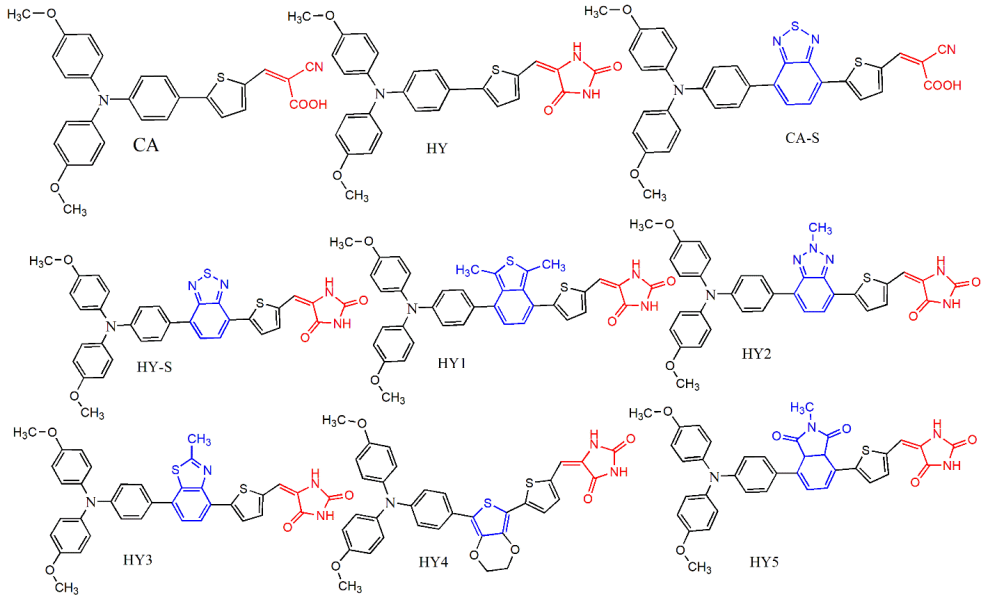

Figure 3: Molecular structures of dyes under consideration, the CA and HY have no internal linkers while the rest contain varied internal linkers

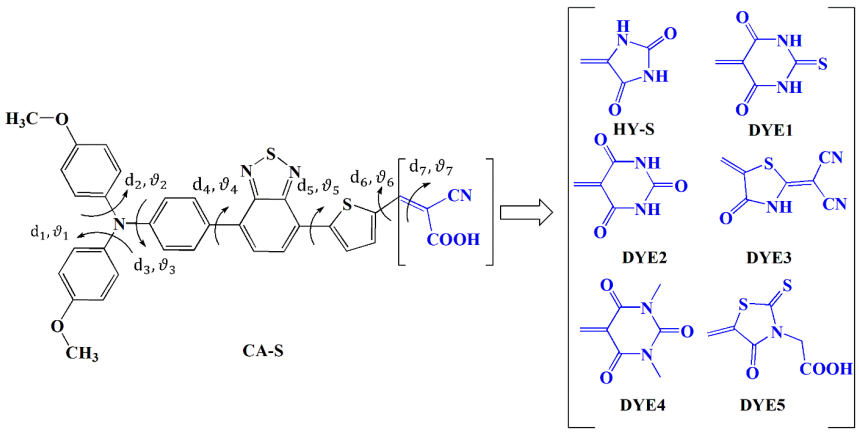

Figure 4: Molecular structures of dyes featuring cyanoacrylic and heterocyclic anchoring groups. The structural difference between the sensitizers is on the anchoring units

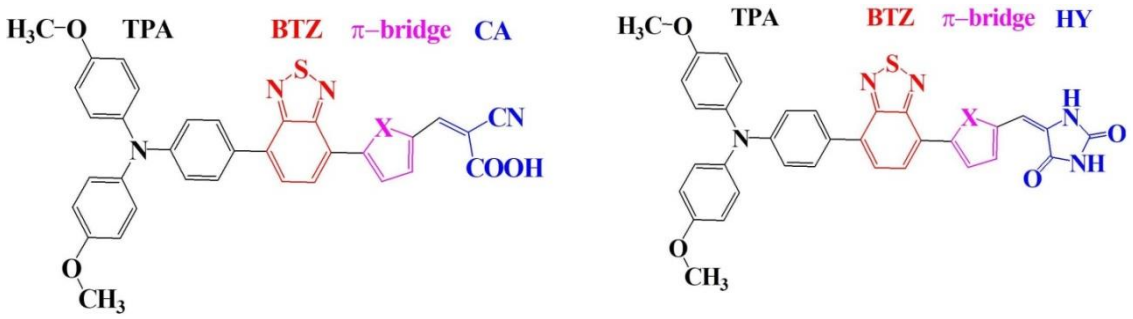

Figure 5: A brief structure of D-π-π-A architecture design for triphenylamine derivatives CA-X (left) and HY-X (right), the heteroatoms X include O, NH, S, Se and Te

3.2 Computational Details

3.2.1 Computation of Geometry and Electronic Properties of Dye Molecules

The 3-D molecular structures were generated using the Avogadro software package (Hanwell *et al*., 2012). The Merk molecular force field (MMFF94) and Universal force field (UFF) available within the code were applied to minimize conformational energies for the designed models. Next, the coordinates for energy minimized geometries were extracted for building input files for DFT computations. The DFT and time-dependent DFT (TD-DFT) frameworks were used to study the designed molecules' characteristics. Full geometry optimization performed using DFT according to Becke's three parameters gradient-corrected exchange potential and the Lee-Yang-Parr gradient-corrected correlation potential (B3LYP) the hybrid functional (Becke, 1996) using 6-31G(d,p) and 6-31+G(d,p) basis sets. The convergence of a geometry search is reached when the largest component of the gradient is less than optimization tolerance (1×10^{-4}) and the root mean square gradient less than 1/3 of optimization tolerance. Vibrational frequency calculations were performed at the same level of theory as for optimization. The absence of imaginary verified that obtained geometries through optimization correspond to minima on the potential energy surface. All calculations were carried out for chloroform ($CHCl_3$) solvent; the solvent's choice is based on polarity. Since the designed dyes are nonpolar molecules, they are expected to dissolve in less polar solvent such as chloroform (Gvishi *et al*., 1993). Furthermore, the photophysical properties for benchmark dyes (CA-S and HY-S) were measured using UV-Vis absorption in $CHCl_3$ (Guo *et al*., 2016). The calculations were performed using Firefly software (Granovsky, 2013) formally known as GAMESS-US (Schmidt *et al*., 1993) and Orca (Neese, 2008;

Neese, 2018) and Gaussian (Frisch *et al*., 2009). The visualization of the frequency calculations' output files for the analysis of the vibrational modes was carried out using the graphical software for visualization of quantum chemistry computations Chemcraft (Zhurko & Zhurko, 2015).

3.2.2 Validation of the Functional and Basis Set for Electronic Spectra Computations

To select the suitable theoretical approach for the simulation of electronic spectra, several functionals and basis sets were examined and available experimental data on maximum absorption wavelengths λ_{max}^{abs} for the CA-S and HY-S dyes (Guo *et al*., 2016) used as the benchmarks. Firstly, different DFT XC functionals, namely: B3LYP (Becke, 1993), CAM-B3LYP (Yanai *et al*., 2004), ωB97XD (Chai & Head-Gordon, 2008), PBEPBE (PBE0) (Perdew *et al*., 1996), MPW1PW91 (Adamo & Barone, 1998) and HSEH1PB (Heyd & Scuseria, 2004), were employed with the 6-31G+(d) basis set. Secondly, the best XC functionals were applied with different basis sets to the control dyes. The percentage deviations between the computed and the experimental data for every combination of basis set and functional are depicted in Fig. 6a.

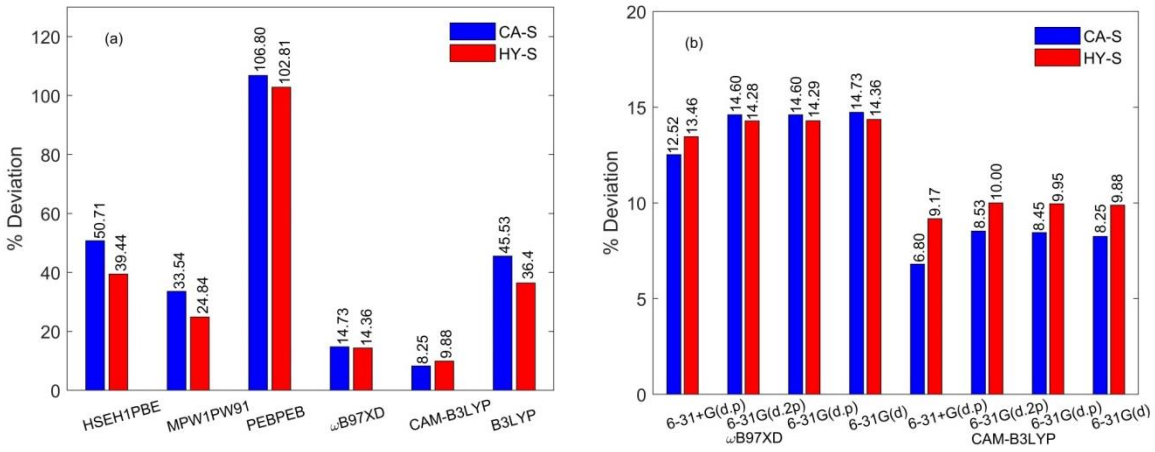

Figure 6: The comparison in the percentage deviation between the calculated and experimental maximum wavelengths for CA-S and HY-S for chloroform solvent. Simulation is done using the CPCM model (a) with the variation of functionals using 6-31G(d) basis set and (b) with variation in basis sets using both ωB97XD and CAM-B3LYP functionals

Among the six functionals, the ωB97XD and CAM-B3LYP showed a lower deviation from the experimental data: 14 − 15% (ωB97XD) and 8 − 10% (CAM-B3LYP). These two functionals were used further with four basis sets: 6-31G(d), 6-31G(d,p), 6-31G(d,2p) and 6-31G+(d,p). It can be observed from Fig. 6b, the lowest deviations 7 − 9% correspond to the

6-31G+(d,p) basis set coupled with CAM-B3LYP functional. One can assume that this theoretical approach should result in similar accuracy of the computed wavelengths for other dyes under consideration. Worth emphasizing that the DFT functional selection appeared to be a crucial step in the electronic spectra simulation. The wrong choice might result in the overestimation of maximum wavelengths with uncertainties as high as 100% (Fig. 6a). In contrast, the basis sets' variation did not significantly impact the calculated λ_{max} (Fig. 6b). Therefore, the UV-Vis absorption and fluorescent emission spectra of all dye molecules under study were simulated using the hybrid exchange-correlation functional CAM-B3LYP and 6-31G(d,p)/6-31G+(d,p) and for atoms, C, N, O, S and H; for heavy atoms Se and Te, the LANL2DZ basis sets with effective core potentials (ECP) (Hay & Wadt, 1985) were used. Only the lowest ten singlet-singlet transitions with nonzero oscillator strengths ($f > 10^{-4}$) were computed.

3.2.3 Calculation of Chemical Descriptors and Charge Transfer Characteristics

Moreover, the anionic and cationic states of the designed dyes were calculated to evaluate the ionization potentials (IPs) and electron affinities (EAs). Values were obtained by performing single point energy calculations, in which for the ions, the geometries were accepted the same as optimized for neutral molecules in the ground electronic state. The minimum energies at the potential energy surface were taken as reference. Subsequently, the electron was added or removed from the system; next, the open-shell calculations were performed. The EA or IP is taken as the difference between reference energy and open-shell energies when the electron has been added or removed, respectively. According to the relationship developed in the Parr's model (Parr *et al*., 1999), the electronic chemical potential (μ), chemical hardness (η), electrophilicity index (ω) were calculated as expressed by Cerón-Carrasco *et al*. (2014) and Zanjanchi & Beheshtian (2019):

$$\mu = -\frac{1}{2}(\mathrm{IP} + \mathrm{EA}),\ \eta = \frac{1}{2}(\mathrm{IP} - \mathrm{EA}), \omega = \mu^2/\eta, \omega^+ \approx \frac{(\mathrm{IP}+3\mathrm{EA})^2}{16(\mathrm{IP}-\mathrm{EA})}, \omega^- \approx \frac{(3\mathrm{IP}+\mathrm{EA})^2}{16(\mathrm{IP}-\mathrm{EA})}$$

The calculation of reorganization was performed by considering the adiabatic ionization potential (IP_a) and electron affinity (EA_a) (Siddiqui, 2019; Tripathi & Chetti, 2020; Tripathi & Prabhakar, 2018): $\mathrm{IP_a} = E_+^+ - E_0^0$, and $\mathrm{EA_a} = E_0^0 - E_-^-$, where E_0^0 represents the energy of the neutral molecule in the ground state, E_+^+ and E_-^- are the energies of the cationic and anionic states at the optimized geometries of the respective cation and anion. Also, the vertical ionization potential (IP_v) and electron affinity (EA_v) can be expressed as: $\mathrm{IP_v} = E_0^+ - E_0^0$ *and* $\mathrm{EA_v} = E_0^0 - E_0^-$, where E_0^+ and E_0^- are the energies of cationic and anionic states at

the optimized geometry of the neutral molecule. Further hole extraction potential (HEP) and electron extraction potential (EEP) can be estimated through the expressions: $\mathrm{HEP} = \mathrm{E}_{+}^{+} - \mathrm{E}_{+}^{0}$ and $\mathrm{EEP} = \mathrm{E}_{-}^{0} - \mathrm{E}_{-}^{-}$, where E_{+}^{0} and E_{-}^{0} are the energies of the neutral molecule with the geometries of the cation and anion, respectively (Fahim *et al*., 2018; Zhang *et al*., 2020).

Among the electrochemical parameters that can be optimized to achieve higher photoelectric conversion includes the free energy of charge injection (ΔG_{inj}) from the dye excited-state to the semiconductor conduction band (CB) and free energy of dye regeneration (ΔG_{reg}) (Liu *et al*., 2019a). The values of ΔG_{inj} and ΔG_{reg} can be estimated as: $\Delta G_{\mathrm{inj}} = E_{\mathrm{CB}}^{\mathrm{TiO_2}} - E_{\mathrm{ox}}^{\mathrm{dye*}}$, where the $E_{\mathrm{CB}}^{\mathrm{TiO_2}} = -4.05$ eV is the CB of TiO_2. Referring to Koopman's theorem, the $E_{\mathrm{OX}}^{\mathrm{dye*}}$is extracted from the ground state oxidation potential (GSOP) $E_{\mathrm{OX}}^{\mathrm{dye}}$ and the electronic energy associated with photo-induced ICT ΔE (the first transition energy corresponding to λ_{max}), note that, $E_{\mathrm{OX}}^{\mathrm{dye}} = E_{\mathrm{HOMO}}$, then $E_{\mathrm{OX}}^{\mathrm{dye*}}$ is obtained as $E_{\mathrm{OX}}^{\mathrm{dye*}} = E_{\mathrm{OX}}^{\mathrm{dye}} + \Delta E$. However, this technique is only applicable if the entropy change during light absorption is neglected (Lee *et al*., 2015) and in this work, it is assumed the same. Dye regeneration ability is calculated through the expression: $\Delta G_{\mathrm{reg}} = E_{\mathrm{I^-/I_3^-}} - E_{\mathrm{OX}}^{\mathrm{dye}}$, where, $E_{\mathrm{I^-/I_3^-}}$ is the redox potential of $\mathrm{I^-/I_3^-}$ in solvent (Fujisawa *et al*., 2017; Li *et al*., 2017; Liu *et al*., 2019a), the iodide/tri-iodide redox potential −4.8 eV (Preat *et al*., 2011).

3.2.4 Simulation of Dye Adsorption to the TiO_2

The adsorption of dyes featuring heterocyclic anchoring groups on the TiO_2 surface was considered using the two models (slab and cluster), the binding energies were evaluated. For the slab model, the geometry optimization of the dye-TiO_2 systems was performed with the projector augmented plane-waves, using the generalized gradient-correlated approximation (GGA) and the Perdew-Burke-Ernzerhof (PBE) exchange-correlation functional (Perdew *et al*., 1996). Anatase and rutile are two different forms of TiO_2. In the anatase polymorph of TiO_2, each oxygen atom is nearly bonded to two Ti atoms (Arkan & Izadyar, 2018). Anatase form is one of the most proper polymorphs of TiO_2, which is used in DSSCs (Pastore & De Angelis, 2013). The TiO_2 anatase 101 was constructed as the most stable surface. The 4 × 8 supercells was used for calculations; the energy cutoff was set to 400 eV. To include the van der Waals interactions, the DFT-D3 model (Grimme *et al*., 2011) was employed. The onsite Coulombic repulsion (U) of Ti 3d electrons was taken into account using PBE+U. A number

of reports investigated the effect of different computational approaches and their influence on the optoelectronic properties of dye@TiO_2 systems (Deskins & Dupuis, 2007; Roy *et al*., 2018; Jedidi *et al*., 2010; Arroyo-de Dompablo *et al*., 2011). Regarding Coulombic repulsion potential U, it was found that U values 3.5-10 eV produced band gaps in reasonable agreement with the experiment. The U = 8.5 eV was selected for Ti atoms in earlier works by Saranya *et al*. (2018) and Liu *et al*. (2014). Accordingly, the same value was chosen in our study. The Monkhorst-Pack mesh of 1 × 1 × 1 for free sensitizer and 4 × 4 × 1 for the dye-TiO_2 systems were chosen (Monkhorst & Pack, 1976). The adsorption calculations were carried out using The Vienna Ab initio Simulation Package (VASP) (Kresse & Furthmüller, 1996; Kresse & Hafner, 1993). The adsorption energy of adsorption systems was calculated according to the equation:

$$E_{\mathrm{ads}} = E_{\mathrm{dye@(TiO_2)_{slab}}} - \left(E_{\mathrm{dye}} + E_{\mathrm{(TiO_2)_{slab}}}\right)$$

In the second model of the dye – TiO_2 attachment, the anatase TiO_2, the cluster $(TiO_2)_6$ was adopted as optimal by size in balancing the computational cost and reliability of the results (Syzgantseva *et al*., 2011). As it was proved earlier, the hydrogenated TiO_2 clusters exhibit higher stability than corresponding naked clusters. The geometries of the investigated dyes in their complexation forms with hydrogenated $(TiO_2)_6$ cluster were fully optimized without any structural constraints; vibrational frequencies were calculated to confirm that the geometries correspond to minima the potential energy surfaces. The binding energies between the dyes and the TiO_2 cluster were calculated using the following equation:

$$\mathrm{BE} = E_{\mathrm{dye@(TiO_2)_6}} - E_{\mathrm{dye}} - E_{\mathrm{(TiO_2)_6}},$$

where $E_{\mathrm{dye@TiO_2}}$ is the energy of the optimized complex dye@TiO_2, E_{dye} and $E_{\mathrm{TiO_2}}$ are the energy of dye and TiO_2 cluster, respectively. The energy of the hydrogen atom detached from the dye during complexation was taken into account in calculations. The DFT computations were performed using the Gaussian 09 (Frisch *et al*., 2009), Orca (Neese, 2018) software packages. The conductor-like polarizable continuum model (CPCM) (Cossi & Barone, 2001) was considered to account for solvent effect and dyes simulated for chloroform for ten lowest singlet-singlet transitions.

CHAPTER FOUR

RESULTS AND DISCUSSION

4.1 General Introduction

It is demonstrated that through fine-tuning of the molecules in a particular arrangement of the building units, it is possible to modulate their optoelectronic properties and thermal stability. This section presents the results and discussion obtained from the modification of triphenylamine-based dyes where the effects of π-bridge/π-linkers and acceptor groups have been studied. The sensitizers that demonstrate sufficient optoelectronic properties upon incorporating π-linkers and anchoring groups within the D-π_1-π_2-A framework have been recognized as potential candidates for high PCE DSSCs.

4.2 Effects of the π-linkers

In this section, the geometrical, optical, electronic and chemical reactivity parameters of nine organic dyes displayed in Fig. 3 with IUPAC names given in Table 5 have been reported.

Table 5: The International Union of Pure and Applied Chemistry names of the dyes

CA	(E)-3-(5-(4-(bis(4-methoxyphenyl)amino)phenyl)thiophen-2-yl)-2-cyanoacrylic acid
HY	(E)–5-((5-(4-(bis(4-methoxyphenyl)amino)phenyl)thiophen-2 yl) methylene)imidazolidine -2,4-dione
CA-S	(Z)-3-(5-(4-(4-(bis(4-methoxyphenyl)amino)phenyl)benzo[c][1,2,5]thiadiazol-7-yl) thiophene-2-yl)-2-cyanoacrylic acid
HY-S	(E)-5-((5-(4-(4-(bis(4-methoxyphenyl)amino)phenyl)benzo[c][1,2,5]thiadiazol-7-yl) thiophen-2-yl) methylene) imidazolidine-2,4-dione
HY1	(E)-5-((5-(4-(4-(bis(4-methoxyphenyl)amino)phenyl)-1,3-dimethylbenzo[c]thiophen-7-yl) thiophen-2-yl) methylene) imidazolidine-2,4-dione
HY2	(E)-5-((5-(4-(4-(bis(4-methoxyphenyl)amino)phenyl)-2-methyl-2H benzo[d] [1,2,3] triazol-7-yl) thiophen-2-yl)methylene) imidazolidine-2,4-dione
HY3	(E)-5-((5-(7-(4-(bis(4-methoxyphenyl)amino)phenyl)-2-methylbenzo[d]thiazol-4-yl) thiophen-2-yl) methylene)I midazolidine-2-4-dione
HY4	(E)-5-((5-(5-(4-(bis(4-methoxyphenyl)amino)phenyl)-2,3-dihyrothieno[3,4-b][1,4] dioxin-7-yl) thiophen-2-yl) methylene) imidazolidine-2,4-dione
HY5	4-(4-(bis(4-methoxyphenyl)amino)phenyl)-2-methyl-7-(5-((E)-(2,5-dioxoimidazolidin-4-ylidene)methyl)thiophen-2-yl)-2H-isoindole-1,3(3aH,7aH)-dione

Evaluation of geometrical parameters, electronic spectra, highest occupied molecular orbitals (HOMO), lowest unoccupied molecular orbitals (LUMO) and adjacent molecular orbitals (MOs) provided insights on the effects of varied π-spacers and anchoring groups.

4.2.1 Geometrical Properties

It is anticipated that dyes with different geometrical structures may exhibit differences in optical and electronic properties. Some of the selected important geometrical parameters i.e., bond lengths (d, Å) and dihedral angles (ϑ, °) as indicated in Fig. 7 of the investigated dyes, have been reported in Table 6. The structural parameters were found to be dependent on inserted π-spacers. Variation in non-planarity due to triphenyl groups is observed from unmodified dyes (HY and CA) to modified dyes. It was observed that the propeller-shaped of the triphenyl groups induce steric hindrances where the two-terminal phenyl groups are twisted from the plane of the third phenyl ring inducing the non-planarity. The non-planarity is expected to reduce the chances of dye aggregation when anchored to the semiconductor's surface. While CA-S and HY-S remained with comparable distances d_4(C-C) and d_5(C-C), larger values were noted for HY1, HY3 and HY5 dyes.

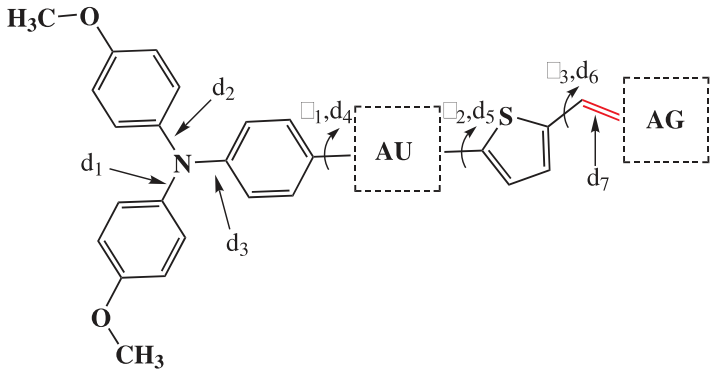

Figure 7: A two-dimensional structure of a dye with π-conjugated system showing bond distances and torsional angles; AU stands for acceptor unit (π-spacer) and AG for anchoring group

The presence of branched methyl groups, methoxy groups and asymmetric effect (HY3) on the respective π-spacers may be accounted for the observed variations. The atoms separated by distances d_1(C-N), d_2(C-N), d_3(C-N) and d_6(C-C) are remote from the AU and these distances remain very close to those in unmodified molecules.

Additionally, essential dihedral angles were analyzed. Significantly smaller dihedral angles were noted for HY-S, HY2 and HY4 for ϑ_1 and $\vartheta_{2,}$ which show that corresponding (-spacer enhances the planarity for these dyes that facilitate charge transfer from donor part to the anchoring group and enhance close packing. Larger dihedral angles are considered a drawback; the property that hinders ICT and such dyes is predicted to exhibit undesirable blue-shift in their electronic spectra.

Table 6: Bond distances (Å) and dihedral angles (°) of the studied dyes for chloroform solvent

Dye	d_1	d_2	d_3	d_4	d_5	d_6	d_7	ϑ_1	ϑ_2	ϑ_3
CA	1.430	1.430	1.400	1.455	−	1.422	1.382	−	−	178.3
HY	1.427	1.427	1.407	1.460	−	1.435	1.361	−	−	179.6
CA-S	1.428	1.428	1.403	1.470	1.456	1.431	1.378	−30.2	1.9	−1.2
HY-S	1.426	1.427	1.407	1.473	1.456	1.436	1.361	31.2	−6.1	−0.4
HY1	1.427	1.426	1.410	1.487	1.475	1.436	1.353	61.1	−66.3	−180.0
HY2	1.426	1.427	1.408	1.473	1.455	1.433	1.354	24.9	−5.2	179.2
HY3	1.427	1.426	1.410	1.480	1.462	1.436	1.361	−41.9	3.5	0.3
HY4	1.425	1.425	1.411	1.458	1.437	1.433	1.362	−4.9	−0.9	0.4
HY5	1.428	1.428	1.406	1.478	1.468	1.436	1.353	44.7	−27.1	−171.8

4.2.2 Ground State Electronic Structures

The effective operation of DSSCs requires that sensitizers possess proper HOMO, LUMO energy levels. Through systematic tuning of optical and electronic properties of dyes, it is possible to achieve desirable properties for the dyes for maximum power conversion efficiency of DSSCs. The HOMO, LUMO energies and energy gaps E_g for the investigated dyes are summarized in Table 7 and energy levels alignment diagram is shown in Fig. 8.

Table 7: The highest occupied molecular orbital energies, lowest unoccupied molecular orbital energies and energy gaps, all values in eV

Dye	$-E_{HOMO}$	$-E_{LUMO}$	E_g
CA	6.11	1.58	4.53
HY	5.94	1.09	4.85
CA-S	6.05	2.04	4.01
HY-S	5.95	1.71	4.24
HY1	5.97	1.03	4.94
HY2	5.91	1.39	4.53
HY3	5.99	1.22	4.77
HY4	5.76	1.27	4.49
HY5	6.08	1.35	4.73

It is noted that the variation of π-conjugated unit significantly affects HOMO and LUMO energies of the studied dyes. Results show that all dyes considered under this study possess

E_{LUMO} above conduction band energy (E_{CB}) of the semiconductor (−4.05 eV) (Fujisawa *et al.*, 2017). Upon insertion of π-spacers, HOMOs for HY2 and HY4 were predominantly lifted up and LUMOs for all dyes shifted towards E_{CB} with the exception of HY1 with reference to hydantoin (Fig. 8). The lowest and highest E_{LUMO} correspond to CA-S and HY1, respectively. Also, E_{HOMO} levels for all designed dyes of I^-/I_3^- (−4.80 eV) (Zhang *et al.*, 2009).

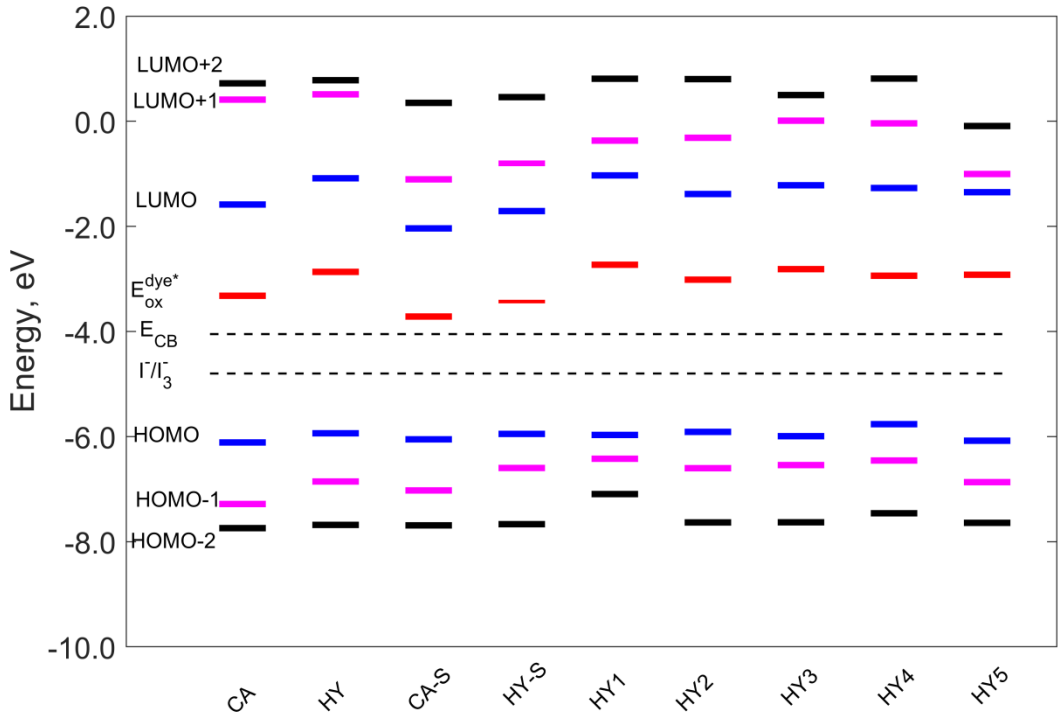

Figure 8: Molecular orbitals energy level diagram of dyes calculated for chloroform solvent

The modified dyes are characterized by the variation of the HOMO-LUMO separation (Table 7). The observed decrease in energy gap in the order HY1 > HY3 > HY5 > HY2 > HY4 > HY-S > CA-S is expected to favour charge transfer from the donor part to the anchoring group through the π-conjugated path. The effect on energy gaps extend beyond the impact of π-spacers introduced, the contribution of anchoring groups on the HOMO, LUMO energy levels is noted, for example, even though CA-S and HY-S have similar π-spacers, the energy gaps of dyes are reduced by 0.51 eV and 0.61 eV when compared to CA and HY, respectively. Unusual features are noted for HY1, which has even higher energy gap than that of unmodified dye; one can suppose that observed unexpected behaviour is due to the presence of methyl branched groups which result in the steric hindrance within the molecule.

Analysis of electron densities distribution over different parts dyes is performed and presented in Fig. 9, HOMOs for the dyes are mostly delocalized over the triphenylamine

group and partially to π-spacers except for HY5 where HOMO is localized on the triphenylamine. Upon excitation of electrons to the LUMOs, electron densities are predominantly contained on the hydantoin and CA groups extending to the adjacent π-spacer, an indication that these charges could be easily transferred to the metal oxide surface. This distribution is vital to facilitate the charge transfer from the dye molecule to the semiconductor surface and reduces the chance of charge recombination. Among the nine dyes investigated, HY-S, HY2, HY4 and CA-S demonstrate suitable charge transfer characteristics when compared to other dyes.

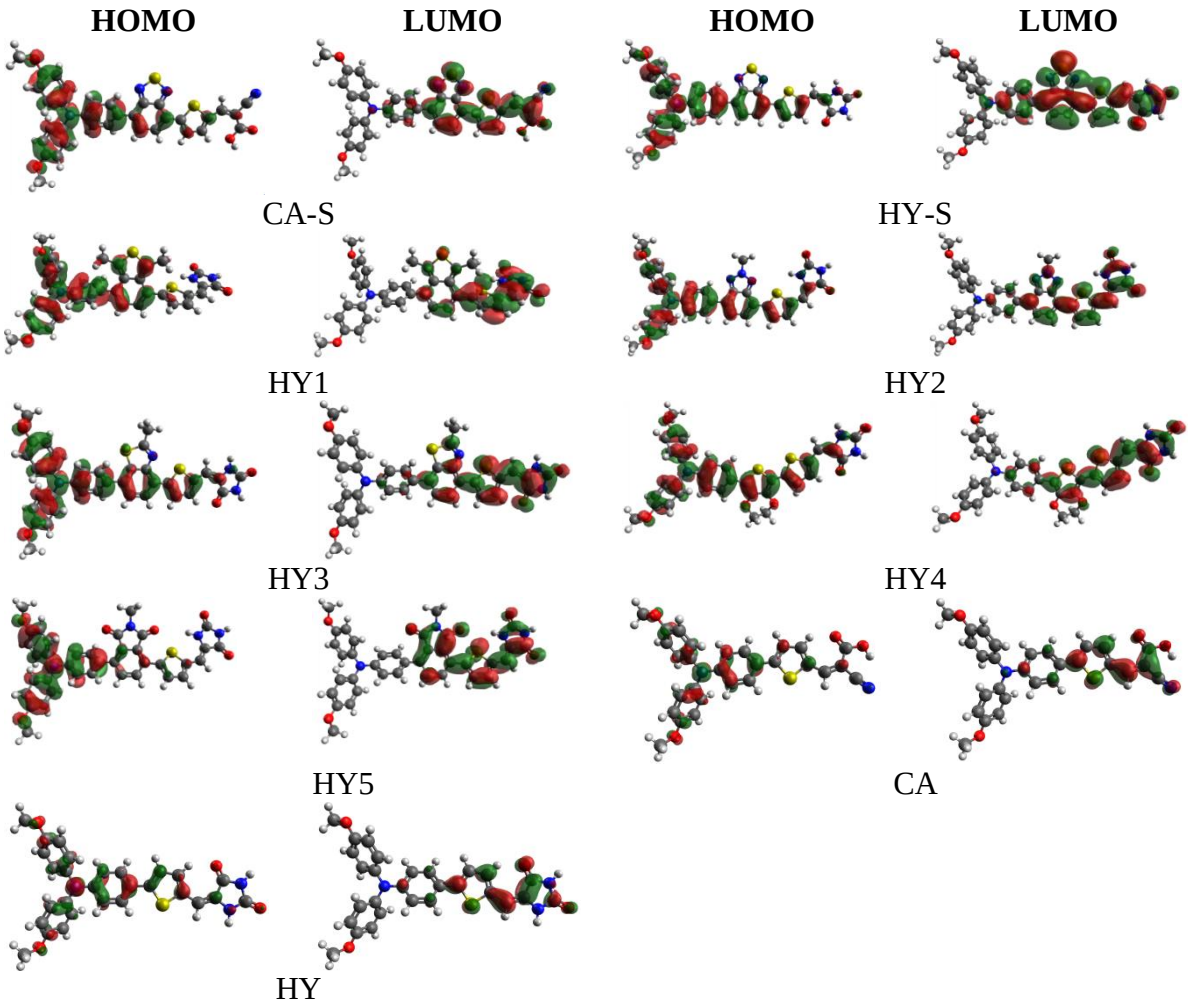

Figure 9: Frontier molecular orbitals for designed dyes

4.2.3 UV-Vis Spectra and Electronic Transitions

In order to gain insight into the excited-state properties, TD-DFT calculations were performed for the ten lowest spin-allowed singlet-singlet transitions. Also, to take into account the solvent effect, chloroform was used for solvent phase calculation. The results on electronic transitions, excitation energies, wavelengths and percentage contributions are

summarized in Table 8 and electronic spectra for unmodified and modified dyes displayed in Fig. 10(a) and (b), respectively. The light-harvesting efficiency (LHE) values at a particular wavelength are calculated through equation LHE = $1-10^{-f}$.

Table 8: Electronic transitions, excitation energies (eV), wavelengths (nm), oscillator strengths and transition assignments, calculated for the designed dyes

Dye	Transition	ΔE	λ	f	Configuration
CA	$S_0 \rightarrow S_1$	2.79	444	1.578	H → L (86%)
	$S_0 \rightarrow S_2$	3.97	313	0.298	H-1 → L (83%)
HY	$S_0 \rightarrow S_1$	3.07	404	1.709	H → L (80%)
	$S_0 \rightarrow S_2$	4.04	307	0.096	H-1 → L (79%)
CA-S	$S_0 \rightarrow S_1$	2.34	531	1.351	H → L (79%); H-1 → L (12%)
	$S_0 \rightarrow S_2$	3.28	378	0.378	H-1 → L (79%); H → L (11%)
	$S_0 \rightarrow S_3$	3.35	370	0.255	H → L+1 (63%); H-1 → L+1 (26%)
	$S_0 \rightarrow S_4$	4.04	307	0.316	H-1 → L+1 (41%); H → L+1 (%)
HY-S	$S_0 \rightarrow S_1$	2.49	498	1.409	H → L (79%); H-1 → L (13%)
	$S_0 \rightarrow S_2$	3.13	396	0.147	H-1 → L (80%); H → L (12%)
	$S_0 \rightarrow S_3$	3.54	350	0.602	H → L+1 (51%); H-1 → L+1 (39%)
HY1	$S_0 \rightarrow S_1$	3.24	383	1.050	H → L (40%); H-1 → L (36%); H → L+1 (12%)
	$S_0 \rightarrow S_4$	4.12	301	0.623	H-2 → L (84%)
HY2	$S_0 \rightarrow S_1$	2.90	428	1.995	H → L (72%); H-1 → L (17%)
	$S_0 \rightarrow S_5$	4.59	270	0.240	H → L+3 (36%); H-1 → L+1 (16%); H-6 → L (14%)
	$S_0 \rightarrow S_9$	4.71	263	0.232	H → L+4 (37%); H-6 → L (14%)
HY3	$S_0 \rightarrow S_1$	3.18	390	2.217	H → L (51%); H-1 → L (39%)
	$S_0 \rightarrow S_4$	4.26	291	0.247	H → L+1 (38%); H → L+2 (15%); H → L+3 (14%)
	$S_0 \rightarrow S_8$	4.71	263	0.258	H → L+6 (51%); H → L+5 (28%)
HY4	$S_0 \rightarrow S_1$	2.82	439	2.079	H → L (75%); H-1 → L (14%)
	$S_0 \rightarrow S_8$	4.63	268	0.206	H → L+5 (54%); H → L+5 (13%); H → L+7 (13%)
	$S_0 \rightarrow S_2$	3.61	343	0.196	H-1 → L (70%); H → L+1 (10%); H → L+4 (66%)
	$S_0 \rightarrow S_3$	3.99	311	0.192	H → L+4 (66%)
HY5	$S_0 \rightarrow S_2$	3.16	393	1.155	H → L+1 (68%)
	$S_0 \rightarrow S_1$			0.672	H → L (49%); H-1 → L (34%)

Designed dyes show maximum wavelength (λ_{max}) in the range 383 − 531 nm, CA-S and HY1 demonstrate highest and lowest λ_{max}, respectively. Oscillator strength higher than a unit characterized major transitions for all dyes, with LHE within ~91 − 99% range. Electronic spectra comparison between unmodified dyes CA and HY is made in Fig. 10(a), HY exhibits intense band at 404 nm, whereas, CA shows a red-shift in comparison to HY with maximum wavelength at 444 nm and the two dyes show comparable oscillator strength. Upon structural modification, molecules HY-S, HY2 and HY4 exhibited red-shift while HY1, HY3 and HY5 blue-shifts were observed in comparison with unmodified counterpart. For dyes HY-S and CA-S with common π-spacer, the calculated maximum wavelength in chloroform were found to be 498 nm (2.49 eV) and 531 nm (2.34 eV), respectively. The calculated electronic spectra

can be co-related to experimentally observed spectral bands at 515 nm (HY-S) and 522 nm (CA-S) in $CHCl_3$ solvent (Guo *et al*., 2016).

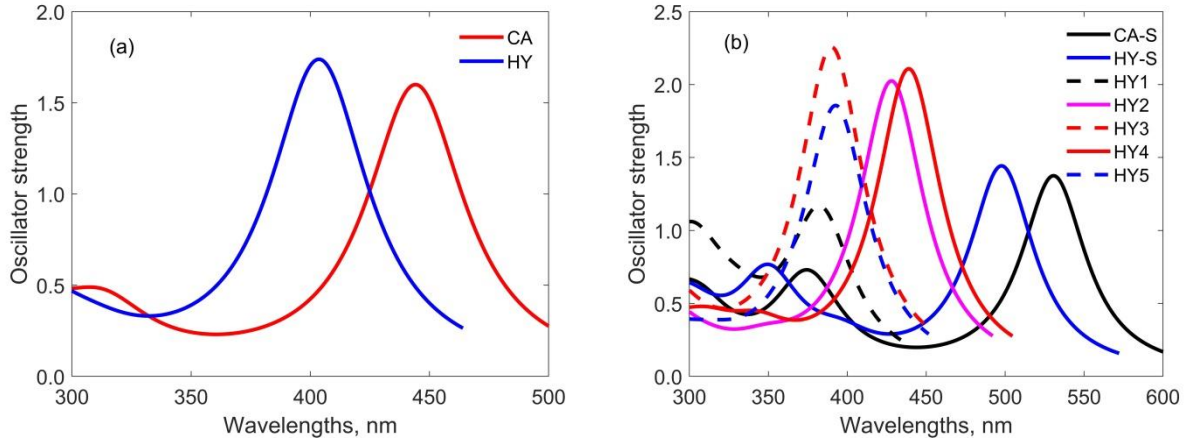

Figure 10: (a) Simulated UV-Vis electronic spectra of dyes without π-spacers; (b) Simulated UV-Vis electronic spectra of dyes containing π-spacers

The CA-S dye is significantly red-shifted compared to HY-S with ~33 nm difference, for both dyes the first electronic transition is characterized by HOMO → LUMO contribution of the same magnitude 79%, while the transitions from HOMO-1 → LUMO were 12% and 13% for CA-S and HY-S, respectively (Table 8). Other modified dyes exhibited HOMO → LUMO transitions below 70%, except HY2 and HY4 with 72% and 75% contribution, respectively. The presence of hydantoin is expected to enhance delocalization of the LUMO onto the anchoring group thus expected to favour ICT.

4.2.4 Exciton Binding Energy

The exciton binding energy (E_b) is defined as the potential energy difference between the neutral singlet exciton and free charge carriers and it is directly related to the charge separation in DSSCs (Wazzan & Irfan, 2018). In order to maximize PCE, the excited-states of the electron and hole pairs must be separated to escape from recombination (Gélinas *et al*., 2014). It is one of the key factors that govern the physics of many optoelectronic organic devices. Thus, understanding the variation of E_b among the considered molecules under this section is not only practically important but also of fundamental interest. It is desired that dye molecules have less exciton binding energy for PCE. The E_b values are obtained as the difference between E_g and the optical band gap, also known as first excitation energy, ΔE (Wazzan & Irfan, 2018). The calculated E_b values are displayed in Table 9; the modified dyes demonstrate lower E_b values in 1.57 − 1.75 eV range. The magnitudes of calculated exciton

binding energies are favourable in the photon to current energy conversion as they are expected to provide effective hole/electron separation.

4.2.5 Charge Transfer Properties

In this part, the focus is on excited-state properties of the designed dyes. Charge separation in DSSCs can be considered as a two-step process; (a) electrons injection into the semiconductor's CB and (b) regeneration of the dye ground state and the two processes are thermodynamically downhill. The electron injection efficiency is closely related to oscillator strength (*f*) and free energy of electron injection (ΔG_{inj}) from the excited-states of dye to the CB of semiconductor (Wang *et al*., 2013). When the absolute value ΔG_{inj} is higher than 0.2 eV (Wei *et al*., 2016; Zanjanchi & Beheshtian, 2019), it can be considered that the injection efficiency of an electron from the excited-state tends to a unit.

For efficient charge injection, LUMOs of the dye must lie above the conduction band edge (Ferdowsi *et al*., 2018). Evaluation of E_{OX}^{dye*} is done by considering that, electron injection occurs from the unrelaxed excited-state. To account for charge separation effect, it is crucial to analyze ΔG_{inj} and ΔG_{reg} summarized in Table 9. All values are negative and this shows that both charge injection and dye regeneration are spontaneous processes for the designed sensitizers.

Table 9: Excited-state oxidation potential, exciton binding energy, the free energy of injection, the free energy of regeneration, all values in eV, excited-state lifetime (ns) and light-harvesting efficiency

Dye	$-E_{OX}^{dye*}$	E_b	$-\Delta G_{inj}$	$-\Delta G_{reg}$	τ	LHE (%)
CA	3.32	1.74	0.73	1.31	1.87	97.4
HY	2.87	1.78	1.18	1.14	1.43	98.0
CA-S	3.72	1.68	0.33	1.25	3.13	95.5
HY-S	3.46	1.75	0.59	1.15	2.63	96.1
HY1	2.73	1.70	1.32	1.17	2.09	91.1
HY2	3.02	1.63	1.04	1.11	1.38	99.0
HY3	2.81	1.60	1.24	1.19	1.03	99.4
HY4	2.94	1.67	1.11	0.96	1.39	99.2
HY5	2.92	1.57	1.13	1.28	2.00	93.0

All dyes considered here could efficiently inject charge into the semiconductor since ΔG_{inj} values are higher than the minimum requirement of 0.2 eV. Among all dyes, CA-S demonstrated the smallest ΔG_{inj} value of 0.33 eV while the highest (1.32 eV) is noted for HY1. The introduction of π-spacers for hydantoin based dyes resulted in the smaller absolute

value of ΔG_{inj} for HY-S, HY2, HY4 and HY5. However, HY3 and HY1exhibit higher values than unmodified dye; this is due to the presence of methyl branched groups on the π-spacer of HY1 and the presence of sulfur replacing of the nitrogen in HY3. Calculated ΔG_{reg} for all studied sensitizers were found to be above the minimal requirement, 0.4 eV (Zanjanchi & Beheshtian, 2019). Among the modified dyes, HY4 possessed the closest E_{HOMO} to the redox potential of the electrolyte followed by HY2, HY-S, HY1, HY3, CA-S and HY5. Therefore, based on this analysis; one can expect efficient charge injection and dye regeneration for all dyes.

4.2.6 Excited-state Lifetime

In this part, the analysis of the excited-state lifetime (τ) is considered. A photoexcited dye has several relaxation pathways, including decay to ground state. It is a requirement that the electron injection time should be shorter than the excited-state decay to the ground state to allow efficient charge transfer (injection) before radiative or photochemical reactions take place (Arunkumar *et al*., 2018; Hardin *et al*., 2012; Listorti *et al*., 2011). Dyes with longer excited-state lifetime are expected to demonstrate better charge transfer efficiency with a low possibility of charge recombination, resulting in high efficiency of the cell. The parameter τ in S_1 state is obtained through Einstein transition probabilities as $\tau = 1.499/(\Delta E^2 f)$ (Hilborn, 1982; Li *et al*., 2019; Wazzan & Irfan, 2018; Xu *et al*., 2019), where ΔE is the first excitation energy.

The results reported in Table 9 shows variations within 1.03 − 3.13 ns, where dyes CA-S and HY-S exhibit higher values. Though, the two dyes possess different anchoring group have shown higher τ values compared to other dyes, this indicates that the featured π-spacer in these two dyes plays a vital role in the stabilization of the excited-state, resulting to longer times for τ in comparison to other π-spacers considered in this work. Thus, it can be concluded that through systematic incorporation of appropriate π-spacers, it is possible to improve the charge transfer characteristics of the dyes.

4.2.7 Chemical Reactivity Parameters

Understanding the IPs and EAs is vital in answering fundamental organic chemistry questions such as whether the molecules are more or less reactive. For many organic compounds, the experimental IP and EA values not frequently available and so for the current thought

molecules. The energy barrier for holes and electrons injection is directly related to the IP and EA; IP reveals the energy change due to the loss of an electron from the neutral state of the dye, whereas EA reveals the change in energy of a neutral dye when an electron is added (Li *et al*., 2019). Smaller IP and larger EA values are desirable to facilitate hole and electron injection. The computed IPs and EAs listed in Table 10 are ranging between 5.84 − 6.39 and 0.64-1.80 eV, respectively.

Table 10: The ionization potential, electron affinity, chemical potential, chemical hardness, electrophilicity, electron-accepting power, electron-donating power, all values in eV

Dye	IP	EA	$-\mu$	h	ω	ω^{+}	ω^{-}
CA	6.39	1.30	3.85	2.55	5.81	1.30	5.15
HY	6.10	0.64	3.37	2.73	4.17	0.74	4.11
CA-S	6.25	1.80	4.02	2.23	7.27	1.90	5.92
HY-S	6.07	1.39	3.73	2.34	5.94	1.40	5.12
HY1	6.16	0.64	3.40	2.76	4.18	0.74	4.14
HY2	6.03	1.04	3.53	2.50	5.00	1.05	4.58
HY3	6.14	0.81	3.48	2.66	4.54	0.86	4.34
HY4	5.84	0.87	3.36	2.48	4.54	0.90	4.26
HY5	6.23	1.02	3.63	2.60	5.06	1.04	4.67

The increase in EA implies that electron injection is more feasible, among hydantoin based dyes HY-S and HY1demonstrated the highest and smallest EA, respectively. Also, HY4, HY2 and HY-S showed lower IP values, while cyanoacrylic acid-based dyes were among the top three dyes with high IP values. Further analysis performed through the full-electron donor-acceptor map (FEDAM) revealed more details (Fig. 11).

The technique was first introduced by Martínez *et al*. (2009); the FEDAM provides qualitative information on the electron-accepting and electron-donating abilities of the dyes. It is a graphical representation of EA versus IP, the graph divided into four quadrants namely: good acceptor and bad donor (I), bad acceptor and bad donor (II), bad acceptor and good donor (III), good acceptor and good donor (IV). Results from Table 10 and Fig. 11 show that HY1, HY3 and HY5 possess the highest IP and lowest EA values. Thus, these three dyes are categorized as both bad acceptor and bad donor in the limit of the present analysis and the dyes of interest can be found in I, III and IV quadrants, i.e. HY-S, HY2, HY4 and CA-S.

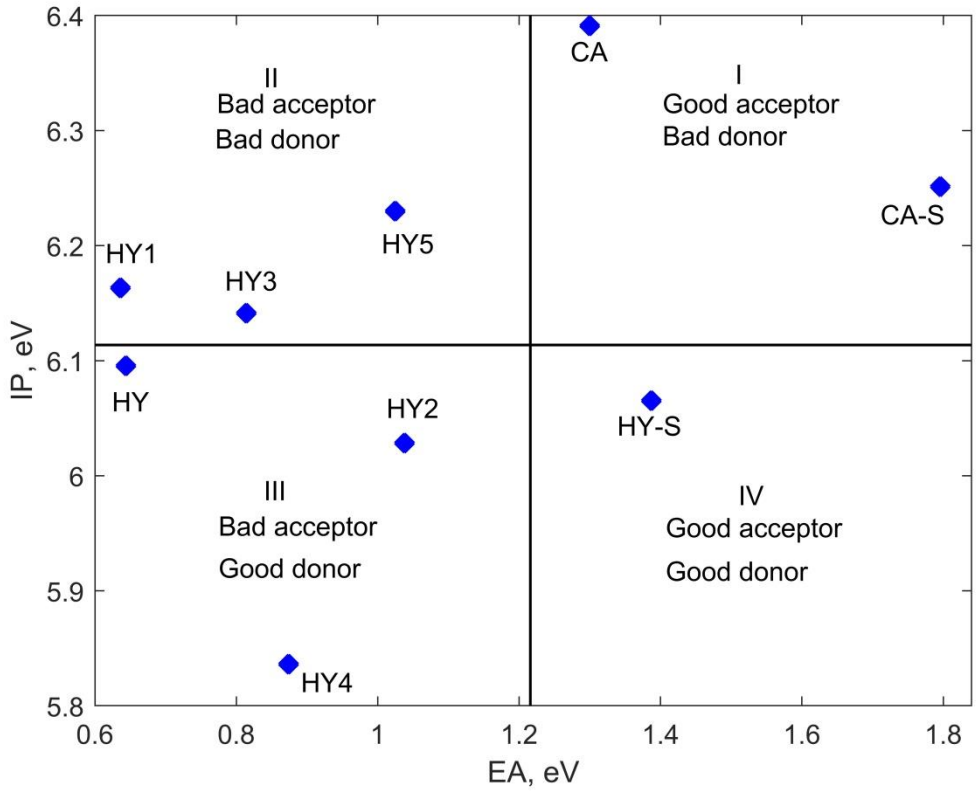

Figure 11: The full-electron-donor-acceptor map for the studied sensitizers

To describe the chemical properties of designed dyes, chemical descriptors were calculated based on Koopman's theorem. Chemical potential/chemical reactivity (μ), the chemical hardness (*h*), the electrophilicity index/stabilization energy (ω) the electron-accepting power (ω^+) and the electron-donating power (ω^-) are listed in Table 10. The parameters μ and *h* are used to describe the tendency of charge to escape from the system in the ground-state and the resistance of the dye to charge transfer, dyes with higher and lower *h* are known as hard and soft molecules, respectively. Seen from Table 10, unmodified dyes (CA and HY) possess higher chemical hardness values in comparison to modified counterparts, for the modified dyes, *h* decreases in the following order: HY1 > HY3 > HY5 > HY2 > HY4 > HY-S > CA-S. The observed lower chemical hardness relates to the π-spacers inserted, for example, the common π-spacer present in CA-S and HY-S results in the reduced chemical hardness of the dyes. The presence of branched groups (HY1 and HY5), also the asymmetric effect in the π-spacer (HY3) may have resulted in increased chemical hardness. Smaller *h* is of interest as it reduces the resistance to ICT, this is further confirmed by the linear dependence between *h* and E_g ($h = 0.4563 \times E_g - 0.139$, $R^2 = 0.987$), that means dyes with wider energy gap demonstrate high chemical hardness. There is no obvious trend in the calculated chemical

reactivity parameter values for hydantoin dyes. In comparison, CA-S exhibits the highest magnitude (4.02 eV), a small difference in magnitude ~0.37 eV was observed between the highest and lowest μ absolute values whereby hydantoin dyes possess μ within the range 3.36 − 3.73 eV.

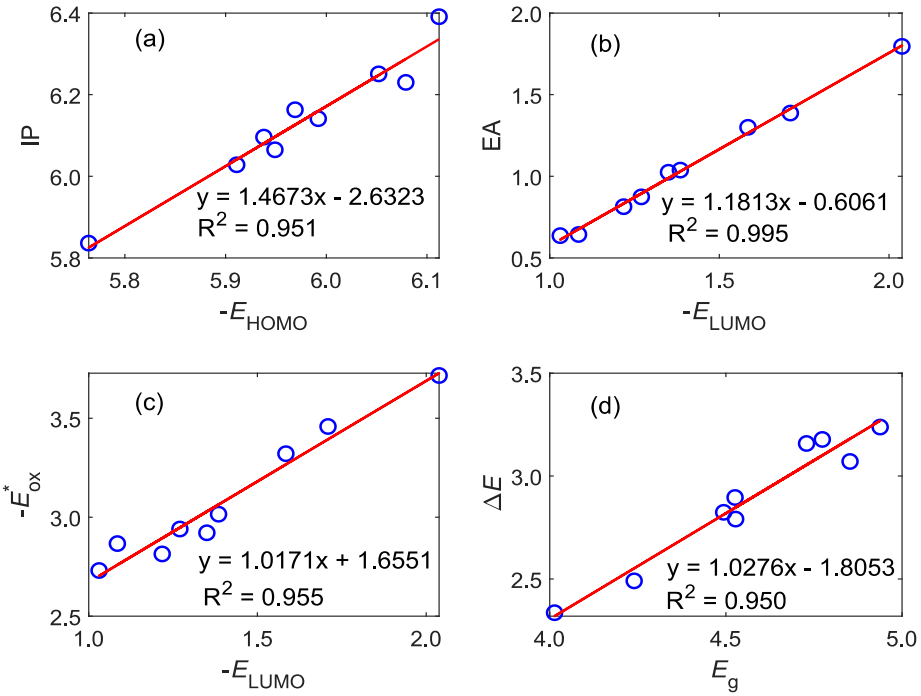

Figure 12: Linear regression analysis of the relationships between electronic energies: (a) ionization potentials and highest occupied molecular orbital energies, (b) electron affinities and lowest unoccupied molecular orbital energies, (c) excited-state oxidation potentials and lowest unoccupied molecular orbital energies and (d) vertical transition energies and energy gap

Electron-accepting power (ω^+), as the name suggests, represents the capability of the material to accept the charge. It is expected that dyes with a higher ω^+ and lower *h* will result in better performance. Calculated ω^+ values are consistent with UV-Vis spectra, where red-shifted (CA-S, HY-S, HY2 and HY4) spectra show good electron-withdrawing ability. Studied dyes show the same trend in terms of stabilization energy (ω) and electron-donating-power (ω^-). The HY-S demonstrates the highest ω, ω^- and ω^+ values among hydantoin dyes. Generally, it is observed that dyes small chemical hardness correspond to dyes with suitable ΔG_{inj}, ΔG_{reg} and higher ω.

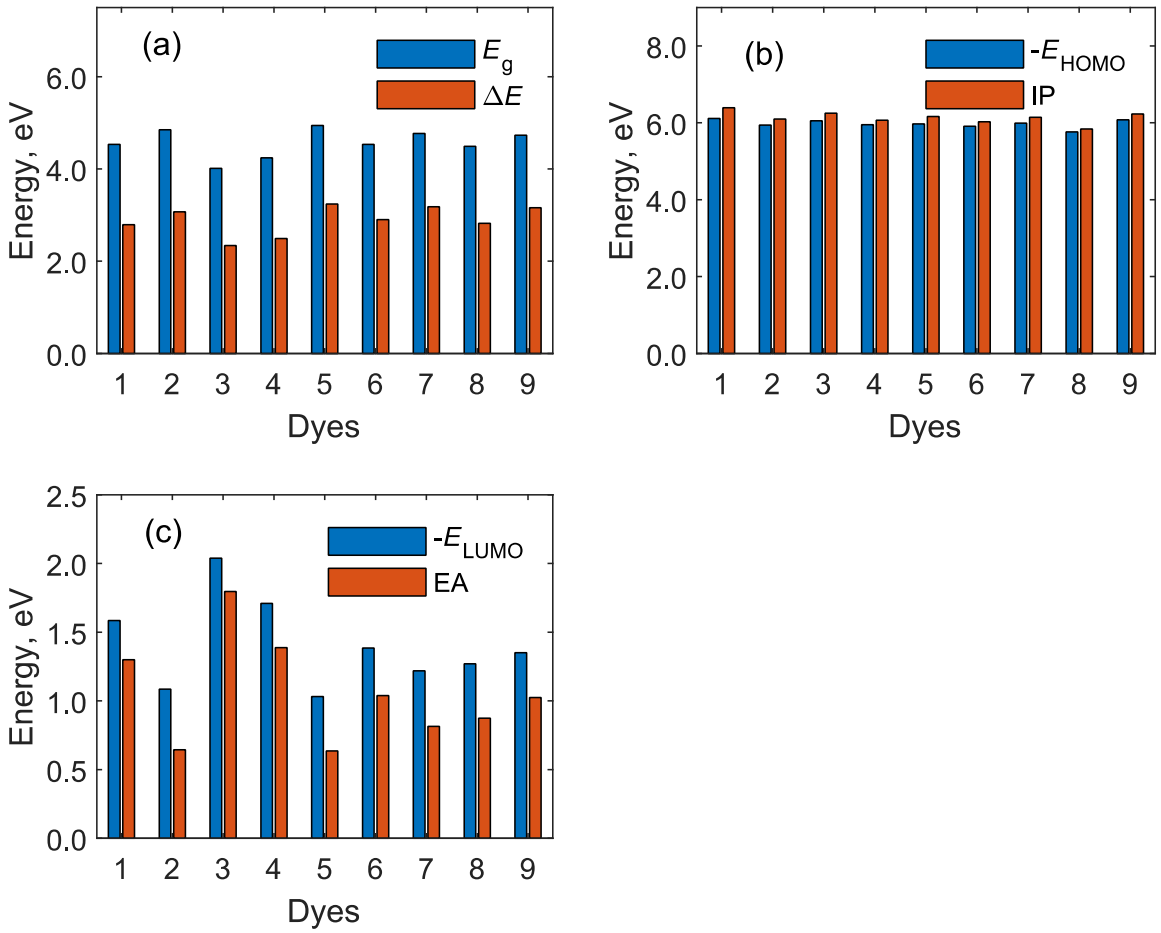

Figure 13: Electronic energies comparison for nine dyes molecules, 1 − CA, 2 − HY and 3 – CA-S, 4 – HY-S, 5 − 9 are HY1 − HY5, respectively; (a) energy gaps and vertical transition energies (b) highest occupied molecular orbital energies and ionization potentials: (c) lowest unoccupied molecular orbital energies and excited-state oxidation potentials

Linear regression analysis between computed electronic energies is given in Fig. 12. A reasonable linear correlation is observed for each couple of parameters with a high determination coefficient R^2 between 0.950 − 0.995, all correlations are positive, the higher is the magnitude E_{HOMO}, the higher is IP, et cetera. Comparison between electronic energies is also represented via bar diagram Fig. 13. It is seen that the energy gap exceeds the excitation energy by 1.57 − 1.78 eV. The IP values are a little bit higher than the magnitude of HOMO energies, while EA less compared to the extent of LUMO energies.

Therefore, appropriate energy levels, reduced energy gap, lower first excitation energies, higher EA and lower IP values for dyes will result in enhanced performance of DSSCs. Generally, from this analysis, HY-S, HY2 and HY4 are selected as best candidates with

desirable charge transfer properties compared to others presented in this work and one can expect improving power conversion efficiency of DSSCs.

In this dissertation, it is demonstrated that optoelectronic properties and chemical reactivity parameters can be improved through systematic modification of dyes by introducing appropriate π-linkers and anchoring groups with the aid of quantum chemical methods. The molecular engineered triphenylamine-based dyes featuring D-π-A architecture have been considered and investigated for suitable properties for DSSCs applications. It was observed that the replacement of the commonly used anchoring group cyanoacrylic acid by hydantoin anchoring group resulted in higher values of free energy of injection and excited-state lifetimes. The observed red-shift in electronic spectra for hydantoin cyanoacrylic acid dyes were consistent with Guo and co-workers' experimental findings (Guo *et al*., 2016). More importantly, the findings confirm that HY-S is both good acceptor and donor dye.

The fact that the heterocyclic anchoring group has demonstrated superior optoelectronic properties, in the subsequent section, attention is paid to the exploration of other heterocyclic anchoring groups. To investigate charge transfer characteristics between the dye and semiconductor, a TiO_2 slab is considered, binding energies were calculated depending on binding mode. The employed method in studying the reported properties significantly reduces the cost and time spent through traditional experiments, thus enabling the design of novel materials with improved efficiencies without sacrificing many resources. Therefore, the results and information reported in this dissertation could be useful in the development of DSSCs based on these dyes or some analogues.

4.3 The Influence of Heterocyclic Anchoring Groups

This section aims to improve the optoelectronic properties and the sensitizers' stability when bound to the semiconductor by featuring heterocyclic anchoring groups compared to cyanoacrylic acid. Detailed analysis on photophysical and photoelectrochemical properties of designed sensitizers: cyanoacrylic acid (CA-S), imidazolidine-2,4-dione (HY-S), pyrimidine-2,4,6(1H,3H,5H)-trione (DYE1), 1,3-dimethylpyrimidine-2,4,6(1H,3H,5H)-trione (DYE2), 2-thioxodihydropyrimidine-4,6(1H,5H)-dione (DYE3), 2-(4-oxothiazolidin-2-ylidene) malononitrile(DYE4) and 2-(4-oxo-2-thioxothiazolidin-3-yl)acetic acid (DYE5) shown in Fig. 4.

The geometrical parameters, light-harvesting efficiency, electronic spectra, chemical descriptors, free energies of charge injection and dye regeneration, reorganization, and adsorption stability have been reported.

4.3.1 Geometrical Properties

Selected geometrical parameters bond lengths (d, Å) and dihedral angles (ϑ, °) indicated in Fig. 4 and listed in Table 11 were extracted from the optimized geometries. The respective parameters look-alike in all seven dye molecules.

Table 11: The calculated bond distances (Å) and dihedral angles (°) for the investigated sensitizers

Dye	d_1	d_2	d_3	d_4	d_5	d_6	d_7
CA-S	1.428	1.428	1.403	1.470	1.456	1.431	1.378
HY-S	1.427	1.426	1.407	1.473	1.456	1.436	1.361
DYE1	1.428	1.428	1.403	1.469	1.455	1.421	1.379
DYE2	1.428	1.428	1.402	1.468	1.454	1.418	1.381
DYE3	1.428	1.427	1.404	1.470	1.456	1.423	1.378
DYE4	1.429	1.428	1.403	1.469	1.455	1.428	1.369
DYE5	1.428	1.428	1.403	1.470	1.455	1.427	1.363
	ϑ_1	ϑ_2	ϑ_3	ϑ_4	ϑ_5	ϑ_6	ϑ_7
CA-S	49.7	49.0	28.2	29.6	30.2	1.9	178.9
HY-S	48.6	47.8	31.3	31.1	31.2	6.1	179.1
DYE1	50.3	49.7	28.6	29.5	29.8	2.8	179.8
DYE2	50.7	49.8	27.6	28.5	29.8	2.1	179.9
DYE3	49.3	49.4	29.5	30.1	29.8	1.1	178.9
DYE4	49.6	49.3	29.2	29.4	30.2	0.0	180.0
DYE5	48.5	51.6	29.6	27.5	31.1	5.1	178.9

The C-N bond lengths within the TPA group are approximately equal to 1.43 Å (d_1, d_2), while d_3 is nearly 1.40 Å. The C-C distances between the TPA and benzothiazole (BTZ) $d_4 \approx$ 1.47 Å, BTZ – thiophene $d_5 \approx 1.45$ Å and d_6 is 1.42 − 1.43 Å; and the double bond d_7(C=C) joining the anchoring group is in the range 1.36 − 1.38 Å. For dihedral angles, the three phenyl groups in the TPA moiety are twisted one to another by ~50° and the third is turned by ~30° to the rest part of the molecule; this non-planarity of the structure is important as it may reduce dye aggregation. On the other hand, the thiophene π-linker part forms almost a planar configuration as ϑ_6 and ϑ_7 are close to 0°/180°; and this planarity may facilitate ICT from the donor unit to the anchoring group. Summarizing this section one can conclude that variation of anchoring groups does not affect the geometry of the remaining part of the molecules noticeably.

4.3.2 Electronic Spectra

The performance of cells relates to broader coverage of the solar spectrum and LHE of sensitizers. The LHE values are obtained through the oscillator strengths *f* at maximum absorption wavelengths (λ_{max}). The electronic absorption spectra of the dyes for chloroform solvent have been simulated; characteristics of the most relevant electronic transitions are displayed in Table 12. The computed maximum wavelengths for CA-S (531 nm) and HY-S (498 nm) accord with experimental observations 522 and 515 nm, respectively (Guo *et al.*, 2016). Generally, two principal peaks are observed in all dyes' UV-Vis spectra; the first maxima within 450 − 600 nm range and the second one from 300 to 450 nm (Fig. 14).

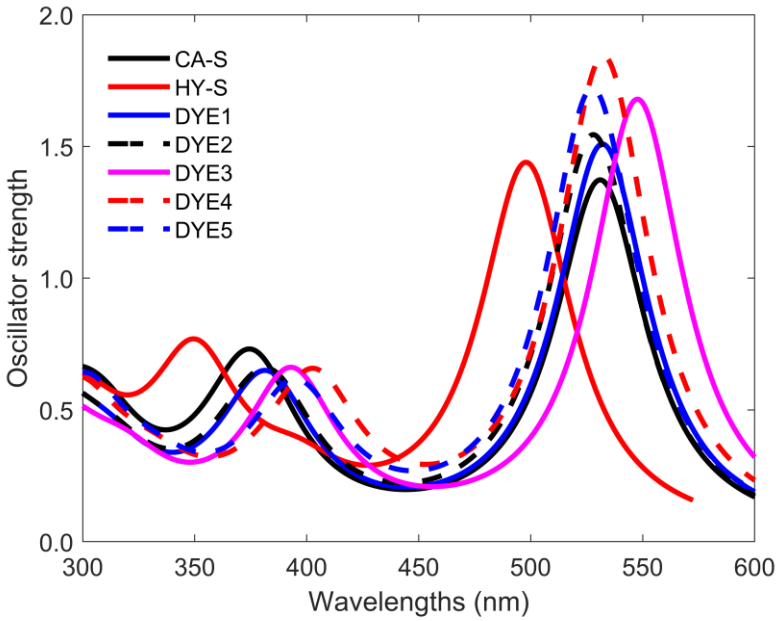

Figure 14: Simulated electronic absorption spectra of the designed dyes for chloroform solvent

From the electronic transition configurations, the excitations at λ_{max} are assigned to HOMO → LUMO and the second peaks are contributed mostly from HOMO−1 → LUMO transitions. Among the dyes with heterocyclic anchoring groups, the greatest oscillator strength for the first S_0-S_1 transition is 1.82 (DYE4) and the lowest 1.41 (HY-S). All dyes from HY-S to DYE5 exhibit higher *f* than cyanoacrylic acid-based DEY1 (1.35). Influence of anchoring groups on the λ_{max} can be seen from the calculated spectra. The DYE3 shows the most red-shifted absorption peak at 548 nm, while HY-S exhibits the peak at the least value, 497 nm; and for other dyes, the λ_{max} values are in the range 528 − 533 nm. Calculation of the excited-state lifetime is performed to assess the decay process from excited to the ground state. A higher lifetime can facilitate charge transfer and reduce energy loss. Designed dyes

demonstrate the comparable moderate capability of retarding charge recombination; the difference between the maximum and minimum τ is not significant ~0.8 ns.

Table 12: Electronic transitions, excitation energies (eV), wavelengths (nm), oscillator strengths, excited-state lifetimes (ns), light-harvesting efficiencies and transition assignments

Dye	Transitions	Δ*E*	λ	*f*	τ	LHE	Contributions
CA-S	$S_0 \rightarrow S_1$	2.33	531	1.35	3.13	95.5	H → L(79%); H−1 → L(12%)
	$S_0 \rightarrow S_2$	3.28	378	0.39			H−1 →L(78%);H → L(11%)
HY-S	$S_0 \rightarrow S_1$	2.49	498	1.41	2.64	96.1	H →L(79%); H−1 → L(13%)
	$S_0 \rightarrow S_2$	3.13	396	0.15			H−1 →L(80%);H → L(12%)
DYE1	$S_0 \rightarrow S_1$	2.33	532	1.49	2.85	96.7	H →L(77%); H−1 → L(14%)
	$S_0 \rightarrow S_2$	3.23	383	0.44			H−1 →L(74%);H → L(11%)
DYE2	$S_0 \rightarrow S_1$	2.35	528	1.52	2.75	97.0	H →L(76%); H−1 → L(14%)
	$S_0 \rightarrow S_2$	3.22	385	0.44			H−1 →L(70%);H → L(10%)
DYE3	$S_0 \rightarrow S_1$	2.26	548	1.66	2.71	97.8	H → L(74%); H−1 → L(15%)
	$S_0 \rightarrow S_2$	3.15	393	0.54			L(70%);H → L+1(10%)
		3.16	392	0.03			H→L+1(51%);H−1→ L+1(24%)
DYE4	$S_0 \rightarrow S_1$	2.33	533	1.82	2.34	98.5	H →L(71%); H−1 →L (17%)
	$S_0 \rightarrow S_3$	3.07	403	0.52			H−1 → L(60%);H → L+1(19%)
	$S_0 \rightarrow S_2$	3.22	385	0.05			H→L+1(38%);H−1→L+1 (28%)
DYE5	$S_0 \rightarrow S_1$	2.35	528	1.69	2.46	98.0	H → L(69%); H−1 → L(17%)
	$S_0 \rightarrow S_2$	3.07	405	0.07			H−4→L(31%);H−4→ L+1(28%)
		3.14	394	0.43			H−1 → L(50%);H → L+1(20%)

Electron density spatial distribution over the frontier molecular orbitals (FMOs) is displayed in Fig. 15. The analysis shows that in the HOMOs electrons are delocalized over the triphenyl rings and in LUMOs charge density is mainly located near or over the anchoring units; such characteristic distribution is beneficial for ultra-fast charge injection from the dye to the semiconductor (Ji Zhang *et al*., 2018). Regarding the anchoring groups effect on the FMOs, it is not exhibited in the HOMOs which are common in all dyes,-but it is apparently observed in the LUMOs. For example, the two dyes CA-S and DYE5 possess a carboxylic group in the anchoring unit, in the CA-S, LUMO extends over cyanoacrylic acid suitable for charge transfer. In contrast, DYE5 exhibits less LUMO charge density (Fig. 14), which may result in weaker dye-semiconductor electronic coupling hence poor electron injection.

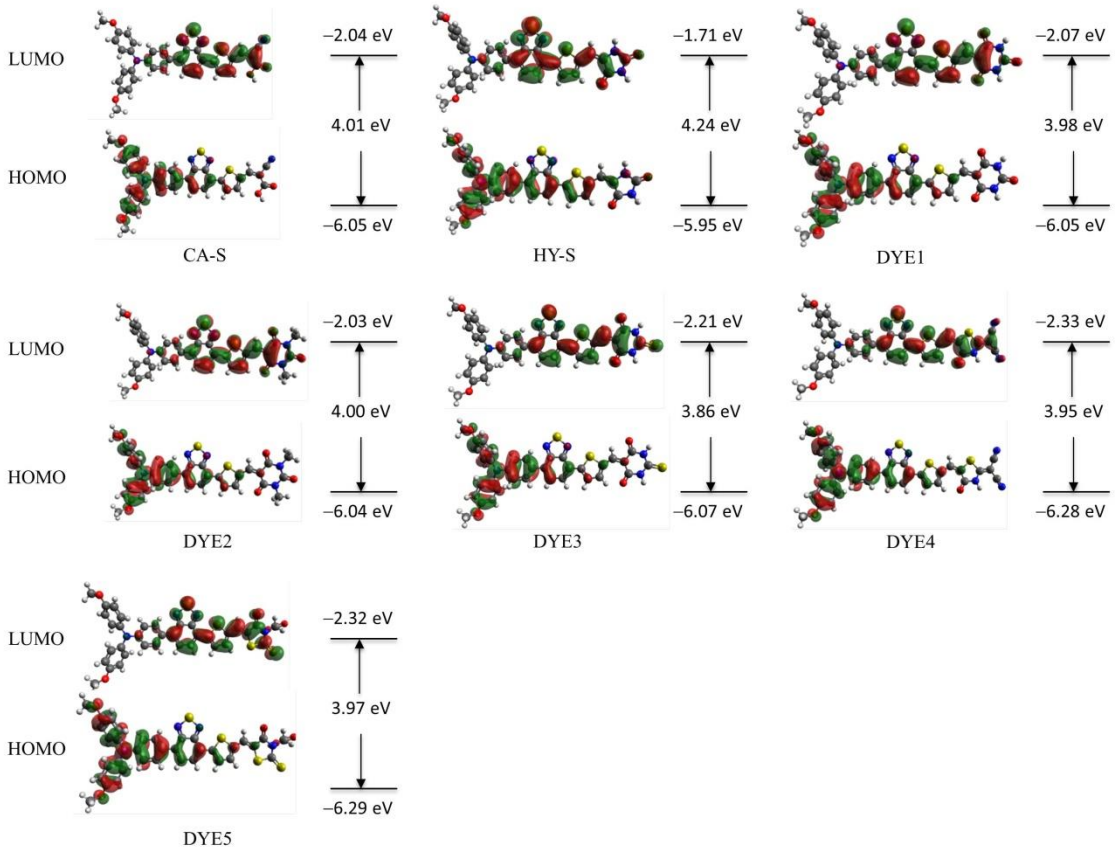

Figure 15: Graphical representation of frontier molecular orbitals, the HOMO, LUMO energies and energy gaps of the studied dyes

4.3.3 Electron Injection and Dye Regeneration

As already discussed in section 4.1.5, photo-induced electronic excitation and subsequent spatial charge separation are the key to accelerate charge transfer processes in the DSSCs operating system. The calculated values of E_{ox}^{dye}, E_{ox}^{dye*}, ΔG_{inj} and ΔG_{reg} are presented in Table 13. It is seen that all dyes meet the requirements on the GSOP and ESOP position. The GSOP and ESOP values range between −5.95 eV to −6.29 eV and −3.95 eV to −3.46 eV, respectively. The HY-S possesses the highest GSOP and ESOP, while the DYE5 and DYE5 exhibit the lowest values. The findings show that ΔG_{inj} for the designed dyes are negative, ranging from −0.10 eV to −0.59 eV, this predicts spontaneous electron injection from the excited dye to TiO_2 conduction band. For all sensitizers (except for DYE4 and DYE5) show ΔG_{inj} values higher than the minimum requirement 0.2 eV (Wei *et al*., 2016; Zanjanchi & Beheshtian, 2019). The dye possessing hydantoin anchoring (HY-S) exhibits the highest ΔG_{inj} about 0.59 eV. According to the Marcus theory, the larger the ΔG_{inj} value, the faster the

electron injection rate. The dyes HY-S, DYE2, DYE1 and DYE3 are expected to provide fast charge injection among hydantoin dyes.

Table 13: Ground and excited-state oxidation potentials, free energies of charge injection and dye regeneration and the electronic coupling constants, all values in eV

Dye	$-E_{ox}^{dye}$	$-E_{ox}^{dye*}$	$-\Delta G_{inj}$	$-\Delta G_{reg}$
CA-S	6.05	3.72	0.33	1.25
HY-S	5.95	3.46	0.59	1.25
DYE1	6.05	3.72	0.33	1.25
DYE2	6.04	3.69	0.36	1.24
DYE3	6.07	3.80	0.25	1.27
DYE4	6.28	3.95	0.10	1.48
DYE5	6.29	3.94	0.11	1.49

The investigated dyes demonstrate thermodynamically favourable regeneration ability as all ΔG_{reg} values are negative, indicating that GSOPs are lower than the electrolyte's redox level. The ICT properties of sensitizers can be well understood through the analysis of molecular orbital energy levels.

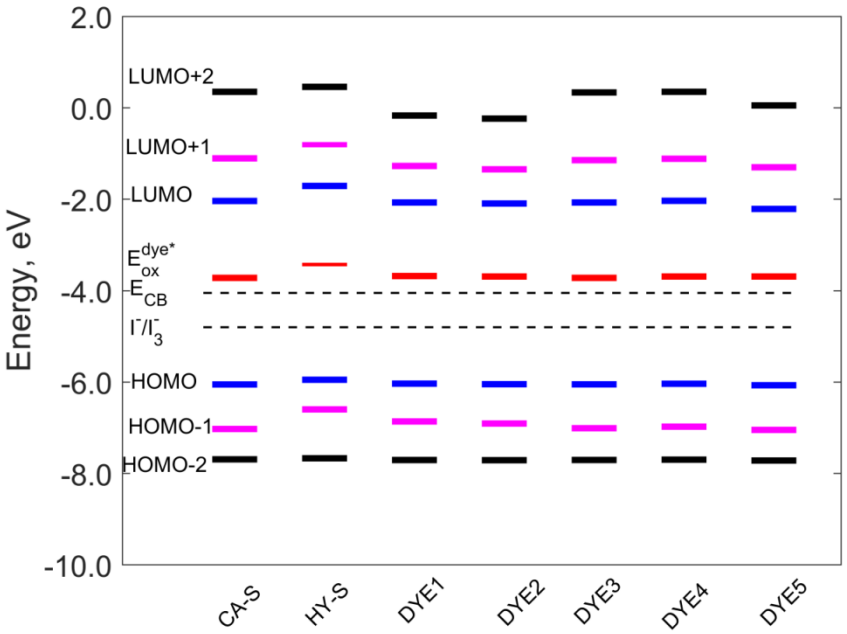

Figure 16: Schematic energy level alignment of the sensitizers with TiO_2 conduction band and electrolyte redox potential, calculations performed for chloroform solvent

For efficient DSSCs, the GSOP should be lower than the potential of I^-/I_3^- redox couple while the ESOP should be higher than the E_{CB} of TiO_2 semiconductor. The energy level alignment diagram Fig. 16 represents the most relevant FMOs, ESOPs, and ECB of TiO_2 and

the redox potential of the electrolyte. Featuring heterocyclic anchoring groups in the sensitizers demonstrate the reduction of excitation energies ΔE and hence longer wavelengths λ_{max} than HY-S. Therefore, calculated thermodynamic and electrochemical parameters exhibit evidence that the dyes considered have a great chance to provide efficient charge injection and dye regeneration and thus are feasible for DSSC applications.

4.3.4 Ionization Potential, Electron Affinity and Reorganization Energy

The IP and EA are closely related to intermolecular charge transfer efficiency. Both adiabatic and vertical IP and EA were computed for the sensitizers under consideration. Smaller IP and larger EA values are of interest to facilitate hole and fast electron injection, respectively (He *et al*., 2017). Variation of vertical and adiabatic characteristics in the series of the dye molecules is shown in Table 14 and Fig. 17.

Table 14: The calculated ionization potentials, electron affinities, hole extraction and electron extraction potentials and hardness of the investigated dyes, all values in eV

Dye	IP_v	IP_a	EA_v	EA_a	HEP	EEP	h_v	h_a
CA-S	5.99	5.90	1.84	2.01	5.81	2.20	2.07	1.94
HY-S	5.72	5.62	1.46	1.64	5.52	1.84	2.13	1.99
DYE1	5.96	5.86	1.86	2.05	5.77	2.24	2.05	1.91
DYE2	5.91	5.82	1.80	1.98	5.73	2.16	2.05	1.92
DYE3	6.00	5.90	2.03	2.20	5.81	2.38	1.98	1.85
DYE4	5.96	5.87	2.05	2.20	5.79	2.37	1.96	1.83
DYE5	5.98	5.89	2.04	2.19	5.79	2.35	1.97	1.85

Clearly seen, the IPs do not vary noticeably in the series except a small drop (by ~0.1 eV) for the HY-S. The latter has the lowest adiabatic and vertical EAs followed by DYE2, CA-S and DYE1; equivalence in the EA values can be observed for DYE3, 6 & 7 dyes. Further, the HEP and EEP values shown in Table 14 exhibit similar trends as IP and EA. These trends reflect the variation in HOMO and LUMO energies of the dye molecules.

The reactivity parameters, electron-accepting (ω^+) and electron-donating (ω^-) powers and chemical hardness (h), have been calculated based on the formulae detailed by Chermette (1999) and Gazquez *et al*. (2007). From Fig. 17 one can observe that the ω^+ and ω^- values decrease in the order: DYE4, DYE5, DYE3, DYE1, CA-S, DYE2 and HY-S. Chemical hardness signifies resistance towards polarization of the molecules upon small perturbation. Soft molecules are easier polarizable than hard ones due to less excitation energy required; thus, lower chemical hardness indicates a higher charge transfer feasibility, which is

anticipated to favour a bigger cell conversion efficiency. It is then predicted that the dyes HY-S and CA-S have greater chemical hardness compared to designed dyes (Table 14). Therefore, based on the analysis on h, ω^+ and ω^- the newly designed dyes DYE4, DYE5, DYE3 and DYE1, are more reactive and thus could be more appropriate for DSSCs application. The electron and hole reorganization energies (λ_e and λ_h) can be obtained as follows:

$$\lambda_e = (E_0^- - E_-^-) + (E_-^0 - E_0^0) \text{ and } \quad \lambda_h = (E_0^- - E_+^+) + (E_+^0 - E_0^0)$$

These energies are referred to a measure of the energetic cost of rearranging the molecules between neutral and ionic states within the surrounding dielectric solvent environment (Moia *et al*., 2014; Vaissier *et al*., 2013).

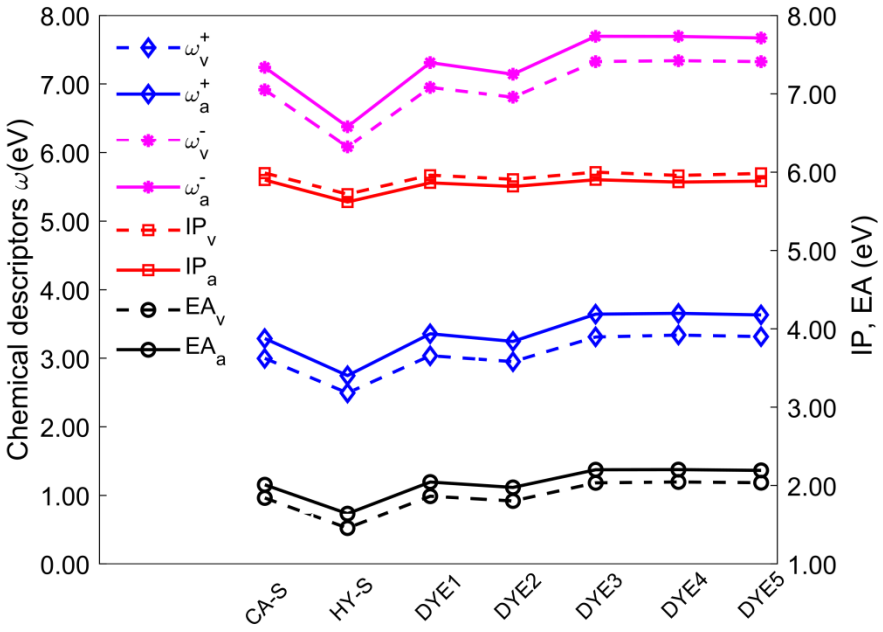

Figure 17: Vertical and adiabatic characteristics of the dye molecules: Ionization potentials, electron affinities and chemical descriptors

Thus, reorganization can be divided into two, (1) solvent (λ_s) and (2) internal (λ_i), reorganization energies. It is demonstrated in Balanay and Kim (2009) and Haque *et al.* (2000) that λ_s show the minimal influence on the electron-transfer dynamics compared to λ_i. For the purpose of simplification, only internal reorganization energy is considered and rename λ_i to λ. Total reorganization energy λ can be obtained as the sum of λ_e and λ_h. Comparison between electron and hole reorganization energies, λ_e and λ_h, is illustrated in Fig. 18. Noticeable variations ranging from 0.16 to 0.38 eV can be seen for λ_e while λ_h values

remain almost similar, ranging from 0.17 to 0.20 eV, for all dyes considered. Small reorganization energies, 0.2 − 0.3 eV and less facilitate charge transport processes between dye molecules (Lin *et al*., 2005; Tripathi & Prabhakar, 2018). From values of λ_h and λ_e obtained, all dyes should possess high hole mobility while high electron mobility is anticipated to be attained by the DYE2– DYE5 and these dyes may be considered as candidates for ambipolar charge transport materials.

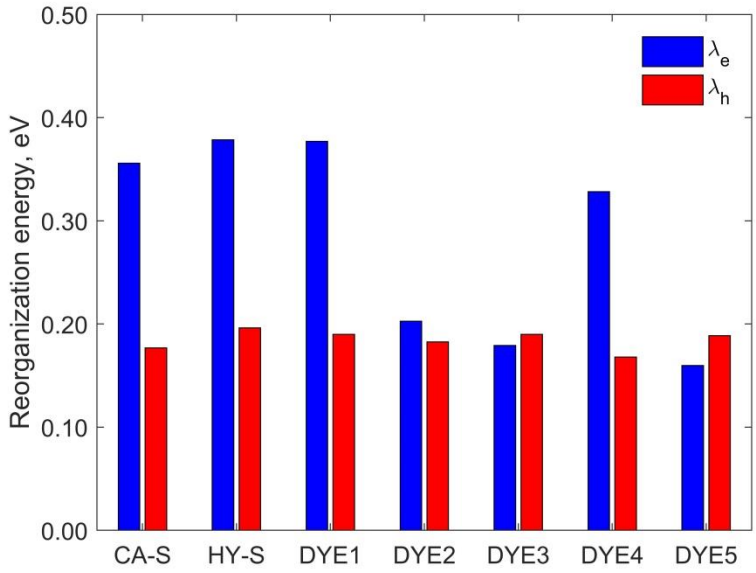

Figure 18: The electron and hole reorganization energies of the studied dyes

4.3.5 Adsorption of Dyes to a TiO_2 Layer

The dye's adsorption mode on the semiconductor plays an important role in solar cell performance since it can influence the electron injection yield (Al-Qurashi *et al*., 2020; Arkan & Izadyar, 2018). In this section, calculations of binding energies for different adsorption modes are considered. The adsorption modes studied here include monodentate (M), bridging bidentate (BB) and the bridging tridentate (BT) carried out for the seven dyes on TiO_2 anatase 101. It was observed that some of the configurations have been altered or distorted during the optimization process; only the stable modes are considered in this section. The optimized dye-TiO_2 systems are illustrated in Fig. 19.

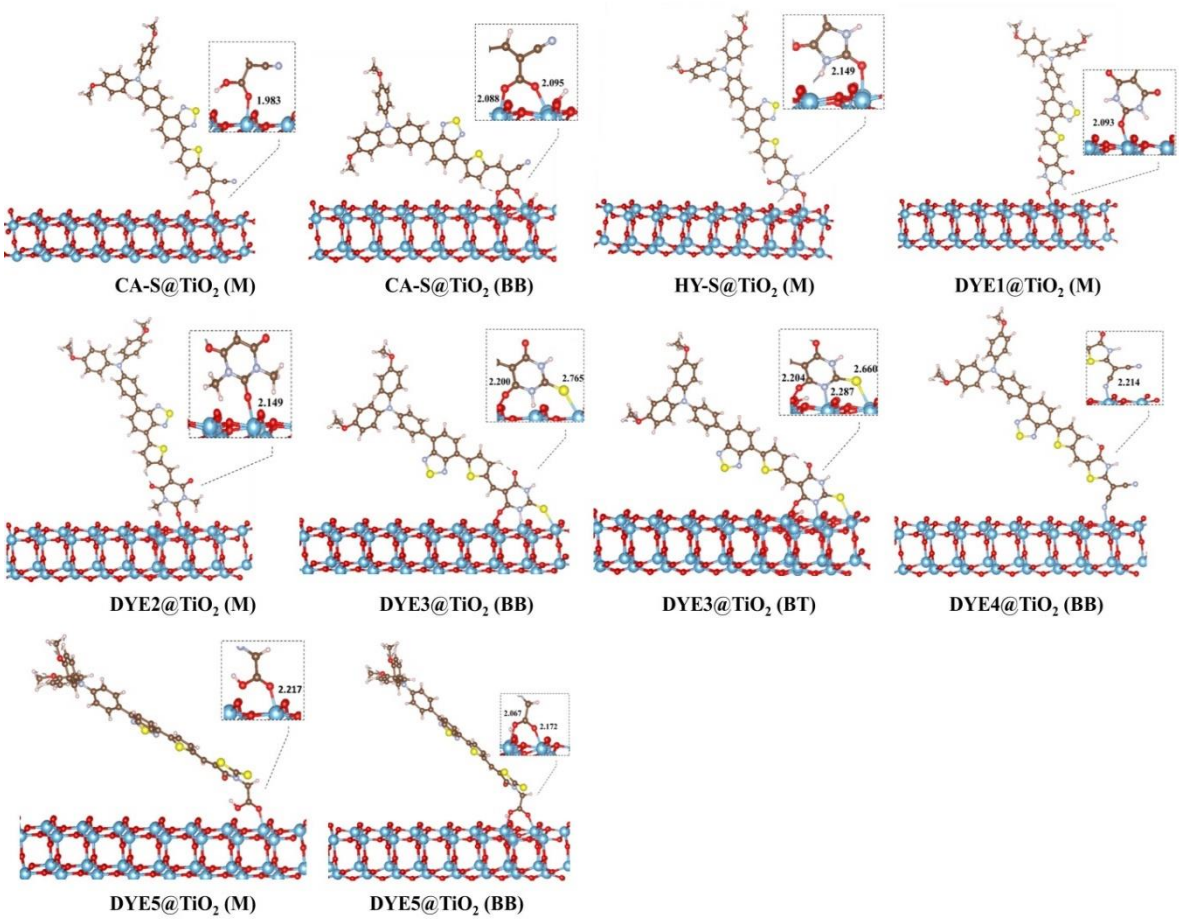

Figure 19: The optimized structural modes of the adsorption of the dyes on TiO_2 anatase 101 surface along with Ti–O, Ti–N and Ti–S bond distances, as calculated with PBE+U functional

Accordingly, dye-TiO_2 adsorption systems are divided into three types. The first type contains complexes HY-S@TiO_2, DYE1@TiO_2, DYE2@TiO_2 and DYE4@TiO_2, which are bound only via the monodentate configuration. The second type comprises CA-S@TiO_2 and DYE5@TiO_2 systems with the carboxylic acid as part of the anchoring group; these dyes exhibit both M and BB modes. The third one is the DYE3@TiO_2 system, in which the anchoring fragment interacts with the TiO_2 surface as the BB and BT modes. The adsorption energies (E_{ads}, eV) are listed in Table 15, along with the bond distances (d, Å) between the interacting atoms of the dye and TiO_2.

In most binding modes, the Ti-O bonds are formed and the bond lengths of Ti-O fall in the range from 1.98 to 2.22 Å; this is in accordance with results by Zhang *et al*. (2018) reported the Ti-O distance interval of 1.99 − 2.13 Å for CA-S@TiO_2 and HY-S@TiO_2 systems. The calculated bond lengths Ti-O for the dye featuring the cyanoacrylic acid anchoring group are comparable with the values 2.05 − 2.13 Å found in the work by Roy *et al*. (2018). For all

complexes, adsorption energies are between –0.11 and –1.75 eV; the DYE4@TiO_2 (with malononitrile group as anchoring fragment) is the least stable complex with E_{ads} = –0.114 eV while the dyes CA-S, DYE3 and DYE5 form much more stronger links with the semiconductor via the bidentate bridging modes, the adsorption energies are between –1.62 and –1.75 eV. This result shows that the bidentate chelating being more favourable than monodentate bindings agrees with findings (Chen *et al*., 2009; Pastore & De Angelis, 2010). The observed stability of bridging bidentate mode can lead to an increase in the rate of electron injection and improved solar cells lifetime.

Table 15: The calculated bond distances (Å) and adsorption energies (eV) for the seven adsorption systems

Systems	Adsorption geometry	d	$-E_{ads}$
CA-S@TiO_2	M	1.983 (Ti-O)	0.252
	BB	2.095 (Ti-O); 2.088 (Ti-O)	1.752
HY-S@TiO_2	M	2.149 (Ti-O)	1.231
DYE1@TiO_2	M	2.093 (Ti-O)	1.050
DYE2@TiO_2	M	2.106 (Ti-O)	0.878
DYE3@TiO_2	BB	2.200 (Ti-O); 2.765 (Ti-S)	1.621
	BT	2.204 (Ti-O); 2.287 (Ti-N); 2.660 (Ti-S)	1.299
DYE4@TiO_2	M	2.214 (Ti-N)	0.114
DYE5@TiO_2	M	2.217 (Ti-O)	1.074
	BB	2.172 (Ti-O); 2.067 (Ti-O)	1.659

The DYE1 and DYE2 have comparable anchoring groups; the replacement of H with methyl groups in DYE1 results in DYE2. The steric hindrance due to methyl groups result into elongated Ti-O bond when DYE2 is bound to TiO_2, which explains the weaker binding observed for DYE2@TiO_2 system. Worth to note, the DYE3@TiO_2 can be formed as the BB complex via the Ti-O and Ti-S bonds as well as the BT complex through the Ti-O, Ti-N and Ti-S bonds. Interestingly the bidentate bridging configuration leads to a more stabilized system than the bridging tridentate configuration by about of 0.32 eV. This additional stabilization of the BB system may be explained by the hydrogen bonding NH···Ti (Fig. 19), which brings a complementary contact with the surface. The importance of hydrogen bond in dyes adsorption with TiO_2 surface was reported earlier (Ambrosio *et al*., 2012; Ji Zhang *et al*., 2018). The monodentate mode generally shows much weaker adsorption energies when compared to the bridging bidentate and the bridging tridentate modes.

Overall, among the seven anchoring groups, the cyanoacrylic acid (CA-S@TiO_2 and DYE5@TiO_2) and 2-thioxodihydropyrimidine-4,6(1H,5H)-dione (DYE3), lead to the most

stable systems when the dye is adsorbed via the bidentate bridging mode. It is worthy to note that final experimental studies on other materials except the CA-S and HY-S molecules are pending. In connection with this, it may be noted that the BTZ and thiophene units play a vital role in ICT; therefore, further investigation of other units could improve the optoelectronic properties of novel materials.

4.4 The Influence of Heteroatoms in π-Conjugated Linkers

The structural features of most π-linkers permit facile modification; the alteration of auxiliary π-linker (thiophene) could be the simplest method of tuning a dye spectral properties. Inspired by work (Guo *et al*., 2016), in the previous section, optoelectronic properties of TPA dyes were investigated through variation of π-conjugated units (Deogratias *et al*., 2020). Nevertheless, the role of five-membered auxiliary π-linkers C_4H_4X with varying heteroatom X in the D-π-π-A molecular architecture is not yet fully understood. Thus, in the present section, the focus is paid on the effect of heteroatoms X = O, NH, S, Se or Te in the ring C_4H_4X on optoelectronic properties of methoxy-substituted triphenylamine dyes with cyanoacrylic acid and hydantoin anchoring groups. The molecular structures of the dyes are shown in Fig. 5.

4.4.1 Geometrical Properties

To analyze the geometry of the dye molecules, the most relevant geometrical parameters have been considered (Fig. 20); the optimized values of the selected bond lengths and angles are listed in Table 16.

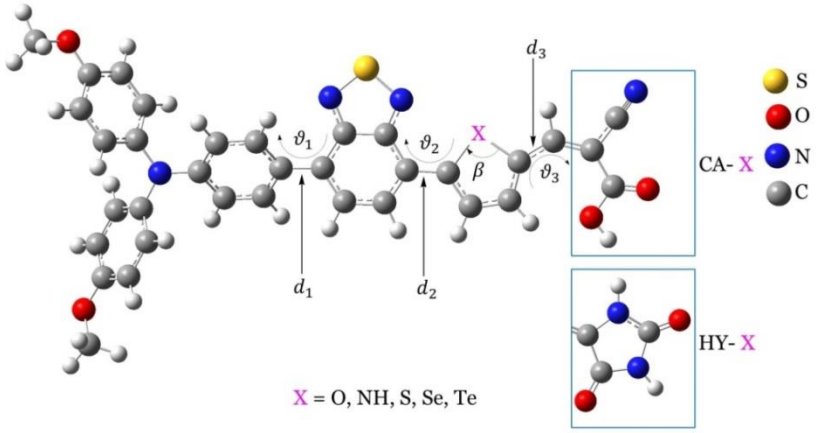

Figure 20: Selected geometrical parameters; bond lengths d_i, bond angle β and dihedral angles ϑi for dye molecules

The variation of heteroatoms leads to a minor change in respective bond distances d_i(C-C) not greater than 0.01 Å; the difference in torsion angles does not exceed 5° for ϑ_1, 8° for ϑ_2 and 11° for ϑ_3. Meanwhile, the valence angle β(C-X-C) changes significantly within either the CA- or HY-group, from 82° (X = Te) to 108 – 111° (X = NH); the angle decreases with the increasing size of the chalcogen atom.

Regarding the TPA moiety, the three phenyl groups are twisted one to another by 52° to 55° while the third phenyl group is twisted by 32° – 36° with the rest part of the molecule. This morphology is favourable since the self-aggregation of dyes would be effectively suppressed.

Table 16: Selected geometrical parameters for the studied dyes, the bond distance (Å) and angles (°)

Dyes	d_1	d_2	d_3	ϑ_1	ϑ_2	ϑ_3	β
CA-O	1.470	1.447	1.415	33.7	3.6	0.5	108.7
CA-NH	1.472	1.453	1.416	34.3	0.2	0.5	111.2
CA-S	1.470	1.455	1.425	32.2	0.3	1.6	92.6
CA-Se	1.469	1.450	1.423	31.6	1.3	0.8	88.1
CA-Te	1.469	1.450	1.425	32.9	3.7	11.0	82.1
HY-O	1.474	1.450	1.426	35.8	2.3	0.3	108.4
HY-NH	1.474	1.453	1.429	36.3	0.9	0.3	108.4
HY-S	1.473	1.458	1.435	35.6	7.6	0.3	92.4
HY-Se	1.473	1.454	1.433	35.1	2.6	0.0	88.0
HY-Te	1.473	1.453	1.435	34.3	1.1	0.2	82.1

4.4.2 Frontier Molecular Orbitals

Frontier molecular orbitals of a sensitizer play a vital role in describing intra- and intermolecular charge transfer processes in a DSSC. The maximum absorption wavelength λ_{max}^{abs} corresponds to the vertical excitation from the ground S_0 to the first excited-state S_1 where electron transition from HOMO to LUMO contributes mostly (Liu *et al*., 2019b). Graphical representation of the electron density distributions over frontier orbitals, HOMO and LUMO, is shown in Fig. 21. The HOMO electron density is predominantly delocalized over the TPA unit (donor part) for all molecules. Comparing the HOMOs of the cyanoacrylic acid and hydantoin dyes, the latter possess more expanded electron density distribution over the dye molecule. The LUMOs are spread over acceptors and π-linkers; only a few traces can be found on the TPA fragment. The LUMOs are delocalized over the acceptor fragment should result in stronger dye-semiconductor electronic coupling leading to efficient electron injection (Ho & Wong, 2016). While transition occurs from HOMO to LUMO, the electron density transfers from the triphenylamine unit to the π-conjugate bridge direction, which is

beneficial for charge injection from the dye to the semiconductor. To understand in detail the HOMO and LUMO distributions over different parts of the molecule, the structure was subdivided into four fragments; namely, TPA, BTZ, π-bridge and cyanoacrylic acid or hydantoin anchoring group (Fig. 5) and the contribution from each fragment to the HOMO and LUMO counted as shown in Fig. 22 and also in Table 17 and Table 18.

Table 17: The percentage fragment contribution to the highest occupied molecular orbitals and lowest unoccupied molecular orbitals of cyanoacrylic acid dyes computed for chloroform

Fragment	CA-O		CA-NH		CA-S		CA-Se		CA-Te	
	HOMO	LUMO	HOMO	LUMO	HOMO	LUMO	HOMO	LUMO	HOMO	LUMO
TPA	85.13	7.43	83.99	6.76	84.94	7.27	84.07	7.54	83.91	7.24
BTZ	9.27	48.65	9.40	69.16	9.42	46.68	9.62	47.47	9.33	48.19
π-bridge	3.15	17.13	3.72	8.89	3.40	21.97	3.87	22.78	4.26	22.09
CA	2.45	26.79	2.89	15.19	2.25	24.07	2.44	22.21	2.50	22.48

Table 18: The percentage fragment contribution to the highest occupied molecular orbitals and lowest unoccupied molecular orbitals of HY dyes computed for chloroform

Fragment	HY-O		HY-NH		HY-S		HY-Se		HY-Te	
	HOMO	LUMO	HOMO	HOMO	HOMO	LUMO	HOMO	LUMO	HOMO	LUMO
TPA	77.19	6.24	67.73	67.73	78.81	6.04	77.18	6.04	76.52	6.11
BTZ	11.00	65.90	12.26	12.26	10.91	62.40	11.17	61.86	10.94	61.43
π-bridge	7.00	10.02	11.89	11.89	6.13	14.19	6.99	15.32	7.59	16.05
HY	4.80	17.84	8.12	8.12	4.16	17.36	4.66	16.78	4.95	16.4

One can observe that the contribution to the HOMO originates mostly from the TPA unit followed by BTZ, π-bridge and the anchoring group. The cyanoacrylic acid dyes possess higher HOMO composition (84 – 85%) for the TPA unit compared to hydantoin dyes (68 – 79%) and the HOMOs occupy not only TPA but also other parts of the molecule. The observed overlap on BTZ and π-bridge in hydantoin dyes is of interest as is expected to facilitate charge evolution from HOMO to LUMO (Wazzan, 2019).

Regarding the LUMO composition, the BTZ unit contributes in the main (47 – 70%) among the three parts of the acceptor, whereas the anchoring group brings less (10 – 30%), with the lowest percentage in the pyrrole dyes; a signal that these dyes may not exhibit efficient charges injection to the semiconductor. The observed spatially well-separated electron

density between HOMO and LUMO is expected to hinder electron-hole recombination, which results in efficient ICT upon photoexcitation (Wang *et al*., 2014).

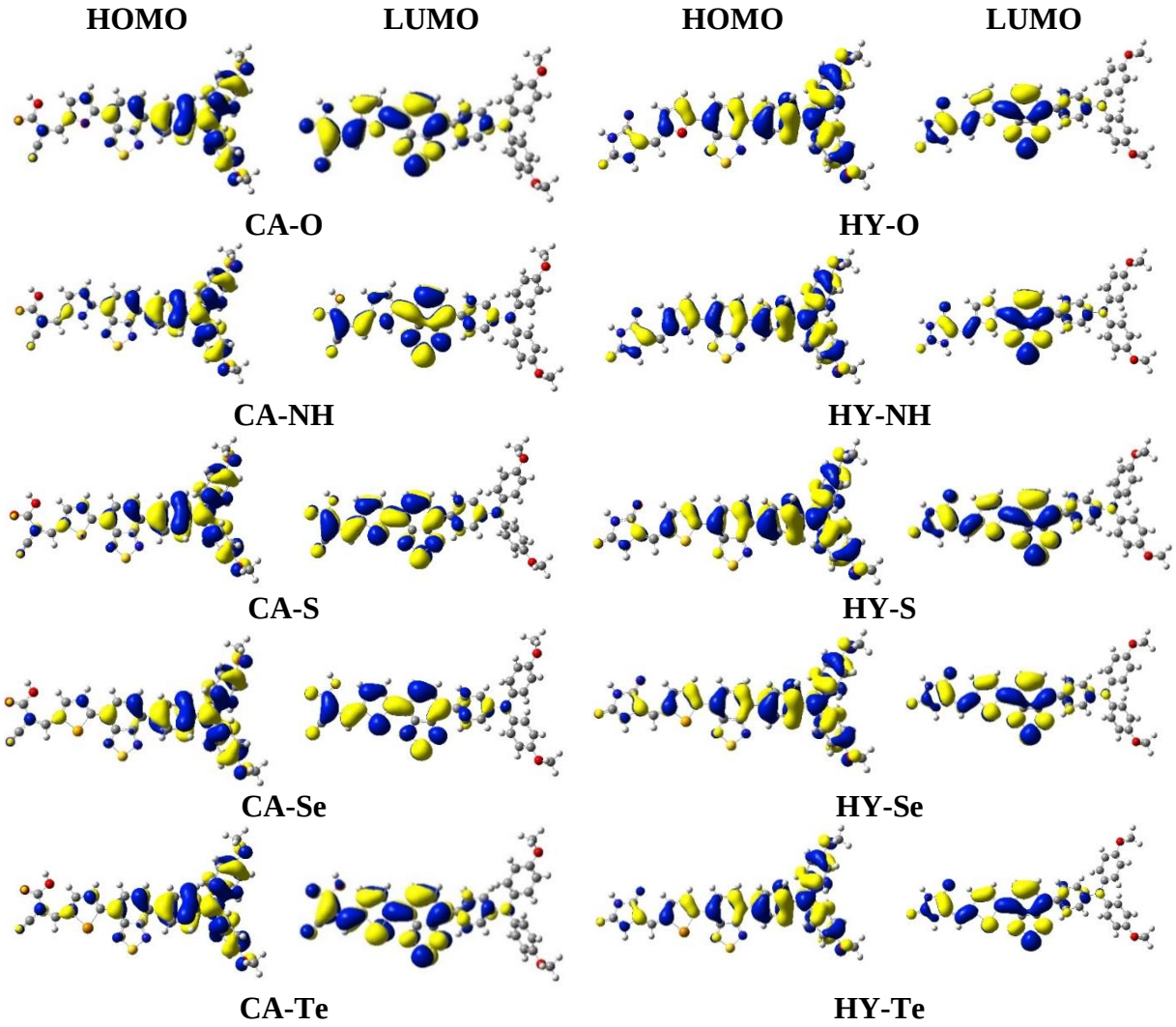

Figure 21: Frontier molecular orbitals HOMO and LUMO of the dye molecules calculated using CAM-B3LYP/6-31+G(d,p) with PCM, chloroform solvent

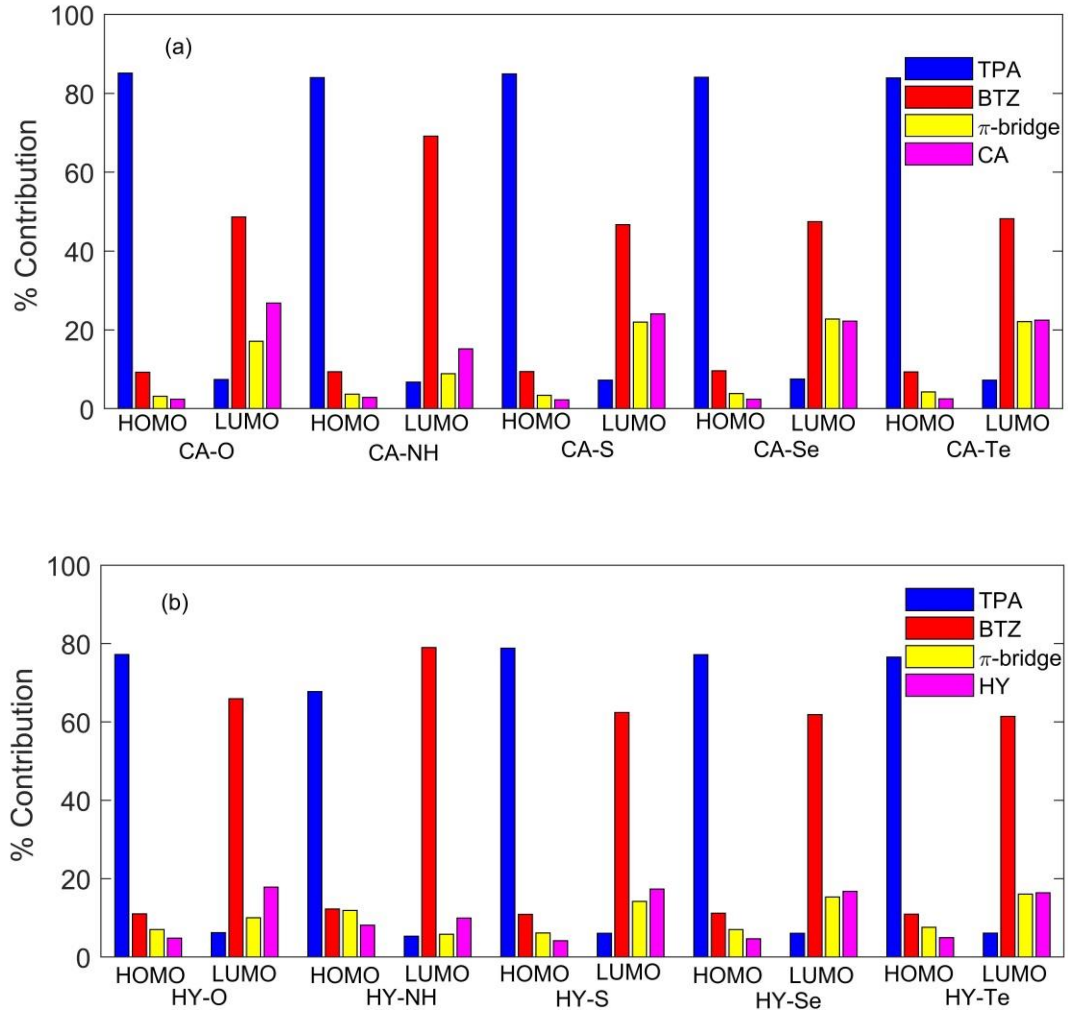

Figure 22: The percentage fragment contribution to the HOMO and LUMO orbitals computed at CAM-B3LYP/6-31G+(d,p) with PCM, chloroform solvent: (a) cyanoacrylic acid-based dyes, (b) hydantoin based dyes

4.4.3 Absorption and Emission Electronic Spectra

Among the drawbacks of metal-free sensitizers is their relatively narrow absorption bands with maxima in the higher energy range (violet or ultra-violet) (Ho & Wong, 2016). Broadly extended spectra in near infra-red regions are of interest to provide good overlap with solar emission spectrum for high photocurrent response. The characteristics of electronic transitions have been explored within the TD-DFT framework. The calculated maximum absorption wavelengths (λ_{max}^{abs}) and emission wavelengths (λ_{max}^{em}), the corresponding oscillator strengths (f_{abs} and f_{em}), transitions assignments and light-harvesting efficiencies (LHE) for the dyes under study are listed in Table 19; the predicted absorption and emission spectra are presented in Fig. 23.

Table 19: Maximum electronic absorption and emission wavelengths, absorption and emission oscillator strengths, light-harvesting efficiencies, major molecular orbital transition contributions of the dyes containing different heteroatoms in the π-linkers for both cyanoacrlic acid and hydantoin anchoring groups calculated for chloroform

Dye	Absorption				Emission		
	λ_{max}^{abs}, nm	f_{abs}	LHE (%)	Contribution (%)	λ_{max}^{em}	f_{em}	Contribution (%)
CA-O	516	1.496	96.8	H→L (60) H-1→L (31)	661	1.804	H←L (66) H-1←L (20)
CA-NH	515	1.304	95.0	H→L (61) H-1→L (30)	667	1.425	H←L (67) H-1←L (18)
CA-S	532	1.508	96.9	H→L (60) H-1→L (33)	666	1.784	H←L (66) H-1←L (21)
CA-Se	545	1.511	96.9	H→L (61) H-1→L (31)	709	1.799	H←L (66) H-1←L (20)
CA-Te	556	1.493	96.8	H→L (60) H→L+1 (12)	732	1.647	H←L (59) H-1←L (11)
HY-O	504	1.424	96.2	H→L (61) H-1→L (31)	637	1.531	H←L (68) H-1←L (15)
HY-NH	526	1.198	93.7	H→L (64) H-1→L (25)	694	1.183	H←L (68) H-1←L (11)
HY-S	510	1.437	96.3	H→L (60) H-1→L (31)	673	1.564	H←L (67) H-1←L (16)
HY-Se	524	1.434	96.3	H→L (61) H-1→L (31)	699	1.551	H←L (67) H-1←L (15)
HY-Te	537	1.429	96.3	H→L (60) H→L+1 (6)	719	1.532	H←L (60) H-1←L (5)

In the absorption spectra, all studied sensitizers exhibit two major bands. The most intensive are seen at around 450 – 600 nm. They correspond to the $S_o \rightarrow S_1$ excitations and originate mainly from HOMO to LUMO transitions. The second bands with lower intensities at 370 – 420 nm correspond to the HOMO-1 → LUMO transitions. Compared to hydantoin dyes, the cyanoacrylic acid counterparts show slightly red-shifted electronic spectra (maximum by 22 nm), except the molecules containing the pyrrole unit. From the observed small differences in the λ_{max}^{abs}, it is anticipated that hydantoin dyes exhibit competitive characteristics to cyanoacrylic acid analogues. As for the hetero-units impact, the tellurophene dyes exhibit the first band position at longest wavelength followed by selenophene dyes. Worth to mention, our results λ_{max}^{abs} for the two dyes, CA-S 532 nm and HY-S 510 nm, corroborate well with respective experimental findings, 522 and 515 nm (Guo *et al*., 2016).

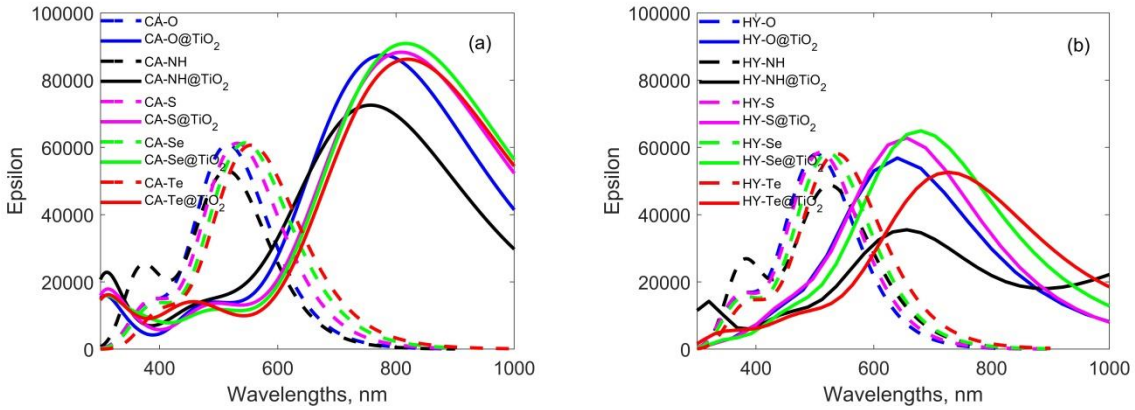

Figure 23: The simulated UV-Vis absorption and emission spectra for (a) cyanoacrylic acid dyes and (b) hydantoin dyes, calculated at CAM-B3LYP/6-31+G(d,p)/LANL2DZ with PCM (chloroform)

Absorption bands in near IR region of the electronic spectra are associated with low excitation energies E_x which correlate with energy gaps E_g (Table 20), the lower energy gaps are expected to favour ICT. Generally, the electronegativity of central atom among the heterocycles decreases in the following order furan > pyrrole > thiophene > selenophene > tellurophene (Fringuelli *et al*., 1977). In this work, it has been found that the E_g values decrease with decrease in electronegativity of the heteroatoms. Therefore, the dyes containing tellurophene, selenophene and thiophene π-linkers are regarded as the best due to most red-shifted absorption maxima.

As for emission spectra, they demonstrate similar to absorption spectra trends (Fig. 23). The studied sensitizers show maximum emission wavelengths 637 − 732 nm. Thus the maxima are shifted by ~130 – 180 nm regarding the absorption maxima. This bathochromic shift is typical for the TPA-based dyes (Li *et al*., 2020; Tan *et al*., 2013; Zhang *et al*., 2019). The observed larger Stokes shifts are due to stronger ICT effect. The bathochromic emission can be easily perceived for tellurophene sensitizers relative to other dyes with λ_{max}^{em} = 732 and 719 nm for CA-Te and HY-Te dyes, respectively. In general, both anchoring groups and π-linkers can be accounted for the observed differences in the emission spectra between the dyes.

The larger the *f* values, the larger the LHEs, which are expected to improve the performance of the DSSCs. The calculated f_{abs} for the studied dyes are well above a unit and the corresponding LHEs ranging between 94% and 97%. Both cyanoacrylic acid and hydantoin dyes containing pyrrole units demonstrate the least LHEs in each dye series.

4.4.4 Intramolecular Charge Transfer Characteristics

The key parameters for efficient charge injection and dye regeneration include GSOP and ESOP. Experiences have shown that for efficient charge injection into the CB and subsequent dye regeneration, the difference between a dye ESOP and semiconductor CB (that is the free energy of charge injection ΔG_{inj}) should be at least ~0.2 eV (by magnitude) while the difference between the dye GSOP and electrolyte redox couple (free energy of dye regeneration ΔG_{reg}) should be at least ~0.4 eV (Pastore *et al*., 2010; Wei *et al*., 2016; Zanjanchi & Beheshtian, 2019). The values of GSOP, ESOP, E_x and ΔG_{inj} and ΔG_{reg} are displayed in Table 20.

Table 20: The ground and excited-state potentials, free energies of charge injection and dye regeneration and energy gaps of the dyes containing different heteroatoms in the π-linkers for both cyanoacrlic acid and hydantoin anchoring groups, all values in eV

Dye	$-E_{ox}^{dye}$	$-E_{ox}^{dye*}$	E_x	$-\Delta G_{inj}$	$-\Delta G_{reg}$	E_g
CA-O	6.35	3.95	2.40	0.10	1.55	4.08
CA-NH	6.33	3.93	2.41	0.12	1.53	4.16
CA-S	6.35	4.02	2.33	0.03	1.55	3.98
CA-Se	6.35	4.08	2.28	−0.03	1.55	3.92
CA-Te	6.34	4.10	2.23	−0.05	1.54	3.88
HY-O	6.24	3.77	2.46	0.28	1.44	4.30
HY-NH	6.17	3.82	2.36	0.23	1.37	4.24
HY-S	6.25	3.82	2.43	0.23	1.45	4.23
HY-Se	6.25	3.88	2.37	0.17	1.45	4.17
HY-Te	6.22	3.91	2.31	0.14	1.42	4.10

By considering the calculated values of ΔG_{inj} and ΔG_{reg}, they are affected more by anchoring groups than heteroatoms. For all molecules, except CA-Se and CA-Te, the ΔG_{inj} values are negative, indicating that charge injection from excited-state proceeds spontaneously. It is worth noting that the ΔG_{inj} values for hydantoin dyes are more negative when compared with cyanoacrylic acid counterparts, for which the absolute values of ΔG_{inj} are less than 0.12 eV. In each series of dyes (cyanoacrylic acid or HY), the same ΔG_{reg} values are seen with a mean value around −1.5 eV for cyanoacrylic acid and –1.4 eV for hydantoin dyes. The negative values of ΔG_{reg} indicate that dye regeneration is predicted to be spontaneous.

Figure 24 shows the energy level diagram of frontier and adjacent MOs together with the conduction band E_{CB} of TiO_2 and redox potential of electrolyte I^-/I_3^-. One can observe that all investigated sensitizers exhibited ESOPs very close to the CB of TiO_2 and the HOMO

energy levels are lower than the redox potential of I^-/I_3^- electrolyte. The inclusion of Se or Te in cyanoacrylic acid and hydantoin dyes results in the shift of ESOP closer to the CB of TiO_2. The GSOPs of cyanoacrylic acid dyes parameters are more negative and deeper by 0.10 – 0.16 eV than those of hydantoin dyes.

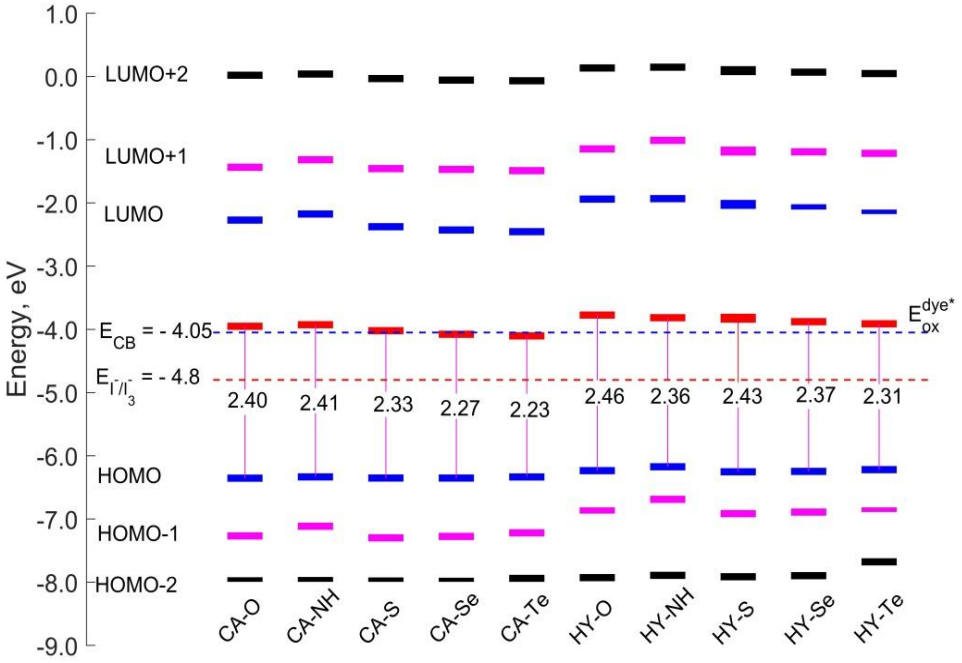

Figure 24: Energy level alignment diagram for the dyes with the TiO_2 conduction band and electrolyte redox potential

ICT characteristics include IPs and EAs, EEPs, HEPs and internal reorganization energies (λ_{int}), which are essential for evaluating the charge injection properties of sensitizers. The lower IP and higher EA values promote holes and electrons injection, respectively. The calculated ICT parameters are listed in Table 21. The vertical IP and EA for cyanoacrylic acid dyes are found within 5.25 – 5.28 eV and 3.02 – 3.27 eV, while those of hydantoin dyes are 5.09 – 5.16 eV and 2.78 – 2.96 eV, respectively. Similarly, a small variation was noted for adiabatic IP and EA; hydantoin dyes show lower ionization potentials and lower EAs than cyanoacrylic acid dyes. The calculated HEP values are found to be 0.18 – 0.19 eV and the EEP 0.11 – 0.13 eV. Furthermore, HY-dyes demonstrate higher hardness than CA-dyes by about 0.1 eV.

Based on the Marcus electron transfer theory (Anderson & Lian, 2005; Marcus, 1965), the rate constant for charge transfer kinetics is higher for a smaller value of reorganization energy

(Tripathi & Prabhakar, 2020). From the calculated hole (λ_{hole}), electron (λ_{elec}) and internal ($\lambda_{int} = \lambda_{hole} + \lambda_{elec}$) reorganization energies Table 21, the $\lambda_{hole} < \lambda_{elec}$, the bigger differences between λ_{hole} and λ_{elec} were observed for hydantoin dyes. Thus the hydantoin dyes are expected to demonstrate higher holes mobility than that for electrons. Thus, it is predicted that hydantoin dyes with λ_{int} 0.45 – 0.49 eV, might yield a bit higher PCE than cyanoacrylic acid counterparts with λ_{int} 0.49 – 0.53 eV.

Table 21: Reorganization energies, adiabatic and vertical ionization potentials and electron affinities, hole and electron extraction potentials and hardness of the eight investigated dyes as calculated for chloroform solvent, all values in eV

Dye	Hole transfer				Electron transfer				λ_{int}	h
	λ_{hole}	AIP	VIP	HEP	λ_{elec}	AEA	VEA	EEP		
CA-O	0.26	5.13	5.27	0.18	0.27	3.25	3.12	0.13	0.53	0.94
CA-NH	0.24	5.12	5.25	0.18	0.27	3.15	3.02	0.12	0.51	0.98
CA-S	0.25	5.14	5.27	0.19	0.26	3.33	3.20	0.13	0.51	0.91
CA-Se	0.25	5.14	5.28	0.19	0.26	3.37	3.24	0.13	0.51	0.89
CA-Te	0.23	5.14	5.26	0.19	0.27	3.40	3.27	0.13	0.50	0.87
HY-O	0.20	5.03	5.14	0.18	0.29	2.94	2.80	0.11	0.49	1.05
HY-NH	0.19	4.99	5.09	0.18	0.29	2.92	2.78	0.11	0.48	1.04
HY-S	0.21	5.04	5.16	0.18	0.28	3.02	2.87	0.12	0.49	1.01
HY-Se	0.21	5.04	5.15	0.18	0.28	3.06	2.92	0.12	0.49	0.99
HY-Te	0.18	5.03	5.13	0.18	0.27	3.09	2.96	0.12	0.45	0.97

$$\lambda_{int} = \lambda_{hole} + \lambda_{elec}$$

4.4.5 Adsorption Characteristics and Binding Energies

The suggested model of the dye adsorption on the TiO_2 surface comprises the hydrogen atom detachment from the anchoring group and binding of the dehydrogenated dye to the TiO_2 cluster (Fig. 25). In the case of the cyanoacrylic acid molecules, the H atom is separated from the carboxylic unit and the dye links to TiO_2 through two oxygen atoms (Fig. 25a). In the case of hydantoin dyes, the H atom detachment occurs from the hydantoin unit's cyclic nitrogen and the dye is adsorbed to TiO_2 through its acyclic ketonic oxygen and cyclic nitrogen (Fig. 25b). The bidentate adsorption was found to be more stable among possible adsorption modes (mono-, bidentate bridging or chelating) (Ji Zhang *et al*., 2018). Thus, in our work, the bidentate bridging mode was considered for the attachment of the dye to the TiO_2 cluster (Fig. 25d).

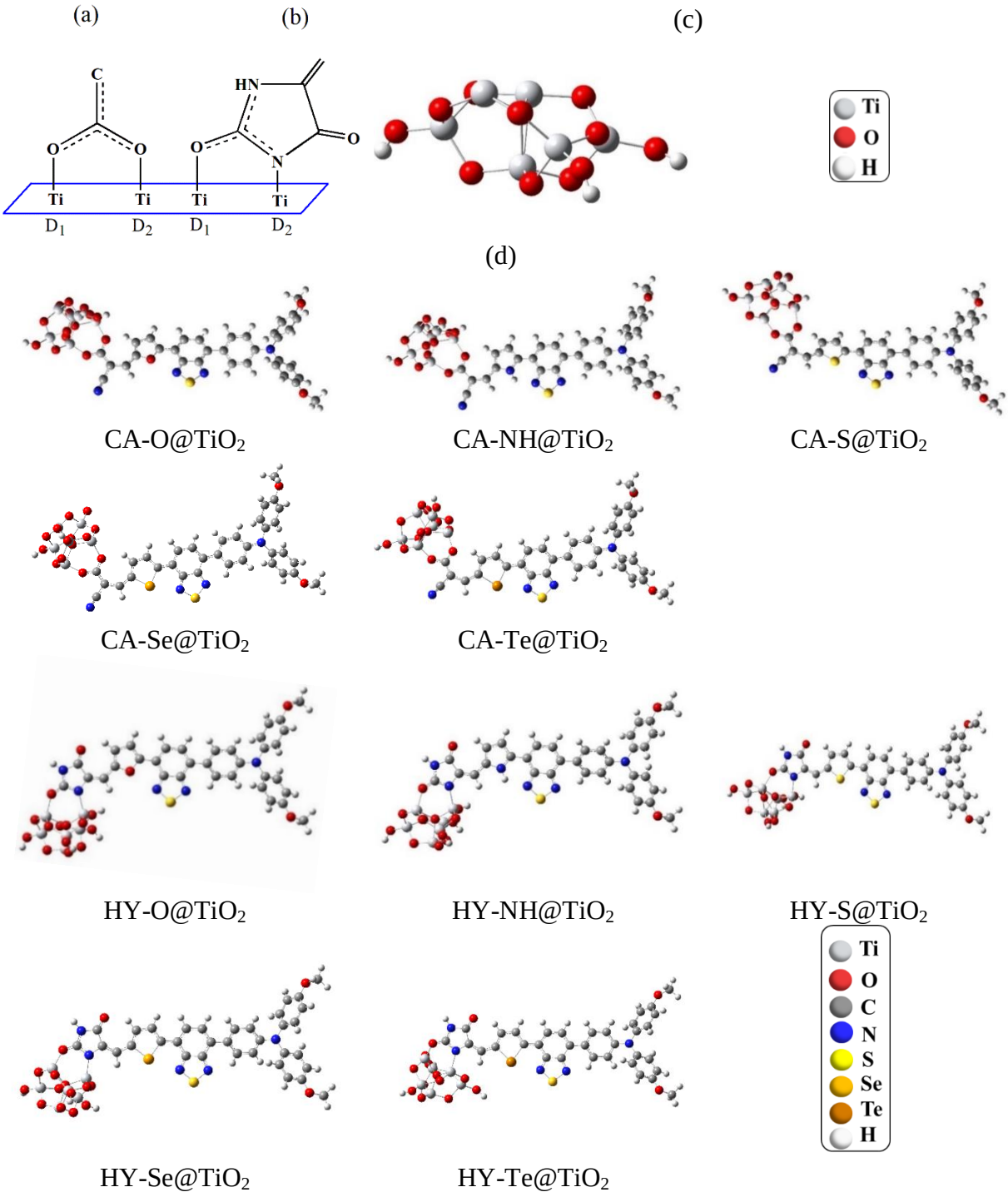

Figure 25: The dyes attachment to the TiO_2 cluster: the bidentate adsorption modes of cyanoacrylic (a) and imidazolidine (b) anchoring groups; the optimized structure of TiO_2 cluster (c); and the optimized dye@TiO_2 systems (d) computed at the B3LYP/6-31+G(d,p)/LANL2DZ level

The energy of the TiO_2 cluster was found to be –1253.5146 au and of hydrogen atom −0.5003 au. The calculated binding energies are displayed in Table 22. All binding energies are negative, indicating that the dye's attachment to the TiO_2 cluster is thermodynamically favourable.

Table 22: The bond distances, electronic energies of free dyes and dye-TiO_2 systems and the binding energies of the studied systems computed for chloroform

System	D_1, Å	D_2, Å	$-E_{dye}$, au	$-E_{dye@TiO_2}$, au	−BE, eV
CA-O@TiO_2	2.048	1.919	2303.4420	3556.7619	8.32
CA-NH@TiO_2	1.882	1.854	2283.6007	3536.9216	8.34
CA-S@TiO_2	1.902	1.833	2626.4133	3879.7312	8.26
CA-Se@TiO_2	1.907	1.830	2237.3978	3490.7567	9.38
CA-Te@TiO_2	1.887	1.835	2236.2187	3489.5813	9.48
HY-O@TiO_2	1.929	2.091	2358.8527	3612.1489	7.67
HY-NH@TiO_2	1.962	2.105	2339.0089	3592.3091	7.78
HY-S@TiO_2	1.929	2.076	2681.8248	3935.1189	7.61
HY-Se@TiO_2	1.927	2.076	2292.8090	3546.1431	8.70
HY-Te@TiO_2	1.963	2.085	2291.6293	3544.9641	8.72

The BE magnitudes change from 8.26 to 9.48 eV for the CA-dye@TiO_2 and from 7.61 to 8.72 eV for the HY-dye@TiO_2 complexes. Thus, the cyanoacrylic acid dyes exhibit stronger attachment to the TiO_2 clusters by 0.56 – 0.76 eV compared with the respective hydantoin dyes. Our binding energies for CA-S@TiO_2 −8.26 eV and HY-S@TiO_2 −7.62 eV accord well with available data in the literature, −8.15 eV and −8.02 eV, respectively (Ji Zhang *et al*., 2018). The observed minor discrepancies are probably due to different models of anatase TiO_2 cluster considered in this work and in Zhang *et al*. (2018).

The bidentate bridging coordination between the dye and TiO_2 is also specified with the bond lengths D_1(Ti-O/all dyes) and D_2(Ti-O/CA-dyes, Ti-N for hydantoin dyes (Fig. 25a-b, Table 22). The CA@TiO_2 complexes exhibit shorter bond lengths than those of corresponding HY@TiO_2 complexes except for furan-containing dyes. It is also worthy to note that in most cases, the BE values correlate well with the bond lengths D_1 and D_2. The binding energies of the dyes@TiO_2 complexes are compared in the histogram representation (Fig. 26). In both types of dyes, the BE's magnitudes vary along the series of heteroatoms being minimal for sulfur followed by a steep increase for the Se and Te. A simple Columbic model was attempted to explain the trends. The Mulliken atomic charges of oxygen, nitrogen and titanium involved in bonding (Table 23) and the distances D_1 and D_2 (Table 22) were considered.

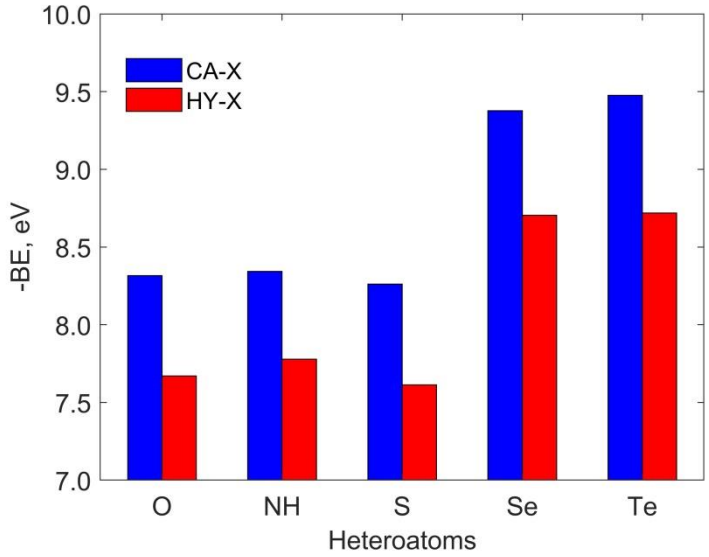

Figure 26: The binding energies of the dyes attached to the TiO_2 cluster as computed at the B3LYP/6-31+G(d,p)/LANL2DZ level for chloroform

It appeared the electrostatic energies obtained do not reproduce the trends in the BE values that implies a more complicated mechanism of interaction involving higher-order multipole moments both of ground and excited-states of the systems may take place. Nevertheless, the binding energy behaviour surprisingly concurs with the variation of charges *q*(X) in Table 23.

Table 23: Mulliken charges analysis of the most relevant elements used in heterocyclic units

Atom X	CA@TiO_2	HY@TiO_2	CA@TiO_2				HY@TiO_2			
			Ti−O				Ti−O/Ti-N			
	q(X)	q(X)	q_1(O)	q_2(O)	q_1(Ti)	q_2(Ti)	q_1(O)	q_2(N)	q_1(Ti)	q_2(Ti)
O	−0.178	−0.212	−0.602	−0.471	1.445	1.587	−0.551	−0.461	1.527	1.428
N	−0.129	−0.108	−0.550	−0.450	1.533	1.646	−0.5770	−0.444	1.468	1.358
S	−0.208	−0.220	−0.608	−0.438	1.599	1.671	−0.547	−0.455	1.549	1.455
Se	0.664	0.655	−0.622	−0.437	1.590	1.678	−0.542	−0.542	1.551	1.438
Te	0.866	0.868	−0.567	−0.458	1.534	1.639	−0.569	−0.442	1.407	1.404

The q(X) trend in the series O – N – S – Se – Te reflects decreasing of the electron withdraw ability and thus increasing polarizability of the heteroatoms that may favour the ICT towards the anchoring group and hence strengthening the dye-TiO_2 bonding.

Two TiO_2 models, namely the anatase (101) slab and $(TiO_2)_6$ cluster, were considered for sensitizer adsorption. The two dyes (CA-S and HY-S) were adsorbed on each TiO_2 adsorption model and the binding energies were calculated. The calculated binding energies for cluster complexes were higher in magnitude than those of the TiO_2 slab complexes. To

account for the bigger differences observed, enthalpies of formation for the slab and cluster were used to evaluate the enthalpy of sublimation. The $\Delta_f H°$(c, TiO_2 anatase, 0) = –935.5 kJ mol^{-1} and $\Delta_f H°$(g, TiO_2, 0) = –320 kJ mol^{-} (Gurvich *et al.*, 1992); hence the sublimation enthalpy is $\Delta_s H°(TiO_2, 0)$ = 615.5 kJ mol^{-1} = 6.38 eV. This value coincides with the difference between the two adsorption models (slab and cluster) for CA-S (eV) and HY-S (6.38 eV) complexes. Worth to mention, the $(TiO_2)_6$ cluster calculation converges much faster than TiO_2 anatase (101) slab.

4.4.6 Optical and Electronic Properties

The electronic absorption spectra of the dye@TiO_2 systems have been investigated at the TD-CAM-B3LYP/6-31+G(d,p)/LANL2DZ for the $CHCl_3$ solvent. The computed characteristics of the first electronic excitations, maximum absorption wavelengths (λ_{max}), oscillator strengths (f) and main MO transitions are listed in Table 24.

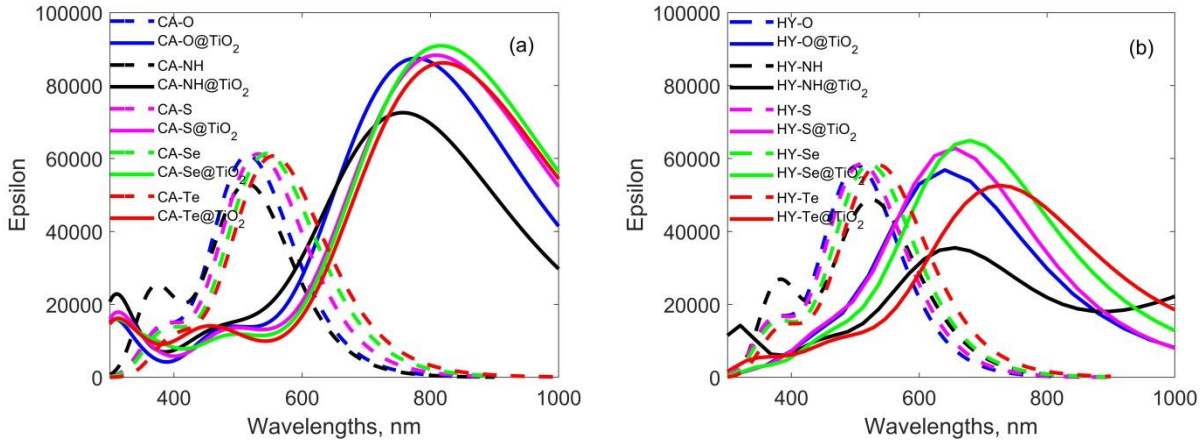

Figure 27: The simulated UV-Vis absorption spectra for (a) cyanoacrylic acid both isolated dyes and complexes; (b) hydantoin both isolated and complexes, calculated at CAM-B3LYP/6-31+G(d,p) with PCM (chloroform)

The complexes exhibit a substantial redshift of electronic spectra with λ_{max} in near/within the infra-red region when compared with isolated dyes (Fig. 27). The shift is more significant for the CA@TiO_2 complexes, ~260 – 280 nm, while for the HY@TiO_2 ~130 – 190 nm. Greater bathochromic shifts are seen for heavier heteroatoms; thus, these findings indicate that replacement of sulfur by selenium or tellurium extends the absorption to lower energy wavelengths.

Table 24: Computed maxima absorption wavelengths, excitation energies, oscillator strengths, light-harvesting efficiencies and major molecular orbital transition contributions for dye-TiO_2 complexes as computed for chloroform solvent

Adsorbed system	λ_{max}, nm	E_x, eV	f	LHE, %	Transition	Contribution, %
CA-O@TiO_2	790	1.57	1.935	98.8	H→L	41
					H→L+1	36
CA-NH@TiO_2	777	1.60	1.551	97.2	H→L	50
					H→L+2	24
CA-S@TiO_2	813	1.53	2.129	99.3	H→L	38
					H→L+1	48
CA-Se@TiO_2	819	1.51	2.215	99.4	H→L	39
					H→L+1	48
CA-Te@TiO_2	822	1.51	2.109	99.2	H→L	41
					H→L+1	43
HY-O@TiO_2	654	1.90	0.388	59.1	H→L+4	25
					H→L+6	43
HY-NH@TiO_2	660	1.88	0.516	69.5	H→L+1	45
					H→L+7	24
HY-S@TiO_2	654	1.90	0.902	87.5	H→L+2	21
					H→L+4	33
HY-Se@TiO_2	711	1.74	0.577	73.5	H-1→L+6	20
					H→L+6	55
HY-Te@TiO_2	718	1.73	0.916	87.9	H-1→L+5	24
					H→L+5	51

In accordance with λ_{max} values, the complexes demonstrate lower excitation energies than corresponding isolated dyes. Regarding the band intensities, the CA@TiO_2 complexes exhibit higher maxima than corresponding isolated dyes, whereas in the spectra of the HY@TiO_2 complexes the band intensities are comparable or less than those of the hydantoin dyes.

Earlier the UV-Vis spectra of pure CA-S and HY-S dye solutions and the dyes adsorbed at the TiO_2 films were measured experimentally (Guo *et al*., 2016); the spectra looked alike and no noticeable change, which might be due to the dye adsorption, was revealed. That implies that in our simulated spectra (Fig. 27), the redshift originates probably from the adopted model of the dye adsorption owing to the dehydrogenated dye binding to the TiO_2 cluster. Thus, it is anticipated that strengthening the dye-TiO_2 bonding will enhance the intermolecular charge transfer and suppress the system's degradation during the DSSC utilization; at the same time broadening and shifting the spectra bands to near IR region should improve the light-harvesting capability.

As for main MO contributions, in the cyanoacrylic acid-TiO_2 dyes complexes, the electronic excitations mostly occur through HOMO → LUMO and HOMO → LUMO + 1 while in the hydantoin-TiO_2 dyes the major transitions involve higher unoccupied orbitals, HOMO →

LUMO + δ (δ = 1, 2, 4, 6 and 7). The charge densities of the frontier and adjacent MOs for the dye@TiO_2 complexes are presented in Fig. 28. In the cyanoacrylic acid systems, the HOMO expands over the TPA and BTZ while LUMO is located on the cyanoacrylic acid anchoring group and TiO_2 cluster. In the hydantoin complexes, the HOMOs are mostly located on the donor group (similar to the cyanoacrylic acid complexes) and the HOMO-1 is delocalized on the entire complex. The electron densities of the unoccupied orbitals are mostly located on the anchoring groups and TiO_2 cluster. Finally, both for CA@TiO_2 and HY@TiO_2, the intermolecular charge transfer is clearly seen to occur from the anchoring groups to the TiO_2 that confirms good abilities of the dyes to sensitize the semiconductor.

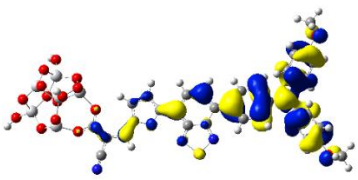

HOMO

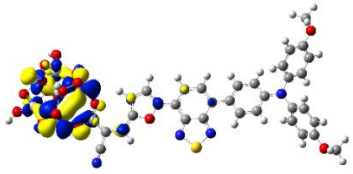

LUMO

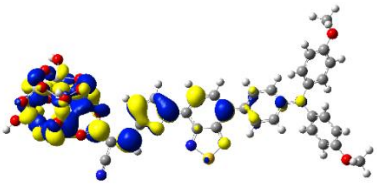

LUMO+1

CA-O@TiO_2

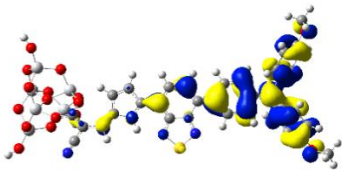

HOMO

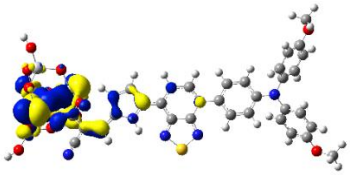

LUMO

LUMO+2

CA-NH@TiO_2

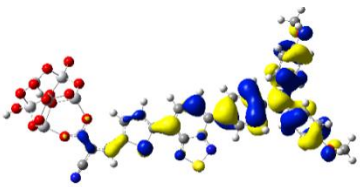

HOMO

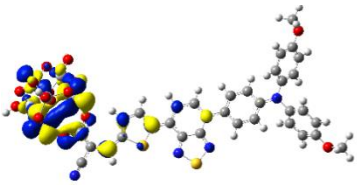

LUMO

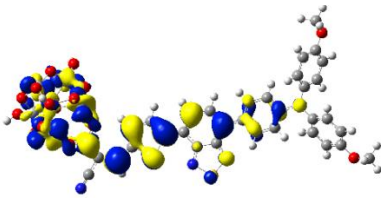

LUMO+1

CA-S@TiO_2

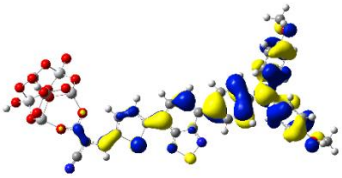

HOMO

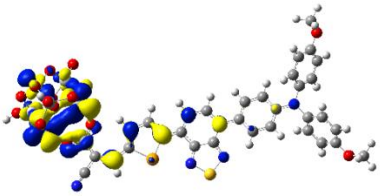

LUMO

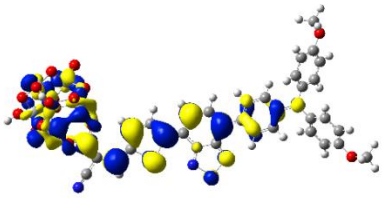

LUMO+1

CA-Se@TiO_2

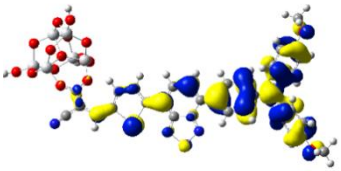

HOMO

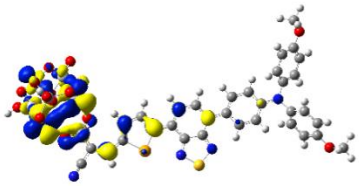

LUMO

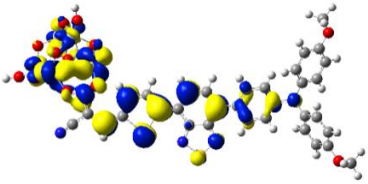

LUMO+1

CA-Te@TiO_2

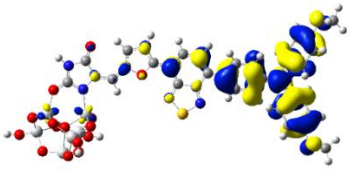

HOMO

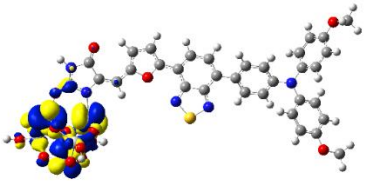

LUMO+4

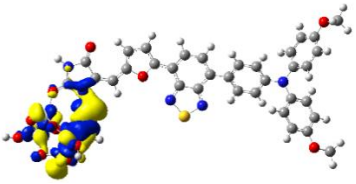

LUMO+6

HY-O@TiO_2

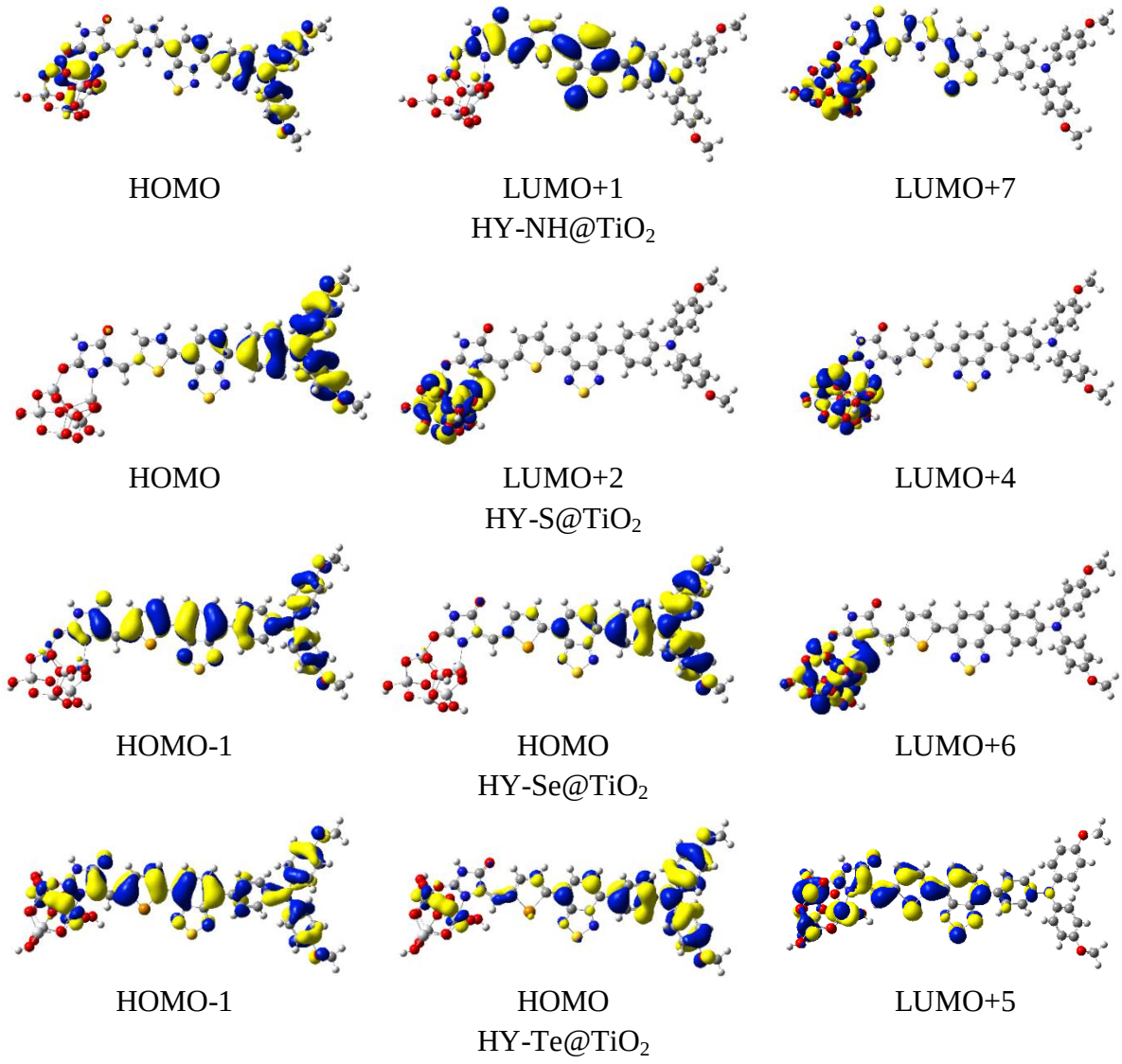

Figure 28: Distribution patterns of the frontier and adjacent molecular orbitals involved into the ground-state to first excited-state transition of the dye-TiO_2 complexes computed for chloroform solvent

CHAPTER FIVE

CONCLUSION AND RECOMMENDATIONS

5.1 Conclusion

Systematic modification of TPA based dyes was performed by using quantum chemical methods towards DSSC applications. The modification was performed on the methoxy substituted TPA by incorporating novel π-linkers and anchoring groups. The π-linkers analogous to Benzothiadiazole, the heterocyclic anchoring groups and the replacement of sulfur of the thiophene by other heteroatoms O, NH, Se and Te have been considered. It is demonstrated that computational approaches can be used to search through a large set of molecules to identify promising candidates for applications by analyzing the optical and electronic properties such as the absorption and emission spectra, chemical reactivity parameters, the intra/inter charge transfer characteristics and binding characteristics to the semiconductor. Through the applied computational approaches it is possible to accelerate the power conversion efficiencies of DSSCs by proposing novel materials to be subjected for experimental investigation, the studies which may result in a more weighted level alignment quality rediscovering. Systematic dye modification and investigation of optoelectronic properties and chemical reactivity parameters by quantum chemistry could help realize high-efficiency DSSCs without sacrificing many resources.

The study on the optoelectronic properties and chemical reactivity parameters obtained from the molecular engineered dyes by adding the π-spacers analogous to Benzothiadiazole showed that:

(i) The geometrical characteristics results in the differences in planarity from unmodified dyes (without π-spacers) to modified dyes. It is predicted that the observed non-planarity decreases the chances of dye aggregation when interacting with the semiconductor.

(ii) For cyanoacrylic acid dyes, the absorption spectrum for modified dyes is red-shifted relative to unmodified dyes, resulting in the improvement of the absorption characteristics. For hydantoin dyes, however, it was noted that the addition of branched π-spacer impairs the characteristics of electronic absorption spectra.

(iii) In general, the presence of nitrogen and sulfur atoms in the added π-spacers had a positive impact on the properties of the materials; in that regard, HY3 displayed poor characteristics of interest compared to HY2 after the replacement of nitrogen atoms (in HY2) by carbon and sulfur atoms. Therefore, it can be confirmed that the presence in the conjugated units of tertiary amine, nitrogen and sulfur increases the ability to donate electrons and enhances the optical and electronic properties, thus favouring electron injection and dye regeneration.

(iv) Although all dyes display comparable free dye regeneration energy, the dyes containing the benzothiadiazole unit exhibit free injection energy closer to the minimum requirement of 0.2 eV and much higher energy is exhibited by the remaining dyes.

(v) Following a thorough study of the geometries, optoelectronic properties and parameters of chemical reactivity, it can be concluded that HY-S, HY2 and HY4 dyes exhibit superior DSSC-interest properties compared to other hydantoin dyes.

Five more dyes (DYE1 − DYE5) containing heterocyclic anchoring groups were designed to investigate the function of heterocyclic anchoring groups. Their geometric, optical and electronic properties were studied, as well as the stability of adsorption when bound to the semiconductor TiO_2.

(i) Various anchoring groups were found to display no pronounced effects on the geometry of the remaining part of the molecules; for the selected geometrical parameters, the only mild variance between the dyes was noted.

(ii) All dyes show sufficient energy level alignment relative to the conduction band of a semiconductor and the redox potential of iodide/tri-iodide; this means that spontaneous charge injection into the conduction band of a semiconductor and dye regenerated can be expected.

(iii) The simulated UV-Vis spectra show intensive maxima in the range of 450 − 600 nm; different anchoring groups influence the maximum location and the most red-shift is observed for the DYE3 dye-containing 2-thioxodihydropyrimidine-4,6(1H,5H)-dione. Generally, the electronic spectrum of the dyes promises to improve the performance of DSSCs in power conversion.

(iv) The studied dyes showed comparable hole generation ability, the hole reorganization energy ranging between 170 – 200 meV; whereas the energy of

electron reorganization can be found between 160 − 380 meV. The dyes DYE2 − DYE5 can be regarded as candidates for ambipolar charge transport.

(v) The calculated binding energies reveal that dyes adsorption on semiconductor's surface is thermodynamically favourable. The bidentate binding mode provides greater stability than the mono- and tridentate modes of the CA-S@TiO_2, DYE3@TiO_2 and DYE5 @TiO_2. The decreasing trend of binding stability on TiO_2 is CA-S (BB), DYE5 (BB), DYE3 (BB), DYE3 (BT), HY-S (M), DYE5 (M), DYE1 (M), DYE2 (M), CA-S (M) and DYE4 (M).

By the variation of five-membered heterocycles (furan, pyrrole, thiophene, selenophene and tellurophene) as auxiliary π-linkers, the triphenylamine-based dyes have been modified while retaining the two anchoring groups cyanoacrylic acid and hydantoin.

(i) The UV-Vis spectra, the CA-X molecules and their respective HY-X equivalents (where X = O, NH, S, Se and Te) exhibit competitive features with a minor redshift for the former.

(ii) All dyes, except CA-Se and CA-Te, which have an excited-state oxidation potential below the CB, exhibit sufficient energy level alignment with the TiO_2 semiconductor conduction band. Hydantoin-based dyes display superior free charge injection energy, whereas both HY-X and CA-X display comparable free dye regeneration energy.

(iii) Because of lower reorganization energies, the HY-X dyes are expected to exhibit higher electron transfer rates.

(iv) The dyes attachment to the $(TiO_2)_6$ cluster has been simulated; the calculated binding energies demonstrate similar trends for CA-X@TiO_2 and HY-X@TiO_2 complexes with a minimum for X = S followed by a steep increase for X = Se, Te; in addition, the CA-X dyes consistently exhibit stronger binding to the TiO_2 than HY-X. The UV-Vis spectra of the dye@TiO_2 systems have shown an essential redshift up to 280 nm compared with the spectra of individual dyes.

(v) Generally, optoelectronic properties are enhanced with a decrease in heteroatomic electronegativity, so dyes containing Se and Te are considered to be among the best dyes.

5.2 Recommendations

The computed optoelectronic properties indicate that the designed sensitizers may contribute to the improvement of dye-sensitized solar cell power conversion efficiency. Despite the findings presented in this work, further study may be carried out and the following are the recommendations:

(i) In the current research, π-linkers and anchoring groups were considered to enhance TPA dyes' optical and electronic nature. It is proposed that methoxy substitution with other classes of electron donors can be performed to increase the density of the charge.

(ii) The variation of heteroatoms on the five-membered ring heterocycle was carried out in this analysis by replacing thiophene with furan, pyrrole, selenophene and tellurophene and it is proposed that O, NH, Se and Te can be used to replace S of BTZ.

(iii) Simultaneous substitution of S by O, NH, Se and Te for the S of both BTZ and thiophene can be performed in accordance with the recommendation (ii).

(iv) Finally, experimental studies are proposed for engineered materials exhibiting promising optoelectronic properties in addition to CA-S and HY-S dyes and possible candidates include HY2, HY4, DYE1-DYE5, CA-X and HY-X (X = O, NH, Se and Te).

REFERENCES

Adamo, C., & Barone, V. (1998). Exchange functionals with improved long-range behavior and adiabatic connection methods without adjustable parameters: The *m*PW and *m*PW1PW models. *The Journal of Chemical Physics, 108*(2), 664-675. https://doi.org/10.1063/1.475428

Agarwala, P., & Kabra, D. (2017). A review on triphenylamine (TPA) based organic hole transport materials (HTMs) for dye-sensitized solar cells (DSSCs) and perovskite solar cells (PSCs): Evolution and molecular engineering. *Journal of Materials Chemistry A, 5*(4), 1348-1373. https://doi.org/10.1039/C6TA08449D

Ahmed, F., Al Amin, A. Q., Hasanuzzaman, M., & Saidur, R. (2013). Alternative energy resources in Bangladesh and future prospect. *Renewable and Sustainable Energy Reviews, 25,* 698-707. https://doi.org/10.1016/j.rser.2013.05.008

Al-Qurashi, O. S., Wazzan, N. A., & Obot, I. (2020). Exploring the effect of mono-and di-fluorinated triphenylamine-based molecules as electron donors for dye-sensitised solar cells. *Molecular Simulation, 46*(1), 41-53. https://doi.org/10.1080/08927022.2019.1668561

Ambrosio, F., Martsinovich, N., & Troisi, A. (2012). What is the best anchoring group for a dye in a dye-sensitized solar cell? *The Journal of Physical Chemistry Letters, 3*(11), 1531-1535. https://doi.org/10.1021/jz300520p

Anderson, N. A., & Lian, T. (2005). Ultrafast electron transfer at the molecule-semiconductor nanoparticle interface. *Annual Review* of *Physical Chemistry, 56*, 491-519. https://doi.org/10.1146/annurev.physchem.55.091602.094347

Andreoni, W., & Yip, S. (2020). *Theory and Methods for Materials Modeling: An Introduction.* In W. Andreoni & S. Yip (Eds.), Handbook of Materials Modeling: Methods: Theory and Modeling (pp. 3-12). Springer International Publishing. https://doi.org/10.1007/978-3-319-44677-6_106

Arkan, F., & Izadyar, M. (2018). Recent theoretical progress in the organic/metal-organic sensitizers as the free dyes, dye/TiO_2 and dye/electrolyte systems; Structural modifications and solvent effects on their performance. *Renewable and Sustainable Energy Reviews, 94*, 609-655. https://doi.org/10.1016/j.rser.2018.06.054

Arroyo-de Dompablo, M., Morales-García, A., & Taravillo, M. (2011). DFT+ U calculations of crystal lattice, electronic structure and phase stability under pressure of TiO_2 polymorphs. *The Journal of Chemical Physics, 135*(5), 1-10. https:// doi.org /10.1063/1.3617244

Arunkumar, A., Shanavas, S., & Anbarasan, P. M. (2018). First-principles study of efficient phenothiazine-based D-π-A organic sensitizers with various spacers for DSSCs. *Journal of Computational Electronics, 17*(4), 1410-1420. https:// doi.org/ 10.1007/ s10825-018 -1226-5

Balanay, M. P., & Kim, D. H. (2009). Structures and excitation energies of Zn–tetraarylporphyrin analogues: A theoretical study. *Journal of Molecular Structure, 910*(1-3), 20-26. https://doi.org/10.1016/j.theochem. 2009.06.010

Becke, A. D. (1993). Density-functional thermochemistry III. The role of exact exchange. Chem. Phys, *98*(7), 5648-5652. https://doi.org/10.1063/1.464913

Becke, A. D. (1996). Density-functional thermochemistry IV. A new dynamical correlation functional and implications for exact-exchange mixing. *The Journal of Chemical Physics, 104*(3), 1040-1046. https://doi.org/10.1063/1.470829

Bourass, M., Benjelloun, A. T., Benzakour, M., McHarfi, M., Hamidi, M., Bouzzine, S. M., & Bouachrine, M. (2016). DFT and TD-DFT calculation of new thienopyrazine-based small molecules for organic solar cells. *Chemistry Central Journal, 10*(1), 1-11. https://doi.org/10.1186/s13065-016-0216-6

Cerón-Carrasco, J. P., Roy, H. M., Cerezo, J., Jacquemin, D., & Laurent, A. D. (2014). Theoretical insights on the antioxidant activity of edaravone free radical scavengers derivatives. *Chemical Physics Letters, 599*, 73-79. https://doi.org/10.1016/j.cplett. 2014.03.010

Chai, J. D., & Head-Gordon, M. (2008). Long-range corrected hybrid density functionals with damped atom–atom dispersion corrections. *Physical Chemistry Chemical Physics, 10*(44), 6615-6620. https://doi.org/10.1039/B810189B

Chaitanya, K., Ju, X. H., & Heron, B. M. (2014). Theoretical study on the light harvesting efficiency of zinc porphyrin sensitizers for DSSCs. *Royal Society of Chemistry Advances, 4*(51), 26621-26634. https://doi.org/10.1039/C4RA02473G

Chen, C. Y., Wu, S. J., Wu, C. G., Chen, J. G., & Ho, K. C. (2006). A Ruthenium Complex with Superhigh Light-Harvesting Capacity for Dye-Sensitized Solar Cells. *Angewandte Chemie International Edition, 45*(35), 5822-5825. https:// doi.org/10. 1002/ ange. 200601463

Chen, F., Li, X., Hihath, J., Huang, Z., & Tao, N. (2006). Effect of Anchoring Groups on Single-Molecule Conductance: Comparative Study of Thiol-, Amine- and Carboxylic-Acid-Terminated Molecules. *Journal of the American Chemical Society, 128*(49), 15874-15881. https://doi.org/10.1021/ja065864k

Chen, P., Yum, J. H., Angelis, F. D., Mosconi, E., Fantacci, S., Moon, S. J., Baker, R. H., Ko, J., Nazeeruddin, M. K., & Grätzel, M. (2009). High open-circuit voltage solid-state dye-sensitized solar cells with organic dye. *Nano Letters, 9*(6), 2487-2492. https://doi.org/ 10.1021/nl901246g

Chen, Q., Wu, N., Liu, Y., Li, X., & Liu, B. (2016). Twisted coumarin dyes for dye-sensitized solar cells with high photovoltage: adjustment of optical, electrochemical and photovoltaic properties by the molecular structure. *Royal Society of Chemistry Advances, 6*(91), 87969-87977. https://doi.org/10.1039/C6RA17930D

Chermette, H. (1999). Chemical reactivity indexes in density functional theory. *Journal of Computational Chemistry, 20*(1), 129-154. https://doi.org/10.1002/(SICI)1096-987X

Cossi, M., & Barone, V. (2001). Time-dependent density functional theory for molecules in liquid solutions. *The Journal of Chemical Physics, 115*(10), 4708-4717. https://doi. org/10.1063/1.1394921

Cui, Y., Yao, H., Hong, L., Zhang, T., Tang, Y., Lin, B., Xian, K., Gao, B., An, C., Bi, P., Ma, W., & Hou, J. (2020). Organic photovoltaic cell with 17% efficiency and superior processability. *National Science Review, 7*(7), 1239-1246. https://doi.org/10.1093/ nsr/nwz200

Cui, Y., Yao, H., Zhang, J., Zhang, T., Wang, Y., Hong, L., Xian, K., Xu, B., Zhang, S., Peng, J., Wei, Z., Gao, F., & Hou, J. (2019). Over 16% efficiency organic photovoltaic cells enabled by a chlorinated acceptor with increased open-circuit voltages. *Nature Communications, 10*(1), 2515. https://doi.org/10.1038/s41467-019-10351-5

Daltrozzo, E., & Tributsch, H. (1975). On the Mechanism of Spectral Sensitization: Rhodamin B Sensitized Electron Transfer to Zinc Oxide. *19*(6), 308-314. https://pascal-francis. inist.fr/

Davidson, D. J. (2019). Exnovating for a renewable energy transition. *Nature Energy, 4*(4), 254-256. https://doi.org/10.1038/s41560-019-0369-3

De Lima Perini, J. A., Perez-Moya, M., & Nogueira, R. F. P. (2013). Photo-Fenton degradation kinetics of low ciprofloxacin concentration using different iron sources and pH. *Journal of Photochemistry and Photobiology A: Chemistry, 259*, 53-58. https://doi.org/10.1016/ j.jphotochem.2013.03.002

De Souza, J. D. S., De Andrade, L. O. M., Müller, A. V., & Polo, A. S. (2018). *Nanomaterials for Solar Energy Conversion: Dye-Sensitized Solar Cells Based on Ruthenium(II) tris-Heteroleptic Compounds or Natural Dyes*. In F. L. Souza & E. R. Leite (Eds.), Nanoenergy: Nanotechnology Applied for Energy Production (pp. 69-106). Springer International Publishing. https://doi.org/10.1007/978-3-319-62800-4_2

Deogratias, G., Seriani, N., Pogrebnaya, T., & Pogrebnoi, A. (2020). Tuning optoelectronic properties of triphenylamine based dyes through variation of pi-conjugated units and anchoring groups: A DFT/TD-DFT investigation. *Journal of Molecular Graphics and Modelling, 94*, 1-10. https://doi.org/https://doi.org/10.1016/j.jmgm.2019.107480

Deskins, N. A., & Dupuis, M. (2007). Electron transport via polaron hopping in bulk Ti O 2: A density functional theory characterization. *Physical Review B, 75*(19), 19-15. https://doi.org/10.1103/PhysRevB.75.195212

Dhere, N. G. (2007). Toward GW/year of CIGS production within the next decade. *Solar Energy Materials and Solar Cells*, 91(15), 1376-1382. https://doi.org/10.1016/j. solmat.2007.04.003

Ellis, H., Eriksson, S. K., Feldt, S. M., Gabrielsson, E., Lohse, P. W., Lindblad, R., Sun, L., Rensmo, H., Boschloo, G., & Hagfeldt, A. (2013). Linker Unit Modification of Triphenylamine-Based Organic Dyes for Efficient Cobalt Mediated Dye-Sensitized Solar Cells. *The Journal of Physical Chemistry C, 117*(41), 21029-21036. https:// doi.org/ 10.1021/jp403619c

Fahim, Z. M. E., Bouzzine, S. M., Aicha, Y. A., Bouachrine, M., & Hamidi, M. (2018). The bridged effect on the geometric, optoelectronic and charge transfer properties of the triphenylamine–bithiophene-based dyes: A DFT study. *Research on Chemical Intermediates, 44*(3), 2009-2023. https://doi.org/10.1007/s11164-017-3211-1

Feng, S., Sun, Z. Z., & Li, Q. (2019). How to screen a promising anchoring group from heterocyclic components in dye sensitized solar cell:A theoretical investigation. *Electrochimica Acta, 296*, 545-554. https://doi.org/10.1016/j.electacta. 2018.11.090

Ferdowsi, P., Saygili, Y., Zhang, W., Edvinson, T., Kavan, L., Mokhtari, J., Zakeeruddin, S. M., Grätzel, M., & Hagfeldt, A. (2018). Molecular Design of Efficient Organic D–A– –A Dye Featuring Triphenylamine as Donor Fragment for Application in Dye-Sensitized Solar Cells. *Chemistry and Sustainability, Energy and Materials, 11*(2), 494-502. https://doi.org/10.1002/cssc.201701949

Fringuelli, F., Marino, G., & Taticchi, A. (1977). Tellurophene and Related Compounds. In A. R. Katritzky & A. J. Boulton (Eds.). *Advances in Heterocyclic Chemistry*, 21, 119-173). Academic Press. https://doi.org/https://doi.org/10.1016/S0065-2725(08)60731-X

Frisch, M., Trucks, G., Schlegel, H., Scuseria, G., Robb, M., Cheeseman, J., Scalmani, G., Barone, V., Mennucci, B., & Petersson, G. (2009). Gaussian 09; Gaussian, Inc. *Wallingford, CT, 32*, 5648-5652.

Fthenakis, V. M. (2018). *Chapter IV-1-A - Overview of Potential Hazards*. In S. A. Kalogirou (Ed.), McEvoy's Handbook of Photovoltaics (Third Edition) (pp. 1195-1212). Academic Press. https://doi.org/https://doi.org/10.1016/B978-0-12-809921-6. 00035-5

Fujisawa, J. I., Eda, T., & Hanaya, M. (2017). Comparative study of conduction-band and valence-band edges of TiO_2, $SrTiO_3$ and $BaTiO_3$ by ionization potential measurements. *Chemical Physics Letters, 685*, 23-26. https://doi.org/10.1016/j.cplett. 2017.07.031

Galoppini, E. (2004). Linkers for anchoring sensitizers to semiconductor nanoparticles. *Coordination Chemistry Reviews, 248*(13), 1283-1297. https://doi.org/10.1016/j.ccr. 2004.03.016

Gazquez, J. L., Cedillo, A., & Vela, A. (2007). Electrodonating and electroaccepting powers. *The Journal of Physical Chemistry A, 111*(10), 1966-1970. https://doi.org/10.1021/ jp065459f

Gélinas, S., Rao, A., Kumar, A., Smith, S. L., Chin, A. W., Clark, J., van der Poll, T. S., Bazan, G. C., & Friend, R. H. (2014). Ultrafast Long-Range Charge Separation in Organic Semiconductor Photovoltaic Diodes. *Science, 343*(6170), 512-516. https://doi.org /10.1126 /science.1246249

Gerischer, H., Michel-Beyerle, M. E., Rebentrost, F., & Tributsch, H. (1968). Sensitization of charge injection into semiconductors with large band gap. *Electrochimica Acta, 13*(6), 1509-1515. https://doi.org/10.1016/0013-4686(68)80076-3

Graetzel, M., Janssen, R. A. J., Mitzi, D. B., & Sargent, E. H. (2012). Materials interface engineering for solution-processed photovoltaics. *Nature, 488*(7411), 304-312. https:// doi.org/ 10.1038/ nature11476

Granovsky, A. A. (2013). Firefly 8.2.0. http://classic.chem.msu.su /gran/ firefly/index.html

Grätzel, M. (2003). Dye-sensitized solar cells. *Journal of Photochemistry and Photobiology C: Photochemistry Reviews*, *4*(2), 145-153. https://doi.org/10.1016/S1389-5567(03)00026-1

Green, M. A. (2015). Corrigendum to 'Solar cell efficiency tables (version 46)' [Prog. Photovolt: Res. Appl. 2015; 23: 805–812]. *Progress in Photovoltaics: Research and Applications*, 23(9), 1202-1202. https://doi.org/https://doi.org/10.1002/pip.2667

Green, M. A., Dunlop, E. D., Hohl-Ebinger, J., Yoshita, M., Kopidakis, N., & Ho-Baillie, A. W. Y. (2020). Solar cell efficiency tables (Version 55) [https://doi.org/10.1002/pip.3228]. *Progress in Photovoltaics: Research and Applications*, *28*(1), 3-15. https://doi.org/10.1002/pip.3228

Grimme, S., Ehrlich, S., & Goerigk, L. (2011). Effect of the damping function in dispersion corrected density functional theory. *Journal of Computational Chemistry*, *32*(7), 1456-1465. https://doi.org/10.1002/jcc.21759

Guo, F. L., Li, Z. Q., Liu, X. P., Zhou, L., Kong, F. T., Chen, W. C., & Dai, S. Y. (2016). Metal-Free Sensitizers Containing Hydantoin Acceptor as High Performance Anchoring Group for Dye-Sensitized Solar Cells. *Advanced Functional Materials*, *26*(31), 5733-5740. https://doi.org/10.1002/adfm.201601305

Gurvich, L., Yungman, V., Bergman, G., Veitz, I., Gusarov, A., Iorish, V., Leonidov, V., Medvedev, V., Belov, G., & Aristova, N. (1992). *Thermodynamic Properties of Individual Substances. Ivtanthermo for Windows Database on Thermodynamic Properties of Individual Substances and Thermodynamic Modeling Software*, Version 3.0 (Glushko Thermocenter of RAS, Moscow). https://gbelov.tripod.com/ivtWeng.htm

Gvishi, R., Reisfeld, R., & Burshtein, Z. (1993). Spectroscopy and laser action of the "red perylimide dye" in various solvents. *Chemical Physics Letters*, *213*(3), 338-344. https://doi.org/10.1016/0009-2614(93)85142-B

Hagfeldt, A., Boschloo, G., Sun, L., Kloo, L., & Pettersson, H. (2010). Dye-Sensitized Solar Cells. *Chemical Reviews*, *110*(11), 6595-6663. https://doi.org/10.1021/cr900356p

Han, L., Zu, X., Cui, Y., Wu, H., Ye, Q., & Gao, J. (2014). Novel D-A-π-A carbazole dyes containing benzothiadiazole chromophores for dye-sensitized solar cells. *Organic Electronics, 15*(7), 1536-1544. https://doi.org/10.1016/j.orgel. 2014.04.016

Hanwell, M. D., Curtis, D. E., Lonie, D. C., Vandermeersch, T., Zurek, E., & Hutchison, G. R. (2012). Avogadro: An advanced semantic chemical editor, visualization and analysis platform. *Journal of Cheminformatics, 4*(1), 3-17. https:// doi.org/ 10.1186/ 1758-2946-4-17

Haque, S. A., Tachibana, Y., Willis, R. L., Moser, J. E., Grätzel, M., Klug, D. R., & Durrant, J. R. (2000). Parameters influencing charge recombination kinetics in dye-sensitized nanocrystalline titanium dioxide films. *The Journal of Physical Chemistry B, 104*(3), 538-547. https://doi.org/https://doi.org/10.1021/jp991085x

Hardin, B. E., Snaith, H. J., & McGehee, M. D. (2012). The renaissance of dye-sensitized solar cells. *Nature Photonics, 6*(3), 162-169. https://doi.org/10.1038/nphoton.2012.22

Hay, P. J., & Wadt, W. R. (1985). Ab initio effective core potentials for molecular calculations. Potentials for the transition metal atoms Sc to Hg. *The Journal of Chemical Physics, 82*(1), 270-283. https://doi.org/10.1063/1.448799

He, L. J., Wei, W., Chen, J., Jia, R., Wang, J., & Zhang, H. X. (2017). The effect of D–[D e–π–A] n (n= 1, 2, 3) type dyes on the overall performance of DSSCs: a theoretical investigation. *Journal of Materials Chemistry C, 5*(30), 7510-7520. https://doi.org/10. 1039/C7TC02499A

Heyd, J., & Scuseria, G. E. (2004). Efficient hybrid density functional calculations in solids: Assessment of the Heyd–Scuseria–Ernzerhof screened Coulomb hybrid functional. *The Journal of Chemical Physics, 121*(3), 1187-1192. https://doi.org/10.1063/1. 1760074

Hilborn, R. C. (1982). Einstein coefficients, cross sections, f values, dipole moments and all that. *American Journal of Physics, 50*(11), 982-986. https://doi.org/10.1119/1.12937

Ho, C. L., & Wong, W. Y. (2016). High performance arylamine-based metallated and metal-free organic photosensitizers for dye-sensitized solar cells. *Journal of Photochemistry and Photobiology C: Photochemistry Reviews, 28*, 138-158. https://doi. org/10.1016/ j.jphotochemrev.2016.05.002

Hosseini, S. E., & Wahid, M. A. (2020). Hydrogen from solar energy, a clean energy carrier from a sustainable source of energy. *International Journal of Energy Research, 44*(6), 4110-4131. https://doi.org/10.1002/er.4930

Hsu, K. F., Loo, S., Guo, F., Chen, W., Dyck, J. S., Uher, C., Hogan, T., Polychroniadis, E. K., & Kanatzidis, M. G. (2004). Cubic $AgPb_mSbTe_{2+m}$: Bulk Thermoelectric Materials with High Figure of Merit. *Science, 303*(5659), 818-821. https://doi.org/10. 1126/science.1092963

Hua, C., & D'Alessandro, D. M. (2017). Systematic Tuning of Zn(II) Frameworks with Furan, Thiophene and Selenophene Dipyridyl and Dicarboxylate Ligands. *Crystal Growth and Design, 17*(12), 6262-6272. https://doi.org/10.1021/acs.cgd.7b00940

Huang, W. K., Cheng, C. W., Chang, S. M., Lee, Y. P., & Diau, E. W. G. (2010). Synthesis and electron-transfer properties of benzimidazole-functionalized ruthenium complexes for highly efficient dye-sensitized solar cells. *Chemical Communications*, 46(47), 8992-8994. https://doi.org/10.1039/C0CC03517C

Hug, H., Bader, M., Mair, P., & Glatzel, T. (2014). Biophotovoltaics: Natural pigments in dye-sensitized solar cells. *Applied Energy, 115*, 216-225. https://doi.org/10.1016/j. apenergy.2013.10.055

Jackson, P., Hariskos, D., Wuerz, R., Kiowski, O., Bauer, A., Friedlmeier, T. M., & Powalla, M. (2015). Properties of Cu (In, Ga) Se2 solar cells with new record efficiencies up to 21.7%. *Physica Status Solidi (RRL)–Rapid Research Letters*, *9*(1), 28-31. https://doi.org/10.1002/pssr.201409520

James, S., & Contractor, R. (2018). Study on Nature-inspired Fractal Design-based Flexible Counter Electrodes for Dye-Sensitized Solar Cells Fabricated using Additive Manufacturing. *Scientific Reports, 8*(1), 1-12. https://doi.org/10.1038/s41598-018-35388-2

Jedidi, A., Markovits, A., Minot, C., Bouzriba, S., & Abderraba, M. (2010). Modeling Localized Photoinduced Electrons in Rutile-TiO_2 Using Periodic DFT+U Methodology. *Langmuir*, *26*(21), 16232-16238. https://doi.org/10.1021/la101359m

Jia, H. L., Peng, Z. J., Gong, B. Q., Huang, C. Y., & Guan, M. Y. (2019). New 2D–π–2A organic dyes with bipyridine anchoring groups for DSSCs [10.1039/C9NJ00087A]. *New Journal of Chemistry*, *43*(15), 5820-5825. https://doi.org/10.1039/C9NJ00087A

Joshi, A. S., Dincer, I., & Reddy, B. V. (2011). Solar hydrogen production: A comparative performance assessment. *International Journal of Hydrogen Energy*, *36*(17), 11246-11257. https://doi.org/10.1016/j.ijhydene.2010.11.122

Juhász, J. I., Großerhode, C., Storck, J. L., Kohn, S., Grethe, T., Grassmann, C., Schwarz-Pfeiffer, A., Grimmelsmann, N., Meissner, H., Blachowicz, T., & Ehrmann, A. (2018). Influence of graphite-coating methods on the DSSC performance. *Optik*, *174*, 40-45. https://doi.org/10.1016/j.ijleo.2018.08.041

Kakiage, K., Aoyama, Y., Yano, T., Oya, K., Fujisawa, J. I., & Hanaya, M. (2015). Highly-efficient dye-sensitized solar cells with collaborative sensitization by silyl-anchor and carboxy-anchor dyes. *Chemical Communications*, *51*(88), 15894-15897. https://doi.org/10.1039/C5CC06759F

Kavan, L., & Grätzel, M. (1989). Nafion modified TiO2 electrodes: photoresponse and sensitization by Ru(II)-bipyridyl complexes. *Electrochimica Acta*, *34*(9), 1327-1334. https://doi.org/10.1016/0013-4686(89)85029-7

Kavlak, G., McNerney, J., & Trancik, J. E. (2018). Evaluating the causes of cost reduction in photovoltaic modules. *Energy Policy*, *123*, 700-710. https://doi.org/10.1016/j.enpol.2018.08.015

Khan, F., & Kim, J. H. (2019). Emission-wavelength-dependent photoluminescence decay lifetime of N-functionalized graphene quantum dot downconverters: Impact on conversion efficiency of Cu(In, Ga)Se_2 solar cells. *Scientific Reports*, *9*(1), 1-9. https://doi.org/10.1038/s41598-019-47068-w

Kim, S. H., Jung, J. Y., Wehrspohn, R. B., & Lee, J. H. (2020). All-Room-Temperature Processed 17.25%-Crystalline Silicon Solar Cell. American Chemical Society Applied Energy Materials, 3(4), 3180-3185. https://doi.org/10.1021/acsaem.0c00133

Kohn, W. and Sham, L.J. (1965) Self-Consistent Equations Including Exchange and Correlation Effects. Physical Review, 140, 1133-1138. http: //dx. doi.org/ 10.1103/ PhysRev.140.A1133

Kumar, K. D., Kříž, J., Bennett, N., Chen, B., Upadhayaya, H., Reddy, K. R., & Sadhu, V. (2020). Functionalized metal oxide nanoparticles for efficient dye-sensitized solar cells (DSSCs): A review. *Materials Science for Energy Technologies, 3*, 472-481. https://doi.org/10.1016/j.mset.2020.03.003

Kresse, G., & Furthmüller, J. (1996). Efficiency of ab-initio total energy calculations for metals and semiconductors using a plane-wave basis set. *Computational Materials Science, 6*(1), 15-50. https://doi.org/10.1016/0927-0256(96)00008-0

Kresse, G., & Hafner, J. (1993). Ab initio molecular dynamics for liquid metals. *Physical Review B, 47*(1), 558-561. https://doi.org/10.1103/PhysRevB.47.558

Lee, D. H., Lee, M. J., Song, H. M., Song, B. J., Seo, K. D., Pastore, M., Anselmi, C., Fantacci, S., De Angelis, F., Nazeeruddin, M. K., Gräetzel, M., & Kim, H. K. (2011). Organic dyes incorporating low-band-gap chromophores based on π-extended benzothiadiazole for dye-sensitized solar cells. *Dyes and Pigments, 91*(2), 192-198. https://doi.org/10. 1016/j.dyepig.2011.03.015

Lee, K., & Sotzing, G. A. (2001). Poly(thieno[3,4-b]thiophene). A New Stable Low Band Gap Conducting Polymer. *Macromolecules, 34*(17), 5746-5747. https://doi.org/10. 1021/ma0106245

Lee, M. W., Kim, J. Y., Son, H. J., Kim, J. Y., Kim, B., Kim, H., Lee, D. K., Kim, K., Lee, D.-H., & Ko, M. J. (2015). Tailoring of Energy Levels in D-π-A Organic Dyes via Fluorination of Acceptor Units for Efficient Dye-Sensitized Solar Cells. *Scientific Reports, 5*(1), 1-7. https://doi.org/10.1038/srep07711

Li, B., Wang, L., Kang, B., Wang, P., & Qiu, Y. (2006). Review of recent progress in solid-state dye-sensitized solar cells. *Solar Energy Materials and Solar Cells*, *90*(5), 549-573. https://doi.org/10.1016/j.solmat.2005.04.039

Li, G., Sheng, L., Li, T., Hu, J., Li, P., & Wang, K. (2019). Engineering flexible dye-sensitized solar cells for portable electronics. *Solar Energy*, *177*, 80-98. https://doi. org/10.1016/j.solener.2018.11.017

Li, P., Cui, Y., Song, C., & Zhang, H. (2017). A systematic study of phenoxazine-based organic sensitizers for solar cells. *Dyes and Pigments, 137*, 12-23. https://doi.org/10. 1016/j. dyepig.2016.09.060

Li, R., Lv, X., Shi, D., Zhou, D., Cheng, Y., Zhang, G., & Wang, P. (2009). Dye-Sensitized Solar Cells Based on Organic Sensitizers with Different Conjugated Linkers: Furan, Bifuran, Thiophene, Bithiophene, Selenophene and Biselenophene. *The Journal of Physical Chemistry C, 113*(17), 7469-7479. https://doi.org/10.1021/jp900972v

Li, Y., Liu, J., Liu, D., Li, X., & Xu, Y. (2019). D-A-π-A based organic dyes for efficient DSSCs: A theoretical study on the role of π-spacer. *Computational Materials Science, 161*, 163-176. https://doi.org/https://doi.org/10.1016/j.commatsci.2019.01.033

Li, Y., Liu, S., Ni, H., Zhang, H., Zhang, H., Chuah, C., Ma, C., Wong, K. S., Lam, J. W. Y., Kwok, R. T. K., Qian, J., Lu, X., & Tang, B. Z. (2020). ACQ-to-AIE Transformation: Tuning Molecular Packing by Regioisomerization for Two-Photon NIR Bioimaging. *Angewandte Chemie International Edition, 59*(31), 12822-12826. https://doi.org/10. 1002/anie. 202005785

Liang, M., Xu, W., Cai, F., Chen, P., Peng, B., Chen, J., & Li, Z. (2007). New Triphenylamine-Based Organic Dyes for Efficient Dye-Sensitized Solar Cells. *The Journal of Physical Chemistry C, 111*(11), 4465-4472. https://doi.org/10.1021/ jp067930a

Lin, B. C., Cheng, C. P., You, Z. Q., & Hsu, C. P. (2005). Charge transport properties of tris (8-hydroxyquinolinato) aluminum (III): Why it is an electron transporter. *Journal of the American Chemical Society, 127*(1), 66-67. https://doi.org/10.1021/ja045087t

Lin, J. T., Chen, P. C., Yen, Y. S., Hsu, Y. C., Chou, H. H., & Yeh, M. C. P. (2009). Organic Dyes Containing Furan Moiety for High-Performance Dye-Sensitized Solar Cells. *Organic Letters, 11*(1), 97-100. https://doi.org/10.1021/ol8025236

Listorti, A., O'Regan, B., & Durrant, J. R. (2011). Electron Transfer Dynamics in Dye-Sensitized Solar Cells. *Chemistry of Materials, 23*(15), 3381-3399. https://doi.org/10.1021/cm200651e

Liu, H., Liu, L., Fu, Y., Liu, E., & Xue, B. (2019a). Theoretical Design of D− π–A–A Sensitizers with Narrow Band Gap and Broad Spectral Response Based on Boron Dipyrromethene for Dye-Sensitized Solar Cells. *Journal of Chemical Information and Modeling, 59*(5), 2248-2256. https://doi.org/10.1021/acs.jcim.9b00187

Liu, H., Liu, L., Fu, Y., Liu, E., & Xue, B. (2019b). Theoretical Design of D−π–A–A Sensitizers with Narrow Band Gap and Broad Spectral Response Based on Boron Dipyrromethene for Dye-Sensitized Solar Cells. *Journal of Chemical Information and Modeling, 59*(5), 2248-2256. https://doi.org/10.1021/acs.jcim.9b00187

Liu, Q. L., Zhao, Z. Y., & Liu, Q. J. (2014). Analysis of sulfur modification mechanism for anatase and rutile TiO_2 by different doping modes based on GGA+ U calculations. *Royal Society of Chemistry Advances, 4*(61), 32100-32107. https://doi.org/10.1039/C4RA03891F

Luo, J. S., Wan, Z. Q., & Jia, C. Y. (2016). Recent advances in phenothiazine-based dyes for dye-sensitized solar cells. *Chinese Chemical Letters, 27*(8), 1304-1318. https://doi.org /10.1016/j.cclet.2016.07.002

Mahadevi, P., & Sumathi, S. (2020). Mini review on the performance of Schiff base and their metal complexes as photosensitizers in dye-sensitized solar cells. *Synthetic Communications, 50*(15), 2237-2249. https://doi.org/10.1080/00397911.2020.1748200

Mahmood, A. (2016). Triphenylamine based dyes for dye sensitized solar cells: A review. *Solar Energy, 123*, 127-144. https://doi.org/10.1016/j.solener.2015.11.015

Marcus, R. A. (1965). On the theory of electron-transfer reactions. VI. Unified treatment for homogeneous and electrode reactions. *The Journal of Chemical Physics, 43*(2), 679-701. https://doi.org/10.1063/1.1696792

Marinado, T., Nonomura, K., Nissfolk, J., Karlsson, M. K., Hagberg, D. P., Sun, L., Mori, S., & Hagfeldt, A. (2010). How the Nature of Triphenylamine-Polyene Dyes in Dye-Sensitized Solar Cells Affects the Open-Circuit Voltage and Electron Lifetimes. *Langmuir, 26*(4), 2592-2598. https://doi.org/10.1021/la902897z

Marques, F. C., Cortes, A. D. S., & Mei, P. R. (2019). Solar Cells Fabricated in Upgraded Metallurgical Silicon, Obtained Through Vacuum Degassing and Czochralski Growth. *Silicon, 11*(1), 77-83. https://doi.org/10.1007/s12633-018-9860-x

Martínez, A., Vargas, R., & Galano, A. (2009). What is Important to Prevent Oxidative Stress? A Theoretical Study on Electron-Transfer Reactions between Carotenoids and Free Radicals. *The Journal of Physical Chemistry B, 113*(35), 12113-12120. https://doi. org/10.1021/jp903958h

Marziano, V., Pugliese, A., Merler, S., & Ajelli, M. (2017). Detecting a Surprisingly Low Transmission Distance in the Early Phase of the 2009 Influenza Pandemic. *Scientific Reports, 7*(1), 1-9. https://doi.org/10.1038/s41598-017-12415-2

Materna, K. L., Crabtree, R. H., & Brudvig, G. W. (2017). Anchoring groups for photocatalytic water oxidation on metal oxide surfaces. *Chemical Society Reviews, 46*(20), 6099-6110. https://doi.org/10.1039/C7CS00314E

Matsushita, S., Tsuruoka, A., Kobayashi, E., Isobe, T., & Nakajima, A. (2017). Redox reactions by thermally excited charge carriers: Towards sensitized thermal cells. *Materials Horizons, 4*(4), 649-656. https://doi.org/10.1039/C7MH00108H

Moia, D., Vaissier, V., López-Duarte, I., Torres, T., Nazeeruddin, M. K., O'Regan, B. C., Nelson, J., & Barnes, P. R. (2014). The reorganization energy of intermolecular hole hopping between dyes anchored to surfaces. *Chemical Science, 5*(1), 281-290. https://doi.org/10.1039/c3sc52359d

Monkhorst, H. J., & Pack, J. D. (1976). Special points for Brillouin-zone integrations. *Physical Review B, 13*(12), 5188-5192. https://doi.org/10.1103/PhysRevB. 13.5188

Moriarty, P., & Honnery, D. (2012). What is the global potential for renewable energy? *Renewable and Sustainable Energy Reviews, 16*(1), 244-252. https://doi.org/10.1016/j.rser.2011.07.151

Murakami, T. N., Yoshida, E., & Koumura, N. (2014). Carbazole dye with phosphonic acid anchoring groups for long-term heat stability of dye-sensitized solar cells. *Electrochimica Acta, 131*, 174-183. https://doi.org/10.1016/j.electacta. 2013.12.013

Namba, S., & Hishiki, Y. (1965). Color Sensitization of Zinc Oxide with Cyanine Dyes1. *The Journal of Physical Chemistry, 69*(3), 774-779. https://doi.org/10.1021/j100887a010

Narayan, M. R. (2012). Review: Dye sensitized solar cells based on natural photosensitizers. *Renewable and Sustainable Energy Reviews, 16*(1), 208-215. https://doi.org/10.1016/j.rser.2011.07.148

Narula, K. (2014). Is sustainable energy security of India increasing or decreasing? *International Journal of Sustainable Energy, 33*(6), 1054-1075. https://doi.org/10.1080/14786451.2013.811411

Neef, C. J., Brotherston, I. D., & Ferraris, J. P. (1999). Synthesis and Electronic Properties of Poly(2-phenylthieno[3,4-b]thiophene): A New Low Band Gap Polymer. *Chemistry of Materials, 11*(8), 1957-1958. https://doi.org/10.1021/cm9901109

Neese, F. (2008). ORCA-an ab initio density functional and semiempirical program package, version 2.7. *University of Bonn*.

Neese, F. (2018). Software update: The ORCA program system, version 4.0. *Wiley Interdisciplinary Reviews: Computational Molecular Science, 8*(1), 1-6. https://doi.org/10.1002/wcms.1327

O'Regan, B., & Grätzel, M. (1991). A low-cost, high-efficiency solar cell based on dye-sensitized colloidal TiO_2 films. *Nature, 353*(6346), 737-740. https://doi.org/10.1038/353737a0

Omar, A., Ali, M. S., & Abd Rahim, N. (2020). Electron transport properties analysis of titanium dioxide dye-sensitized solar cells (TiO_2-DSSCs) based natural dyes using electrochemical impedance spectroscopy concept: A review. *Solar Energy, 207*, 1088-1121. https://doi.org/10.1016/j.solener.2020.07.028

Pachauri, S. (2011). Reaching an international consensus on defining modern energy access. *Current Opinion in Environmental Sustainability, 3*(4), 235-240. https://doi.org/10.1016/j.cosust.2011.07.005

Parr, R. G., Szentpály, L. V., & Liu, S. (1999). Electrophilicity Index. *Journal of the American Chemical Society, 121*(9), 1922-1924. https://doi.org/10.1021/ja983494x

Pastore, M., & De Angelis, F. (2010). Aggregation of organic dyes on TiO_2 in dye-sensitized solar cells models: an ab initio investigation. *American Chemical Society nano, 4*(1), 556-562. https://doi.org/10.1021/nn901518s

Pastore, M., & De Angelis, F. (2013). Modeling materials and processes in dye-sensitized solar cells: understanding the mechanism, improving the efficiency. In *Multiscale modelling of organic and hybrid photovoltaics*, 151-236. Springer. https://doi.org/10.1007/128_2013_468

Pastore, M., Fantacci, S., & De Angelis, F. (2010). Ab initio determination of ground and excited state oxidation potentials of organic chromophores for dye-sensitized solar cells. *The Journal of Physical Chemistry C, 114*(51), 22742-22750. https:// doi.org/ 10.1021/ jp1088965

Perdew, J. P., Burke, K., & Ernzerhof, M. (1996). Generalized gradient approximation made simple. *Physical Review Letters, 77*(18), 3865-3868. https:// doi. org/ 10.1103/ Phys RevLett. 77.3865

Pimental, D. (1976). World Food Crisis: Energy and Pests. *Bulletin of the Entomological Society of America, 22*(1), 20-26. https://doi.org/10.1093/besa/22.1.20

Pimentel, D., Rodrigues, G., Wang, T., Abrams, R., Goldberg, K., Staecker, H., Ma, E., Brueckner, L., Trovato, L., Chow, C., Govindarajulu, U., & Boerke, S. (1994). Renewable Energy: Economic and Environmental Issues. *BioScience, 44*(8), 536-547. https://doi.org/10.2307/1312281

Preat, J., Hagfeldt, A., & Perpète, E. A. (2011). Investigation of the photoinduced electron injection processes for p-type triphenylamine-sensitized solar cells. *Energy & Environmental Science, 4*(11), 4537-4549. https://doi.org/10.1039/C1EE01638E

Qian, X., Zhu, Y. Z., Song, J., Gao, X. P., & Zheng, J. Y. (2013). New Donor-π-Acceptor Type Triazatruxene Derivatives for Highly Efficient Dye-Sensitized Solar Cells. *Organic Letters, 15*(23), 6034-6037. https://doi.org/10.1021/ol402931u

Ray, D. (2019). Lazard's Levelized Cost of Energy Analysis-Version 13.0. *Lazard: New York, NY, USA*, 20.

Ren, J., & Sovacool, B. K. (2014). Quantifying, measuring and strategizing energy security: Determining the most meaningful dimensions and metrics. *Energy, 76*, 838-849. https://doi.org/10.1016/j.energy.2014.08.083

Rho, W. Y., Song, D. H., Yang, H. Y., Kim, H. S., Son, B. S., Suh, J. S., & Jun, B. H. (2018). Recent advances in plasmonic dye-sensitized solar cells. *Journal of Solid State Chemistry, 258*, 271-282. https://doi.org/10.1016/j.jssc.2017.10.018

Roy, J. K., Kar, S., & Leszczynski, J. (2018). Insight into the optoelectronic properties of designed solar cells efficient tetrahydroquinoline dye-sensitizers on TiO_2 (101) surface: first principles approach. *Scientific Reports, 8*(1), 1-12. https:// doi.org/10. 1038/ s41598 - 018-29368-9

Saranya, G., Yam, C., Gao, S., & Chen, M. (2018). Roles of Chenodeoxycholic Acid Coadsorbent in Anthracene-Based Dye-Sensitized Solar Cells: A Density Functional Theory Study. *The Journal of Physical Chemistry C, 122*(41), 23280-23287. https://doi.org/10.1021/acs.jpcc.8b06495

Schmidt, M. W., Baldridge, K. K., Boatz, J. A., Elbert, S. T., Gordon, M. S., Jensen, J. H., Koseki, S., Matsunaga, N., Nguyen, K. A., & Su, S. (1993). General atomic and molecular electronic structure system. *Journal of Computational Chemistry, 14*(11), 1347-1363. https://doi.org/10.1002/jcc.540141112

Shakeel Ahmad, M., Pandey, A. K., & Abd Rahim, N. (2017). Advancements in the development of TiO_2 photoanodes and its fabrication methods for dye sensitized solar cell (DSSC) applications. A review. *Renewable and Sustainable Energy Reviews, 77*, 89-108. https://doi.org/10.1016/j.rser.2017.03.129

Siddiqui, S. A. (2019). In silico investigation of the coumarin-based organic semiconductors for the possible use in organic electronic devices. *Journal of Physical Organic Chemistry*, *32*(3), 1-10. https://doi.org/10.1002/poc.3905

Sinha, A., & Shahbaz, M. (2018). Estimation of Environmental Kuznets Curve for CO2 emission: Role of renewable energy generation in India. *Renewable Energy*, *119*, 703-711. https://doi.org/10.1016/j.renene.2017.12.058

Solangi, K. H., Islam, M. R., Saidur, R., Rahim, N. A., & Fayaz, H. (2011). A review on global solar energy policy. *Renewable and Sustainable Energy Reviews, 15*(4), 2149-2163. https://doi.org/10.1016/j.rser.2011.01.007

Sotzing, G. A., & Lee, K. (2002). Poly(thieno[3,4-b]thiophene): A p- and n-Dopable Polythiophene Exhibiting High Optical Transparency in the Semiconducting State. *Macromolecules, 35*(19), 7281-7286. https://doi.org/10.1021/ma020367j

Spitler, M. T., & Calvin, M. (1977). Electron transfer at sensitized TiO2 electrodes. *The Journal of Chemical Physics, 66*(10), 4294-4305. https://doi.org/10.1063/1.433739

Sun, W., Wang, C. H., Lv, S. F., Jiang, J. X., Guo, X., & Zhang, F. B. (2020). Bis(benzofurano)pyrrole and hybrid thienopyrrole derivatives for organic thin-film transistors. *Organic Electronics*, 77, 1-11. https://doi.org/10.1016/j.orgel.2019.105548

Sundin, E., & Abrahamsson, M. (2018). Long-lived charge separation in dye–semiconductor assemblies: A pathway to multi-electron transfer reactions. *Chemical Communications, 54*(42), 5289-5298. https://doi.org/10.1039/C8CC01071D

Syzgantseva, O. A., Gonzalez-Navarrete, P., Calatayud, M., Bromley, S., & Minot, C. (2011). Theoretical investigation of the hydrogenation of $(TiO_2)_N$ clusters (N= 1–10). *The Journal of Physical Chemistry C, 115*(32), 15890-15899. https://doi.org/10.1021/jp2050349

Tamang, A., Hongsingthong, A., Jovanov, V., Sichanugrist, P., Khan, B. A., Dewan, R., Konagai, M., & Knipp, D. (2016). Enhanced photon management in silicon thin film solar cells with different front and back interface texture. *Scientific Reports, 6*(1), 1-10. https://doi.org/10.1038/srep29639

Tan, Y., Zhang, Q., Yu, J., Zhao, X., Tian, Y., Cui, Y., Hao, X., Yang, Y., & Qian, G. (2013). Solvent effect on two-photon absorption (TPA) of three novel dyes with large TPA cross-section and red emission. *Dyes and Pigments*, *97*(1), 58-64. https://doi.org/10.1016/j.dyepig.2012.11.024

Tongsopit, S., Kittner, N., Chang, Y., Aksornkij, A., & Wangjiraniran, W. (2016). Energy security in ASEAN: A quantitative approach for sustainable energy policy. *Energy Policy, 90*, 60-72. https://doi.org/10.1016/j.enpol.2015.11.019

Tripathi, A., & Chetti, P. (2020). Enhanced charge transport properties in heteroatomic (NH, O, Se) analogs of benzotrithiophene (BTT) isomers: A DFT insight. *Molecular Simulation, 46*(7), 548-556. https://doi.org/10.1080/08927022.2020.1738425

Tripathi, A., & Prabhakar, C. (2018). Impact of replacement of the central benzene ring in anthracene by a heterocyclic ring on electronic excitations and reorganization energies in anthratetrathiophene molecules. *Journal of the Chinese Chemical Society, 65*(8), 918-924. https://doi.org/10.1002/jccs.201700448

Tripathi, A., & Prabhakar, C. (2020). Optical and charge transport properties of chalcogen (O, S and Se) based acene molecules. *Journal of Molecular Structure, 1203*, 1-24. https://doi.org/10.1016/j.molstruc.2019.127397

Tsoutsos, T., Frantzeskaki, N., & Gekas, V. (2005). Environmental impacts from the solar energy technologies. *Energy Policy, 33*(3), 289-296. https://doi.org/10.1016/S0301-4215(03)00241-6

Upadhyaya, H. M., Senthilarasu, S., Hsu, M. H., & Kumar, D. K. (2013). Recent progress and the status of dye-sensitised solar cell (DSSC) technology with state-of-the-art conversion efficiencies. *Solar Energy Materials and Solar Cells, 119*, 291-295. https://doi.org/10.1016/j.solmat.2013.08.031

Vaissier, V., Barnes, P., Kirkpatrick, J., & Nelson, J. (2013). Influence of polar medium on the reorganization energy of charge transfer between dyes in a dye sensitized film. *Physical Chemistry Chemical Physics, 15*(13), 4804-4814. https:// doi.org/ 10.1039 /C3CP44562 C

Velusamy, M., Justin Thomas, K. R., Lin, J. T., Hsu, Y. C., & Ho, K. C. (2005). Organic Dyes Incorporating Low-Band-Gap Chromophores for Dye-Sensitized Solar Cells. *Organic Letters, 7*(10), 1899-1902. https://doi.org/10.1021/ol050417f

Venkateswararao, A., Thomas, K. R. J., Lee, C. P., Li, C. T., & Ho, K. C. (2014). Organic Dyes Containing Carbazole as Donor and π-Linker: Optical, Electrochemical and Photovoltaic Properties. *American Chemical Society Applied Materials and Interfaces, 6*(4), 2528-2539. https://doi.org/10.1021/am404948w

Wan, T., Ramakrishna, S., & Liu, Y. (2018). Recent progress in electrospinning TiO_2 nanostructured photo-anode of dye-sensitized solar cells. *Journal of Applied Polymer Science, 135*(1), 1-10. https://doi.org/10.1002/app.45649

Wang, D. L., Cui, H. J., Hou, G. J., Zhu, Z. G., Yan, Q. B., & Su, G. (2016). Highly efficient light management for perovskite solar cells. *Scientific Reports, 6*(1), 1-10. https://doi.org/10.1038/srep18922

Wang, J. L., Wu, Z., Miao, J. S., Liu, K. K., Chang, Z. F., Zhang, R. B., Wu, H. B., & Cao, Y. (2015). Solution-Processed Diketopyrrolopyrrole-Containing Small-Molecule Organic Solar Cells with 7.0% Efficiency: In-Depth Investigation on the Effects of Structure Modification and Solvent Vapor Annealing. *Chemistry of Materials, 27*(12), 4338-4348. https://doi.org/10.1021/acs.chemmater.5b00848

Wang, J., Li, H., Ma, N. N., Yan, L. K., & Su, Z. M. (2013). Theoretical studies on organoimido-substituted hexamolybdates dyes for dye-sensitized solar cells (DSSC). *Dyes and Pigments, 99*(2), 440-446. https://doi.org/10.1016/j.dyepig. 2013.05.027

Wang, N., Sun, X., Zhao, Q., Yang, Y., & Wang, P. (2020). Leachability and adverse effects of coal fly ash: A review. *Journal of Hazardous Materials, 396*, 1-26. https://doi.org/10.1016/j.jhazmat.2020.122725

Wang, S., Wang, J., Lin, S., & Li, J. (2019). Public perceptions and acceptance of nuclear energy in China: The role of public knowledge, perceived benefit, perceived risk and public engagement. *Energy Policy, 126*, 352-360. https://doi.org/10.1016/j.enpol. 2018.11.040

Wang, X., Yang, J., Yu, H., Li, F., Fan, L., Sun, W., Liu, Y., Koh, Z. Y., Pan, J., & Yim, W. L. (2014). A benzothiazole–cyclopentadithiophene bridged D-A-π-A sensitizer with enhanced light absorption for high efficiency dye-sensitized solar cells. *Chemical Communications, 50*(30), 3965-3968. https://doi.org/10.1039/C4CC00577E

Wazzan, N., & Irfan, A. (2018). Theoretical study of triphenylamine-based organic dyes with mono-, di- and tri-anchoring groups for dye-sensitized solar cells. *Organic Electronics, 63*, 328-342. https://doi.org/10.1016/j.orgel.2018.09.039

Wazzan, N. A. (2019). A DFT/TDDFT investigation on the efficiency of novel dyes with ortho-fluorophenyl units (A1) and incorporating benzotriazole/benzothiadiazole/ phthalimide units (A2) as organic photosensitizers with D–A2–π–A1 configuration for solar cell applications. *Journal of Computational Electronics, 18*(2), 375-395. https://doi.org/10. 1007/s10825-019-01308-4

Wei, S., Li, K., Lu, X., Zhao, Z., Shao, Y., Dang, Y., Li, S., & Guo, W. (2016). Theoretical insight into electronic structure and optoelectronic properties of heteroleptic Cu (I)-based complexes for dye-sensitized solar cells. *Materials Chemistry and Physics, 173*, 139-145. https://doi.org/10.1016/j.matchemphys.2016.01.049

Wu, Y., Marszalek, M., Zakeeruddin, S. M., Zhang, Q., Tian, H., Grätzel, M., & Zhu, W. (2012). High-conversion-efficiency organic dye-sensitized solar cells: molecular engineering on D-A-π-A featured organic indoline dyes. *Energy and Environmental Science, 5*(8), 8261-8272. https://doi.org/10.1039/C2EE22108J

Xie, Y., Tang, Y., Wu, W., Wang, Y., Liu, J., Li, X., Tian, H., & Zhu, W. H. (2015). Porphyrin Cosensitization for a Photovoltaic Efficiency of 11.5%: A Record for Non-Ruthenium Solar Cells Based on Iodine Electrolyte. *Journal of the American Chemical Society, 137*(44), 14055-14058. https://doi.org/10.1021/jacs.5b09665

Xu, M., Li, R., Pootrakulchote, N., Shi, D., Guo, J., Yi, Z., Zakeeruddin, S. M., Grätzel, M., & Wang, P. (2008). Energy-Level and Molecular Engineering of Organic D-π-A Sensitizers in Dye-Sensitized Solar Cells. *The Journal of Physical Chemistry C, 112*(49), 19770-19776. https://doi.org/10.1021/jp808275z

Xu, Y., Li, M., Fu, Y., Lu, T., Hu, Y., & Lu, W. (2019). Theoretical study of high-efficiency organic dyes with the introduction of different auxiliary heterocyclic acceptors based on IQ1 toward dye-sensitized solar cells. *Journal of Molecular Graphics and Modelling, 86*, 170-178. https://doi.org/10.1016/j.jmgm.2018.10.001

Yan, N., Zhao, C., You, S., Zhang, Y., & Li, W. (2020). Recent progress of thin-film photovoltaics for indoor application. *Chinese Chemical Letters, 31*(3), 643-653. https://doi.org/10.1016/j.cclet.2019.08.022

Yanai, T., Tew, D. P., & Handy, N. C. (2004). A new hybrid exchange–correlation functional using the Coulomb-attenuating method (CAM-B3LYP). *Chemical Physics Letters, 393*(1-3), 51-57. https://doi.org/10.1016/j.cplett.2004.06.011

Yao, H., Ye, L., Zhang, H., Li, S., Zhang, S., & Hou, J. (2016). Molecular Design of Benzodithiophene-Based Organic Photovoltaic Materials. *Chemical Reviews, 116*(12), 7397-7457. https:// doi.org/ 10.1021/ acs.chemrev.6b00176

Yugis, A. R., Mansa, R. F., & Sipaut, C. S. (2015). Review on Metallic and Plastic Flexible Dye Sensitized Solar Cell. *Institute of Physics Conference Series: Materials Science and Engineering, 78*, 1-7. https://doi.org/10.1088/1757-899x/78/1/012003

Zanjanchi, F., & Beheshtian, J. (2019). Natural pigments in dye-sensitized solar cell (DSSC): a DFT-TDDFT study. *Journal of the Iranian Chemical Society, 16*(4), 795-805. https:// doi.org/ 10.1007/ s13738 - 018-1561-2

Zhang, G., Bai, Y., Li, R., Shi, D., Wenger, S., Zakeeruddin, S. M., Grätzel, M., & Wang, P. (2009). Employ a bisthienothiophene linker to construct an organic chromophore for efficient and stable dye-sensitized solar cells. *Energy and Environmental Science, 2*(1), 92-95. https://doi.org/10.1039/B817990E

Zhang, H., Lu, Y., Han, W., Zhu, J., Zhang, Y., & Huang, W. (2020). Solar energy conversion and utilization: Towards the emerging photo-electrochemical devices based on perovskite photovoltaics. *Chemical Engineering Journal, 393*, 1-13. https://doi.org/10.1016/j.cej.2020.124766

Zhang, J., Xu, L., & Wong, W. Y. (2018). Energy materials based on metal Schiff base complexes. *Coordination Chemistry Reviews, 355*, 180-198. https://doi.org/10.1016 /j.ccr.2017.08.007

Zhang, J., Zhu, H. C., Zhong, R. L., Wang, L., & Su, Z. M. (2018). Promising heterocyclic anchoring groups with superior adsorption stability and improved IPCE for high-efficiency noncarboxyl dye sensitized solar cells: A theoretical study. *Organic Electronics, 54*, 104-113. https://doi.org/10.1016/j.orgel.2017. 12.023

Zhang, M., Hua, Z., Liu, W., Liu, H., He, S., Zhu, C., & Zhu, Y. (2020). A DFT study on the photoelectric properties of rubrene and its derivatives. *Journal of Molecular Modeling, 26*(2), 1-8. https://doi.org/10.1007/s00894-020-4295-x

Zhang, Q., Zhang, P., Gong, Y., & Ding, C. (2019). Two-photon AIE based fluorescent probe with large stokes shift for selective and sensitive detection and visualization of hypochlorite. *Sensors and Actuators B: Chemical, 278*, 73-81. https://doi.org/10.1016 /j.snb.2018.09.057

Zheng, B., Chevallier, F., Ciais, P., Yin, Y., Deeter, M. N., Worden, H. M., Wang, Y., Zhang, Q., & He, K. (2018). Rapid decline in carbon monoxide emissions and export from East Asia between years 2005 and 2016. *Environmental Research Letters, 13*(4), 1-9. https://doi.org/10.1088/1748-9326/aab2b3

Zhurko, G. A., & Zhurko, A. D. (2015). ChemCraft graphical program for visualization of computed results. http://www.chemcraftprog.com/.2015

RESEARCH OUTPUTS

List of Publications

Deogratias, G., Al-Qurashi, O. S., Wazzan, N., Pogrebnaya, T., & Pogrebnoi, A. (2020). Effects of heteroatoms in π-conjugated linkers on the optical and electronic properties of modified triphenylamine based dyes: Towards DSSCs' applications. *Journal of Molecular Modeling*, *26*(10), 288. https://doi.org/10.1007/s00894-020-04542-x

Deogratias, G., Al-Qurashi, O. S., Wazzan, N., Seriani, N., Pogrebnaya, T., & Pogrebnoi, A. (2020). Investigation of optoelectronic properties of triphenylamine-based dyes featuring heterocyclic anchoring groups for DSSCs' applications: A theoretical study. *Structural Chemistry*. https://doi.org/10.1007/s11224-020-01596-8

Deogratias, G., Seriani, N., Pogrebnaya, T., & Pogrebnoi, A. (2020). Tuning optoelectronic properties of triphenylamine based dyes through variation of pi-conjugated units and anchoring groups: A DFT/TD-DFT investigation. *Journal of Molecular Graphics and Modelling*, *94*, 107480. https://doi.org/10.1016/j.jmgm.2019.107480

Poster Presentation

Molecular modification of dye constituents through Grafting Anchoring Groups and pi-Spacers: Towards DSSCs Application.